TALLINN UNIVERSITY OF TECHNOLOGY
DOCTORAL THESIS
68/2018

Reliability Aspects of PVD Coatings Sliding under Wear and Corrosive Conditions

JANIS BARONINŠ

TTÜ PRESS

TALLINN UNIVERSITY OF TECHNOLOGY
School of Engineering
Department of Mechanical and Industrial Engineering
This dissertation was accepted for the defence of the degree 17/10/2018

Supervisor: Prof. Irina Hussainova
School of Engineering
Department of Mechanical and Industrial Engineering
Tallinn University of Technology
Tallinn, Estonia

Co-supervisor: PhD Maksim Antonov
Senior Research Scientist, School of Engineering
Department of Mechanical and Industrial Engineering
Tallinn University of Technology
Tallinn, Estonia

Opponents: PhD Arkadi Zikin
Technology Leader, Application Development, Laser Surface Engineering
Oerlikon Metco AG
Wohlen, Switzerland

PhD Sergei Vlassov
Senior Research Fellow, Faculty of Science and Technology
Institute of Physics
University of Tartu
Tartu, Estonia

Defence of the thesis: 14/12/2018, Tallinn

Declaration:
Hereby I declare that this doctoral thesis, my original investigation and achievement, submitted for the doctoral degree at Tallinn University of Technology, has not been previously submitted for doctoral or equivalent academic degree.

Janis Baroninš

----
signature

European Union
European Social Fund

Investing in your future

ISSN 2585-6898 (publication)
ISBN 978-9949-83-350-4 (publication)
ISSN 2585-6901 (PDF)
ISBN 978-9949-83-351-1 (PDF)

TALLINNA TEHNIKAÜLIKOOL
DOKTORITÖÖ
68/2018

PVD pinnete töökindluse aspektid liughõõrdumise ja korrosiooni tingimustes

JANIS BARONINŠ

TTÜ
KIRJASTUS

Contents

List of Publications

The list of author's publications, based on which the thesis has been prepared:

I **Baronins, J.**, Podgursky, V., Antonov, M., Bereznev, S., Hussainova, I., Electrochemical behaviour of TiCN and TiAlN gradient coatings prepared by lateral rotating cathode arc PVD technology. *Key Engineering Materials*, 2016, 721, 414–418.

II Antonov, M., Afshari, H., **Baronins, J.**, Adoberg, E., Raadik, T., Hussainova, I., The effect of temperature and sliding speed on friction and wear of Si_3N_4, Al_2O_3, and ZrO_2 balls tested against AlCrN PVD coating. *Tribology International*, 2018, 118, 500–514.

III **Baronins, J.**, Antonov, M., Bereznev, S., Raadik, T., Hussainova, I., Raman spectroscopy for reliability assessment of multilayered AlCrN coating in tribo-corrosive conditions. *Coatings*, 2018, 8 (7), 229–241.

Author’s contribution to the publications

In these papers the author of the present doctoral thesis created and developed methodology; made formal analysis and investigation; provided data curation; prepared and wrote original draft; provided visualization of the obtained research data; and was involved in the correction of the final versions.

The list of the author's publications not included into thesis

IV Sarjas, H., Surzhenkov, A., **Baroninš, J.**, Viljus, M., Traksmaa, R., Kulu, P., Corrosion behaviour of high velocity oxy-fuel sprayed composite Ni-/Fe-based self-fluxing alloy – cermet coatings. *Journal of Mineral, Metal and Materials Engineering,* 2018, 4, 1–9.

V Antonov, M., **Baronins, J.**, and Hussainova, I. (2018). Transformable multi-sample apparatus for dry erosion testing of materials up to 1000 °C in the presence of corrosive gases. P201800011. Estonia. (industrial property).

VI Kommel, L., **Baroninš, J.**, Dependence of wear of Cu-Cr-S alloy on hardness and electrical conductivity in sliding electrical contact. *Solid State Phenomena*, 2017, 267, 229–233.

VII Yashin, M., **Baroninš, J.**, Menezes, P. L., Viljus, M., Raadik, T., Bogatov, A., Antonov, M., Podgursky, V., Wear rate of nanocrystalline diamond coating under high temperature sliding conditions. *Solid State Phenomena*, 2017, 267, 219–223.

VIII Surzhenkov, A., **Baroninš, J.**, Viljus, M., Traksmaa, R., Kulu, P., Sliding wear of composite stainless steel hardfacing under room and elevated temperature. *Solid State Phenomena*, 2017, 267, 195–200.

IX **Baronins, J.**, Antonov, M., Ivanov, R., Shuliak, V., Hussainova, I., Effect of basalt and silica additives on erosive wear resistance of cast ceramics. *Proceedings of the Estonian Academy of Sciences*, 2016, 65 (2), 144–151.

X Hussainova, I., **Baronins, J.**, Drozdova, M., Antonov, M., Wear performance of hierarchically structured alumina reinforced by hybrid graphene encapsulated alumina nanofibers. *Wear*, 2016, 368–369, 287–295.

Introduction

It is well known, that the movement of bodies pressed against each other inevitably causes a loss or relocation of material in the contact zone. Such reactive environments, like a high temperature oxidative atmosphere or an aqueous media, can intensify a wear rate of tools in service. A tribo-corrosion phenomenon occurs, when simultaneous environmental caused corrosion and sliding caused wear leads to a transformation of a material at a contact surface. A formation of a rust or a segregating oxide layer often leads to a devastating impact on the performance of the metal-based tool products. Therefore, a physical vapour deposition (PVD) of a thin, penetration reducing, and a hard coating is a way of the protection of a steel-based equipment with a minor influence on the final dimensions of a coated product.

An application of such coated parts often requires a relatively basic knowledge about the lifetime of a selected combination of a steel substrate and a PVD coating. Such situations are common in a case of well-developed technologies with an avoided or reduced number of unfavourable wear or corrosion causing factors, like a low speed electrical sliding contact with a mild tribo-corrosive wear mode.

However, products from automotive, aerospace, cutting or drilling tool production industries more commonly meet an unexpectable combination of corrosion modes causing events, due to the operation under drastically changing environmental conditions and uneven applied working parameters.

A deep scratch in the coating of a steel car body is an example of a commonplace event. A passive type coating cannot resist corrosion when a substrate is uncovered, while an anodic coating, like Zn, not only protects more cathodic Fe based steel substrate, but also can sufficiently heal the scratch by covering affected place with Zn corrosion products. This, well known protection method, is a good example of the reliability of a coating in service, which caused an innovative idea of the new experimental method for reliability estimation of the tested AlCrN PVD coating demonstrated in the present thesis.

Today’s trends and demands require a coating to play the role of “prime reliance”. Therefore, a predictable life of operation is a part of the reliability of the coating. Intrinsic variabilities of the coated material and operational environment affect “prime reliance” (Dwivedi et al., 2010).

Static and sliding affected (tribo-corrosive) tests in the aqueous corrosive environment allows in-situ estimation of a PVD coating reliability with electrochemical methods (Ricker et al., 2008).

An incorporation of aluminium into the first generation Ti-based PVD coatings leads to improved oxidation resistance of a coating at elevated temperatures up to 600 °C (Chim et al., 2009). Even better performance can be reached when a presence of Ti is completely avoided. An improvement in the wear resistance of PVD coatings has been found effective by the application of a gradient or multilayer architecture (Antonov et al., 2009; Liew et al., 2013).

Therefore, the motivation was to estimate the reliability of three different types of as received PVD coatings (gradient TiCN and TiAlN, and multilayered AlCrN) under aqueous solution; to find the most durable coating for high temperature sliding applications; and to estimate the main reliability influencing factors under corrosive and tribo-corrosive environmental conditions.

Scientific novelty

Several laboratory scale testing methods were developed and applied to assess and to determine the reliable environmental conditions and sliding parameters for PVD coated stainless steel in a tribopair with a ceramic counter-body. Researchers often report standardized test methods for estimation of repeatability and reproducibility of created PVD coatings under the well-known predefined conditions in laboratory scaled experiments. However, only the very limited number of research papers contain production methods and test results concerning the reliability of different coatings and applied working conditions. It is also not easy to find publications about the testing of the preliminarily affected coatings as the general objective mostly is to “sell” results promoting superior properties of a material obtained from selected specimens with the highest quality. This fact is very surprising when knowing that reliability engineering itself takes the important role in the industrial field. It is understandable that huge databases about tested properties of coatings characterizing their reliability are collected at industrial level as commercial secrets, therefore, not published in open access databases.

The reliability factors of the PVD coatings in sliding tribopair with a ceramic counter-body under 3.5 wt% NaCl aqueous solution and under high temperatures are illustrated with schemes, results of Raman spectroscopy analysis and SEM images in Paper I, Paper II and Paper III. A combination and confirmation from previous scientific reports about the correlation between hydrolyzation or oxidation of the reactive compounds and subsequent passivation of the corrosive compound penetration and solid lubrication effect in the sliding contact zone at the same time is provided in the present PhD thesis. Sliding tests with a ball type counter-body against preliminarily scratched PVD coated stainless steel combines two different testing standards for the first time and is a novel method for determination of the reliability (sensitivity to effects of defects) of coatings with predefined defects, fulfilling the scope of the present PhD thesis.

Abbreviations

AISI	American Iron and Steel Institute
CE	Counter electrode
CoF	Coefficient of friction
DLC	Diamond-like carbon
EDS	Energy-dispersive X-ray spectroscopy
GPES	General Purpose Electrochemical System
ISO	International Organization for Standardization
MML	Mechanically mixed layer
OCP	Open circuit potential
PID	Proportional–integral–derivative
PVD	Physical vapour deposition (-ed)
RE	Reference electrode
R&D	Research and development
sccm	Standard cubic centimetres per minute
SEM	Scanning electron microscope
SS	Stainless steel
Ta-C	Amorphous tetrahedral carbon
TalTech	Tallinn University of Technology
TR	Calculated rise of bulk/flash temperature
UMT	Universal Materials Tester
WE	Working electrode
XRD	X-ray diffraction

Symbols

i_{corr}	Corrosion current density (μA·cm^{-2})
K_1	$3.27 \cdot 10^{-3}$ mm·year^{-1} (constant value)
ρ	Alloy density, g·cm^{-2}
EW_{alloy}	The alloy equivalent weight (dimensionless)
R_{pm}, R_p	Polarization resistance (V·cm^{-2})
$E_{corr\ calc}$	Calculated corrosion potential (V)
$\lvert\beta_a\rvert$	Anodic Tafel slope (V·decade^{-1})
$\lvert\beta_c\rvert$	Cathodic Tafel slope (V·decade^{-1})
CR	Corrosion rate or penetration rate (mm·year^{-1})
P_i	Protective efficiency (%)
P_{open}	Open porosity (%)
F	Normal load (N or kgf)
E1, E2, E3… E18	Tribological sliding events observed on the preliminarily scratched coating (E is used in the text only).

1 THEORETICAL BACKGROUND

Tribology is the field of science and engineering of interacting surfaces of bodies in relative motion (Wood, 2007). It includes the study and application of the principles of friction, lubrication, wear and any other types of surface deterioration (Jost, 1966).

As a branch of mechanical engineering, tribology may get interdisciplinary, when a lot of other fields of engineering meet in any new technological solution by setting many specific durability requirements for an invention. As every aspect of tribology impacts product reliability, the lifetime of automotive and aerospace parts, production systems and machines must be predicted more accurately (Holmberg, 2001). Therefore, reliability engineering deals with the role of the tribology in the large and complex scope. Sustainable development and increasing demand for green technologies (Tzanakis et al., 2012) require an improved component lifetime, reliability of the design, selection of materials (Ashby, 2011), diagnostics, aesthetics estimation and monitoring of conditions. These are just a few examples of reliability engineering aspects indicated that makes application of tribology more complicated nowadays, as shown in Figure 1.

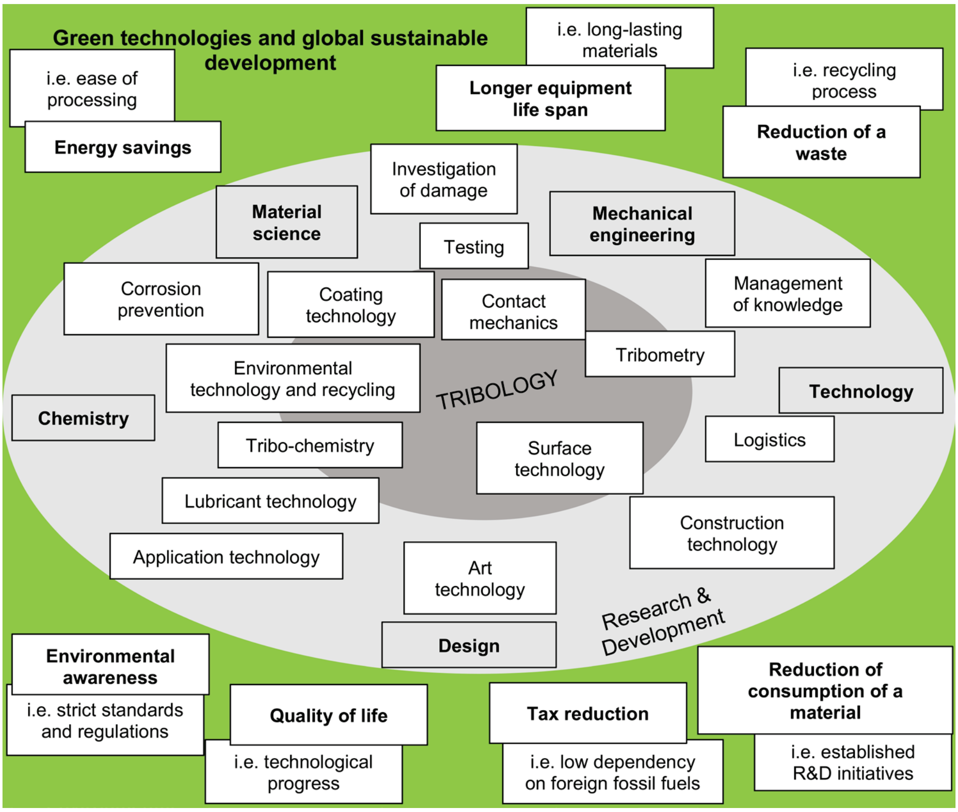

Figure 1. Tribology interaction towards global sustainable development and global green market technologies, adopted and combined from Ref. (Nirmal et al., 2015) *and OPS A La Carte, LLC presentation* (Silverman, 2012) *with author's update.*

Different geometrical scales from nano- up to tera-tribology can be used for experimental methods and for an expression of observed effects. Researchers are accustomed to apply more linear approaches in nano- and micro-tribology level due to the strict reductionism (Holmberg, 2001). It is often required a task to scale up this knowledge to more non-linear approaches when applying a selected tribo-system in real operational conditions. It causes the demand for application reliability.

1.1 General reliability aspects of PVD coatings in tribological applications

Reliability of surfaces in contact:

- Reliability of mechanical elements in contact is related with wear characteristics or other tribological phenomenon's;
- Each wear regime leads to different failure modes;
- Reliability engineering establishes an advanced application of mechanical or electrical components, like roller bearings, electromagnetic relays, etc.

Key aspects of tribology:

- Friction and wear, solid lubrication and corrosion resistance;
- Surface properties, characterization and contact mechanics;
- A type of tribological systems, like seals, gears, bearings, artificial joints, and lubricants;
- Design and manufacturing technology of parts affected by tribological wear;
- Aesthetic property preservation in service (maintenance of design features).

1.1.1 History of reliability of coatings in tribological applications

An ancient history of a material lifetime closely associates with an art. There is an evidence of artistic activity dating as far back as about 500 000 years ago performed by Homo erectus (Joordens et al., 2015). A zig-zag line was found etched by a shark tooth into a shell of a fossilised freshwater clam in Trinil, Indonesia, in the 1890's by Dutch geologist *Eugene Dubois*. It is by far the oldest engraving ever found. However, as a first coating, 40 800 years old prehistoric dots and crimson hand stencils on Spanish cave walls are now the world's oldest known cave art, probably performed by Neanderthals. These two prehistorical artefacts demonstrate an impressive reliability of objects selected and used by the human being, carrying information through thousands of years. The reliability which was not expected.

The evolutionary process facilitated to understand that the purpose of applying the coating may be a decorative, functional, or both. Science and an industrial development caused a wide variety of available coatings nowadays with a set of specific technical parameters not always included in data sheets. Nevertheless, the prediction of a lifetime and a failure-free coating product is still a challenge for reliability determination.

The word 'reliability' can be traced back to 1816 and any test was considered "reliable" if the same satisfactory results would be obtained repeatedly. However, only in the 1940's the modern use of the word 'reliability' was defined by United States (U.S.) military, characterizing a product that would operate when expected and for a specified period. Further activities on statistical control in systems engineering led to new sub-discipline named 'reliability engineering' applied in many fields of engineering (e.g., tribology, materials science, chemical engineering, etc.) (IEEE, 1990). A new development method and general approaches for reliability estimation were created almost every decade and findings were based on a great variety of different techniques and expert knowledge in several fields. Great efforts led to more standardized, faster and more effective computer-assisted hybrid physics-statistics and theoretical reliability simulations instead, or in addition to recent testing method (Tan et al., 2017).

1.1.2 Repeatability, reproducibility and reliability

Specific issues with respect to a process and reliability of a PVD coating should be clarified with appropriate nuances and terminologies. Variabilities can be found in the performance of any PVD coating as a result from different temporal and time-dependent variations caused by any failure in production-related processes internally (mechanical component, electronics, software and even human-caused errors, etc.) and externally (environment, feedstock, etc.). International Organization for Standardization (ISO) defines failure as "termination of the ability of an item to perform a required function" (ISO, 2012). In research level, variations usually cause variables within a single PVD booth (cathode, chamber, electrical supply, etc.). However, spatial variations arising from multiple PVD booths within various locations in the same address and around the world can be found more frequently at an industrial level.

Repeatability, reproducibility, and reliability usually have different approaches customised for exact goals as demonstrated in Table 1. Unlike repeatability and reproducibility, a reliability is a system level definition encompassing all the aspects of the process and coating highlighted during monitoring to meet the required performance goals (Dwivedi, 2010).

Table 1. List of typical approaches to achieve repeatability, reproducibility and reliability (Dwivedi, 2010; Friedrich et al., 1999; Holmberg, 2001).

	Repeatability	**Reproducibility**	**Reliability**
Level	Usually R&D	Usually R&D	Mainly industrial
Nº of persons involved	Usually one	Two or more	Usually group of persons
Nº and type of measured attributes	Usually one and the same	Usually one and the same	From systematic selection during monitoring
Number of measurements	One or multiple	Multiple	According to monitoring results
Measuring equipment and technique	Usually the same and standardized	Usually the same and standardized	May be customized
Possible enhancements	By setting a standard procedure for the measurements	By setting a standard procedure for the measurements	By setting specified environmental and other test conditions
Booth	Usually single	Usually multiple	Usually multiple.
Aspects	Usually one or more the most important ones	Usually one or more the most important ones	All highlighted to requisite performance goals
Goal	Successful steps for achieving outcome	Outcome	Reliability (performance) of product

1.1.3 Reliability of substrate

It is well known that PVD coatings on machine components are quite rare as compared to tools.

A properly prepared substrate can provide an outstanding performance of PVD hard coatings (Sheikh-Ahmad et al., 2001). Such substrate must provide a metallurgical bonding for a coating. Researchers in their papers indicate an importance of proper substrate selection and preparation process in detail, however, a role of set parameters (e.g., adhesion and bonding strength, final roughness, residual stress distribution, etc.) is often neglected. For example, in a case of sliding wear applications, a too high surface roughness of a substrate can cause a shear off a coating and subsequently can expose a substrate material to a tribo-corrosive environment. However, in some applications, a mirror finish can also be unfavourable and may cause high adhesion and bonding between sliding parts. Therefore, a micro-rough finish is usually preferable. Out of that, coaters, producers of PVD units and researchers usually propose, but not limit several main requirements for reliability estimation of a substrate, as demonstrated in Table 2.

Table 2. Examples of aspects and solutions for substrate to improve the reliability (Dwivedi, 2010; Friedrich, 1999; Holmberg, 2001; Sheikh-Ahmad, 2001).

Aspect	Requirement	Possible enhancements
Aspect 1. Substrate durability	Entire component must be compatible with high vacuum conditions. Materials that outgas in vacuum conditions (e.g. high vapour pressure metals, porous materials) should be avoided.	Component can be partially masked with various methods
Aspect 2. Composition of component	Entire component must be compatible with coating process temperatures	The coating process temperature can be adjusted according to specific properties of substrate
Aspect 3. Design of component (substrate)	A component must be designed to achieve required coverage with PVD coating	An effective communication between coater and user must be provided to create a proper holder for component in PVD chamber
	A component must be designed precise enough to achieve the benefit of thin coating in selected applications	Operator must follow the requirement and recommendations for coated component
Aspect 4. Preliminarily preparation of the substrate	Oxides or other impurities affecting adhesion	Operator must follow recommendations for preparation of component
	Imperfections (e.g. slivers and overlapped material caused by aggressive grinding) on functional areas should be removed (Ipaz et al., 2012)	Operator must accurately estimate and provide a quality of the substrate
	A component must be free of surface contaminants like grease, paint, etc.	Operator must follow recommendations for cleaning
A combination of aspect 3 and aspect 4	The roughness of the component surface must not be much greater than the coating thickness	Operator must follow recommendations for surface grinding and polishing

1.1.4 Reliability of PVD process

Researchers often receive coated components with different dimensions and geometry for testing. These parameters of any specimen usually depend on the type of the PVD unit and a potential application of coated material. It is obvious that in most cases researchers test idealized small samples from one laboratory scale deposition unit to achieve the specific goal. However, such an approach not always provides a total reliability achievement of PVD process for industrial level needs. In some cases, researchers affect a PVD process according to possible aspects as demonstrated in Table 3. One of the most important aspects is the hidden process instability during the coating process (Friedrich, 1999). Such an approach often helps to initiate an appearance of local specific change or defect in coating properties. Real components in the mechanical engineering often has dimensions much larger than 100 mm and complicated shapes. Therefore, it often causes a difficulty to provide a complete estimation of local coating defects on simplified shape small specimens (Friedrich, 1999).

Table 3. Examples of aspects and solutions for reliability of PVD coating process (Friedrich, 1999).

Aspect 1 Coating unit and procedure design	**Aspect 2 Component geometry and dimensions**	**Aspect 3 Hidden process instability**
Instable or improper gas supply near the target rim affects composition of coating. Excluded or too low rotation speed of substrate causes varying distance from the electrode surface to the target.	Substrate with the complicated (e.g. rounded) geometry causes a varying angle between the electrode surface and the target	Disturbed transmission from power supply to rotating substrate. Low control speed of bias voltage. Lags in a computer software. Contaminant particles (dust) in the working chamber.
Solution: the sample must be monitored at more than one position by characterizing the deposition unit	Solution: an effective communication between coater and producer of component must be provided to ensure the required thickness and quality of the coating at the most significant areas of coated parts	Solution: coater must check and must exclude such hidden effects in the deposition unit

1.1.5 Reliability of substrate-PVD coating characterization

The first aspect, a characterization of the properties of a PVD coating is closely tied to the characterization of the selected substrate and deposition process. Therefore, a lot of effort has been made worldwide to provide standardized methods. However, often only the test cycle is standardized due to the difficulty to set specific requirements for test parameters, evaluation, deviations and comprehensive information flow (Friedrich, 1999). These requirements then must be selected by the operator of the test unit.

The second aspect, a result of PVD coating characterization test can often demonstrate the significant difference between different measurements. These differences can be found in different locations on the same sample or on different samples obtained from the same coating unit or obtained from different coating units set for the same target coating. As an example, in addition to inhomogeneity, roughness and mechanical oscillations of a coating and a substrate, a crystallographic coating structure can also cause such deviation in local hardness distribution of the coated sample. These irregularities must be assessed in a scale of numerical quality.

The third aspect, selected test parameters influence the test result. The operator of the test unit should follow rules of selected standards. However, in many cases, they are not defined, or application of existing standardized rules leads to a failure of the test or collected data gives insufficient information about limits of the coating under potential work conditions.

Therefore, a PVD coating characterization is one of the most important parts in the total reliability estimation scheme which helps to determine important deviations and irregularities in the properties of a tested coating. All relevant test parameters for characterization must always be documented.

1.1.6 Reliability improvement of a stainless steel in sliding contacts

Highly corrosion resistant austenitic stainless steels (SS) generally exhibit reduced resistance to tribological sliding contacts due to their strong adhesion and transfer tendency to the surface of the counter-body (Saketi et al., 2017; L. Wang et al., 2008). A face-centred cubic crystalline structure dominates in such SS. As SS AISI 316L was used as a substrate in the present PhD thesis, it should be noted that austenitic structure of 300 series SS is achieved primarily by a nickel addition. Above mentioned crystalline structure limits a hardenability of SS by heat treatment (Laroudie et al., 1994). Therefore, a hard PVD coating can improve the environmental friendliness and longer service life of 300 grade SS in sliding contacts (Dinu et al., 2018). It is well known that the high ratio of hardness and Young's modulus may cause adhesion problems in sliding contacts due to the "egg-shell" cracking effect (Beake et al., 2014). Therefore, austenitic SS with a low hardness (≈200 HV) limit an application of PVD coatings due to the deformation under high loads and due to the possible critical softening of SS substrate at temperatures above 500 °C (Saeidi et al., 2017).

Sufficiently high Young's modulus at higher temperatures can be provided by the high-temperature oxidation resistant SS, like 253 MA (155 and 120 $kN \cdot mm^{-2}$ at 600 and 1000 °C, respectively). Such substrate can be successfully applied as the support for harder PVD coatings in tribological applications at temperatures up to 800 °C (Roy et al., 2004).

1.2 Corrosive and tribo-corrosive data for reliability estimation

A degradation of materials through high-temperature or chemical processes, such as oxidation (Mo et al., 2009), corrosion, abrasive and erosive wear cause enormous costs for the European industry. Mechanically induced interactions with electrochemical or chemical processes are involved in tribo-corrosion (Wood, 2017). It is crucial to avoid a failure of machines and components, which can entail catastrophic accidents. Most of the high temperature and/or corrosive resistant parts of a wide variety of devices for many different applications are protected by specially designed coatings (Fenker et al., 2014). Today's trends and demands require a coating to play the role of "prime reliance" (the dependence on something in the best possible quality or trust in something excellent), especially in an engine performance. Therefore, a predictable life of the operation must be provided additionally to the service performance of a coating. Intrinsic variabilities of a coated material and an operational environment affect "prime reliance" (Dwivedi, 2010).

A determination and estimation of the sensitivity of PVD coating to effects of defects toward defect-initiated damage (reliability) with the help of a novel combined method is a key contribution described in the present PhD thesis.

1.2.1 Assessment of reliability with the help of electrochemical methods

The trial-and-error method was the only technique available for material selection and estimation when people started creating the first tools. Today, in addition to this approach, a corrosion testing provides the possibility to compare the relative corrosion resistance of materials with a small number of experiments. Regardless of a relatively short duration of such tests, this comparison is often valid only for similar conditions in real field application. Therefore, these experiments are frequently considered as insufficient-indicators of the actual in-service behaviour of the component and it is necessary to adapt an experimental setup. As in the most of engineering fields, also corrosion engineers meet developers and component designers as main customers. However, in the commercial world, designers create a much higher demand for technological solutions to reduce production, warranty, and liability costs with improved corrosion performance at the same time.

Reliable lifetime prediction for a component used in a corrosive environment requires the identification of corrosion failure modes. Such failure modes can be pitting (if halide ions present), stress-corrosion caused cracking by hydrogen embrittlement and corrosion fatigue (Ricker, 2008). Every failure mode requires an estimation of the expected time-to-failure with evaluated uncertainty in this prediction (Ricker, 1995).

1.2.2 Assessment of reliability at elevated temperatures

The consideration of the behaviour of a PVD coating under static oxidative conditions should be done before testing under high temperature tribo-corrosive conditions. It is clear, that oxidation of metals and other oxide free compounds intensifies at elevated temperatures (Kawate et al., 2003). Most alloys rely on the protective effect of formed oxide scales (Schütze, 1995). Therefore, a presence of oxides between bodies in sliding contact takes place inevitably (Tomala et al., 2013).

A set of most important parameters as aspects have been selected for reliability estimation:

- Type of oxides - based on one (Fe, Cr, Al etc.) or a combination of metal atoms (e.g. Fe, Cr – spinel);
- Mechanical properties of oxides (e.g. hardness, thermal conductivity, fracture toughness, etc.);
- The durability of an oxide layer under thermal and mechanical loading;
- An extent and characteristics of defects in oxide scales;
- "Self-healing" ability – oxide scales recoverability to a sufficiently stable condition after mechanical impact;
- Growing rate of oxide scales.

1.2.3 Methods for tribo-corrosive data collection and estimation

The coexistence of wear and corrosion impacts on economics of engineering systems both directly and indirectly. Loss of material may cause associated equipment downtime for repair and replacement of worn and corroded components (Jiang et al., 2002). Specific wear rate can be assumed as a suitable parameter applied during designing of coated part. Chemo-mechanical mechanisms of tribo-corrosion include a great number of parameters (Fischer et al., 2006; Stack et al., 2006). However, significant differences in test results could be induced from the analysis of the values derived from this parameter due to the following aspects (Ramalho, 2010):

- The level of test procedures and the accuracy of the measurement techniques significantly influences the reliability of the experimentally achieved value;
- The quality of the test equipment and precision of any part of test setup plays an even more important role.

1.3 General concept for improving reliability of PVD coating in tribo-corrosive conditions

The high hardness of PVD coatings provides a resistance of cutting or other tools and parts to a wear characterized by compressive stresses which provide durability of edge, when toughness, sharp edge and a good adhesion to a substrate is required simultaneously (Fernández-Abia et al., 2013). It is well known that durability of PVD coating can be significantly affected by the presence of defects. During last decade a presence of such PVD process caused defects in a coating, like cone-like inclusions, dish-like craters, spherical pin-holes etc. are noticeably reduced both in density on the surface and sizes. It leads to the reduced effect of defects from the coating process on the homogeneity of wear and equality in the evolution of friction parameters. In such situation a wear and mechanical impacts caused reliability issues to get more importance in the durability of a coating in tribo-corrosive conditions. Wear, plastic deformation of the ductile substrate, chipping, and cracking are most common coating failure mechanisms in real operational conditions of tools caused by natural wear, overloading, local mechanical impacts, and other undesirable events. For example, it is well known that detachment can occur when counter-body slides over the area of cracked coating (Bull et al., 2002).

Often these events cause relatively small sized defects on coating as compared with the size of the tool, therefore, operator commonly decides to continue operation with the defected tool until significantly unacceptable failure occurs. In many cases, the user of a device cannot detect a damage of tool himself like in a case of hidden parts in the car engine or air compressor, for example. Thereby, a mechanically defected PVD coating may prove to be much less durable as prediction according to common and usually standardized experimental data.

One of the main tasks of reliability engineering is to predict the lifetime reliability of defected tool when it continuously operates under intended conditions. Therefore, it becomes important to understand the mechanism of defect development and to estimate the failure risks of the tool in given tribo-corrosive conditions. Unfortunately, an application of new approaches in testing without following some standardized methods usually leads to a high cost and unclear description of the applied test method for other researchers.

Accordingly, the author of the present PhD thesis offers a combination of two standardized methods with commercially available equipment for estimation of wear evolution of preliminarily scratched coating as explained and demonstrated below.

1.4 Objectives of the study

The main objective of this study is the development of the procedure(s) for estimation of reliability of applied gradient TiCN, gradient TiAlN and multilayered AlCrN PVD coatings covered steels under sliding wear and corrosive conditions. This objective can be broken down into the following sub-tasks:

1. To assess the suitability of potentiodynamic polarization and tribo-corrosive sliding tests in 3.5 wt% NaCl aqueous solution for determination of defects and estimation of defect evolution of gradient TiCN and TiAlN, and multilayered AlCrN PVD coatings;
2. To explain the reliability factors and reasons of the failure of the selected PVD coating under sliding wear and corrosion in 3.5 wt% NaCl aqueous solution;
3. To provide in-deep understanding in the reliability of the selected (SS) substrate for applications under static elevated temperature conditions supported with microstructural analysis;
4. To provide in-deep understanding in the reliability of the selected PVD coating for applications under static elevated temperature conditions supported with microstructural analysis;
5. To provide in-deep understanding in the reliability of the selected PVD coating for elevated temperature tribo-corrosive applications supported with microstructural analysis;
6. To develop the novel test methodology for the assessment of the reliability (sensitivity to effects of defects) of selected PVD coating under tribological and tribo-corrosive conditions with the intentionally caused preliminarily mechanical influence (deformation or damage).

2 MATERIALS AND METHODS

The limits of equipment like maximum service temperature, sliding speed, corrosion resistance, etc., are, probably, the most important information for designers of new PVD coated steel parts. Therefore, a tribological problem rise when design part is not able to adequately perform during required (predicted) lifetime.

In given experimental model tests both tribo-surfaces are replaced by simulated components in a simplified tribo-couple test mode (Antonov et al., 2009) as ceramic counter-bodies were tested against coated SS specimens. All tests were repeated at least three times. The selected laboratory scale experimental methods and materials approach are proposed for improvement of reliability of AlCrN PVD coating on steel materials for use in aggressive environments, where insufficient technological durability causes a failure of coated steel product on the field.

Applicability of various equipment for various steps of laboratory evaluation of the reliability of coatings intended for elevated temperature or corrosive tribo-applications available at Tallinn University of Technology (TalTech) is demonstrated in Table 4.

2.1 Preparation of samples

The cuboid-shaped samples of molybdenum-containing hot rolled austenitic SS AISI 316L (UNS S31603, dimensions: 25×15×5 mm and chemical composition as shown in the Paper III) and micro-alloyed high temperature oxidation resistant cold rolled SS 253 MA (EN 1.4835, 60 mm in diameter and about 5 mm in thickness, Paper II) supplied by *Outokumpu* were used in the present thesis. Selected Fe based SS 253 MA typically contains C (0.09 wt%). Mn (≤1 wt%), Cr (21 wt%), Ni (11 wt%) and N (0.17 wt%), Si (1.6 wt%) and Ce (0.05 wt%) according to properties provided by the producer. Arithmetical mean roughness $R_a \leq 0.02$ µm was reached using a *Phoenix 4000* (*Buehler*, USA) polishing system by applying SiC papers (*Buehler*, USA) down to grade P4000 (*MicroCut S*, *Buehler*, USA). Substrates were cleaned with isopropanol for 50 min by using the ultrasonic bath. The samples were placed in the coating chamber and sputter-cleaned in argon plasma with the bias voltage of 850 V at 425 °C for 1 h. Gradient layer TiCN and TiAlN and multilayer AlCrN PVD coatings with a target thickness of 3.3 µm were deposited onto substrates in the nitrogen atmosphere using a lateral rotating cathode arc (LARC) technology (*Platit π-80* unit, Switzerland) according to methods demonstrated in Table 5 and Figure 2, respectively.

Class 1 (cracking without adhesive delamination of the coating) adhesion of coating was reached according to VDI 3198 with Rockwell "C" indentation test (VDI - The Association of German Engineers, 2013). Main properties of the multilayer AlCrN coating are demonstrated in Paper II and III.

2.2 Characterization methods of substrate-coating systems and selected counter-bodies

The surface morphology was tested with the scanning electron microscope (SEM) *Hitachi TM1000* equipped with energy-dispersive X-ray spectroscopy (EDS). Kalotest method was used to measure a thickness of a coating with the *kaloMAX* tester in accordance with the method developed by *BAQ* (Germany).

Table 4. Applicability of various equipment for various steps of laboratory evaluation of reliability of coatings intended for elevated temperature or corrosive tribo-applications (available at TalTech, data is taken from Paper III).

	Visual and tactile observation	**Optical microscopy**	**SEM imaging**	**2D contact profilometry**	**3D topography**	***KaloMax* ball cratering**	**Adhesion testing**	**Scratch testing**	**Electrochemical corrosion testing**	**Tribo-corrosive testing***	**EDS**	**Raman spectroscopy**	**X-ray diffraction (XRD)**
Preliminarily evaluation	+	+	+	++	+++	+++	+++	+++	+	NCH	++	++	+++
Wear or corrosion rate	-	+	+	+++	+++	NCH	NCH	NCH	++	+++	-	-	-
Destruction mechanisms	+	+	++	++	+++	NCH	NCH	+	+	++	+	+++	++
Elemental or phase composition of thin tribolayer	-	-	- SE	NCH	NCH	NCH	NCH	-	0	0	-	+++	-
Elemental or phase composition of thick (≈ >1 um) tribolayer	-	0	+ BSE	NCH	NCH	NCH	NCH	-	0	0	++	+++	++
In-Situ measurement of corrosion intensity and/or evolution of coating damage	0	0	NCH	NCH	NCH	NCH	NCH	NCH	+++	+++	-	-	+

Notes: “+” is showing how useful could be the equipment (+ min, ++ average, +++ max)

“-“ means that equipment is rather not useful

“0” - only qualitative estimation or indirect conclusion

NCH – not considered here

SE and BSE - Secondary electron and Backscattered electrons of SEM

*Assisted with potentiostat/galvanostat

Table 5. PVD parameters for gradient TiCN and TiAlN coatings, demonstrated in Paper I.

Type of coating	Bias voltage, V	Pressure, mbar	Cathode arc current, A	Temp., °C	Gas flow rate, sccm		
					Ar	**N_2**	**C_2H_2**
TiCN	(–60) - (–120)	$6 \cdot 10^{-3}$	120 - 130 (Ti only)	450	6	165	7 - 39
TiAlN	(–60) - (–150)	$4 \cdot 10^{-3}$	60 - 125 (Ti and Al)	450	6	150 - 200	-

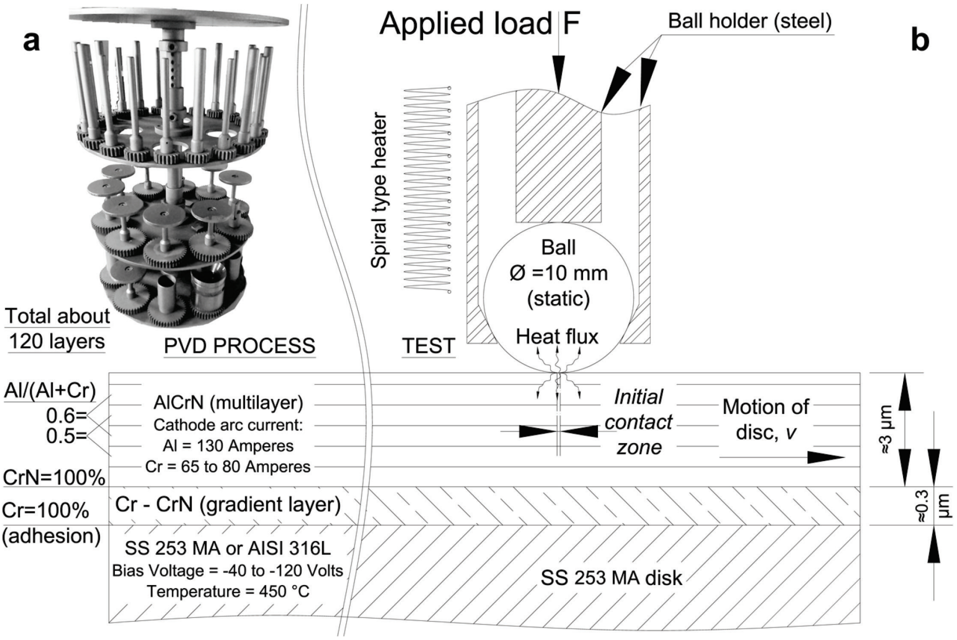

Figure 2. Specimens installed in the carousel type holder (a); and PVD parameters for production of the multilayer AlCrN coating on AISI 316L and 253 MA substrates with schematic illustration of tribological unidirectional sliding tests at room and elevated temperatures under oxidative conditions (b) demonstrated in Paper II and Paper III.

2.3 Potentiodynamic polarization tests

Potentiodynamic polarization measurements were performed in 3.5 wt% NaCl aqueous solution according to method demonstrated in Paper I and Paper III. *Autolab PGSTAT30* galvanostat – potentiostat with *General Purpose Electrochemical System* (*GPES*) software (*Metrohm Autolab B.V.*, Netherlands) was used for data recording. Software *NOVA* (version 2.1.2, *Metrohm Autolab B.V.*, Netherlands) was used for Tafel plot analysis as described in Paper I and Paper III.

According to Faraday's law, the *CR* is calculated from Eq. 1:

$$CR = K_1 \cdot \frac{i_{corr}}{\rho} \cdot EW_{alloy} \qquad \text{Eq. 1}$$

where *CR* – penetration rate (the thickness loss per unit of time), mm·year^{-1}; K_1 = $3.27 \cdot 10^{-3}$ mm·year^{-1} (only consistent valence groupings were used); i_{corr} – corrosion current density, µA·cm^{-2}; ρ – alloy density, g·cm^{-2}; EW_{alloy} – the alloy equivalent weight (dimensionless in this calculation) (ASTM, 2015).

The protective efficiency P_i (%) of the coating is calculated using Eq. 2 (ASTM, 1997):

$$P_i = \left[1 - \frac{i_{corr}}{i_{corr}^0}\right] \times 100 \qquad \text{Eq. 2}$$

where i_{corr} and i_{corr}^0 indicate the corrosion current densities of a coating and a substrate respectively.

The open porosity P_{open}, % of a coating is calculated according to Eq. 3:

$$P_{open} = \left[\frac{R_{pm}}{R_p} \times 10^{-\left|{}^{\Delta E_{corr}}/_{\beta_a}\right|}\right] \times 100 \qquad \text{Eq. 3}$$

where R_{pm} and R_p are the polarization resistances of the substrate and coating-substrate systems (calculated by GPES according to Eq. 4), respectively, ΔE_{corr} is the corrosion potential difference between the substrate and applied coating, and β_a is the anodic Tafel constant of substrate (Yoo et al., 2008).

$$R_p(R_{pm}) = \left(\frac{\delta \Delta E}{\delta i}\right)_{i=0,\ {}^{dE}/_{dt} \to 0} \qquad \text{Eq. 4}$$

where a small potential scan $\Delta E(t)$, V is defined with respect to the corrosion potential, shown in Eq. 5 (ASTM, 1997):

$$\Delta E = E - E_{corr\ calc} \qquad \text{Eq. 5}$$

2.4 Tribo-corrosive tests at open circuit potential

Tribo-corrosion experiments were carried out using the tribotester *UMT-2* (*Universal Materials Tester)* from *CETR* (*Bruker*) (further in the text - tribotester *CETR UMT-2*) in a reciprocating mode (amplitude $1{\cdot}10^{-3}$ m, frequency 1 Hz) according to methods demonstrated in Paper I and Paper III. Specimens were fixed in the electrochemical cell installed on the reciprocating table (designed at TalTech) as shown in Figure 3.

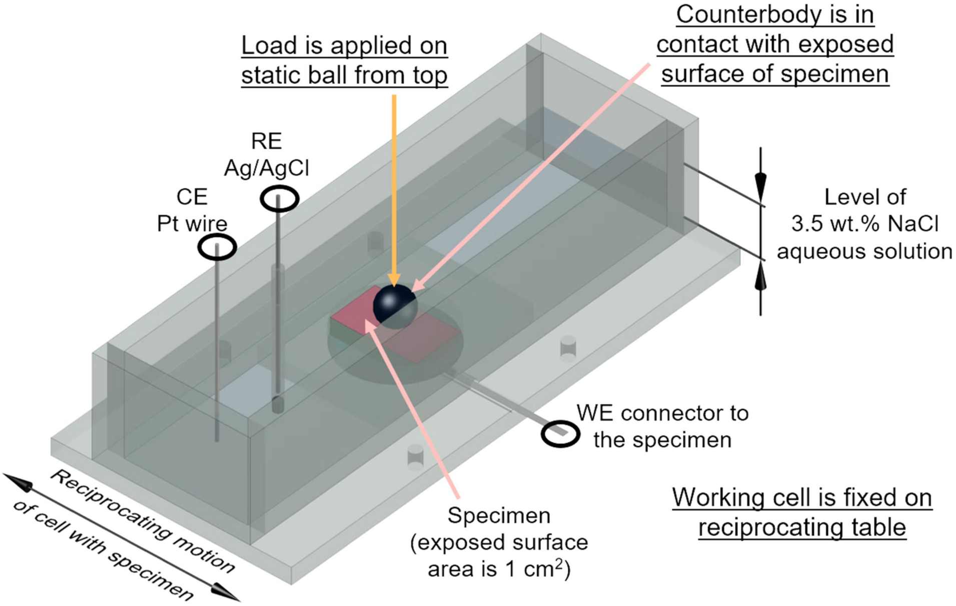

Figure 3. Schematic illustration of reciprocating tribo-corrosion test setup (designed at TalTech, drawing is made according to Paper I and Paper III).

The electrochemical cell was filled with 50 ml of 3.5 wt% NaCl aqueous electrolyte solution. The specimen was connected to the potentiostat as working electrode (WE). Standard Ag/AgCl as reference electrode (RE) and Pt as counter electrode (CE) were used in a three-electrode mode. *EmStat^{3+}* potentiostat and *PSTrace* software (*PalmSens BV*, Netherlands) were used for data recording and processing.

The created system was stabilized for 1 h before starting the test. Recorded test for coated and uncoated materials was divided into three periods: (1) stabilization - 1000 seconds (s); (2) tribo-corrosion – 7200 s in a case of 9.8 N (1 kgf) normal load only; and passivation - 1000 s. A 12 h tribo-corrosion test was additionally done under 9.8 (1 kgf) and 29.42 N (3 kgf) loads with the multilayer AlCrN coated material by increasing a duration of the second period up to 43 200 s and increasing of initial maximum contact pressure from 1.31 up to 1.88 GPa, respectively.

2.5 High temperature static oxidation tests

Coated and bare SS 253 MA substrates and all selected types of ceramic counter-bodies were examined for their high temperature static oxidation behaviour. The oven *Nabertherm L9/B* equipped with the proportional-integral-derivative (PID) P330 controller was employed for static oxidation at 300, 500, 800 °C for 5 h. Bare and coated steels were additionally tested at 900, 1000 and 1100 °C. Heating and cooling rates were set at 5 $°C \cdot min^{-1}$. A duration of static oxidation at selected test temperature was 5 h.

2.6 Dry sliding tests at room and elevated temperatures under oxidative conditions

Tests were performed in an ambient (oxidative) atmospheric conditions using the tribotester *CETR UMT-2* equipped with *S21ME1000* drive according to ASTM G99-05 as presented in Paper II. Schematic illustration of setup, conditions, and test parameters are shown in Figure 2, Table 6 and Table 7, respectively. The normal load of 3 N was applied to provide initial maximum contact pressure close to 1 GPa. The counter-body balls of β-Si_3N_4 (β-Si_3N_4 - 92.2, Y-3.5, Al-3.5, and Ti-0.8 wt%; *Redhill Precision*, Czech Republic), α-Al_2O_3 (*Redhill Precision*, Czech Republic) and yttria-stabilized tetragonal zirconia (YSZ, 95 % ZrO_2, 5 % Y_2O_3, *Tosoh/Nikkato*, Japan) were used in this research.

Accordingly, an analytical calculation of bulk and flash temperatures was done for room temperature situations as demonstrated in Paper II. An equations and a theory from the work about temperature maps for frictional heating in dry sliding (Ashby et al., 1991) were used for this purpose. From a theory, a temperature that would appear at surfaces, if a frictional heat injects uniformly (heat flux, see Figure 2 b) across the apparent contact area, is understood as a 'bulk temperature'. This theoretical assumption does not match the practical results as a real contact area is usually much smaller than apparent contact area. It leads to considerably higher 'flash temperature' at real contact areas.

Table 6. Testing conditions applied to materials (data is combined from Paper II).

Material	**Testing temperature, °C**				
	20	**300**	**500**	**800**	**900, 1000 and 1100**
Si_3N_4 (ball)	T	S/T	S/T	S/T	-
Al_2O_3 (ball)	T	S	S	S/T	-
ZrO_2 (ball)	T	S	S	S/T	-
AlCrN PVD (coating)	T (Si_3N_4, Al_2O_3, ZrO_2)	S/T (Si_3N_4)	S/T (Si_3N_4)	S/T (Si_3N_4, Al_2O_3, ZrO_2)	S
SS 253 MA (substrate)	S	S	S	S	S
Notes: S – static oxidation tests (5 h); T –tribological sliding test against indicated counter-body.					

Table 7. Testing parameters applied to materials (data is combined from Paper II).

Track radius, mm	**10**	**12**	**14**	**16**	**18**	**20**	**22**
Sliding Speed, $m \cdot s^{-1}$	0.002	0.006	0.018	0.054	0.162	0.486	1.458
Duration, s	180.0	133.5	99.1	73.5	54.5	40.4	30.0
Distance, m	21.6	48.1	107.0	238.1	529.7	1178.1	2624.4
Number of revolutions	343	637	1217	2369	4684	9375	18986

2.7 Reliability estimation of preliminarily scratched coating

AlCrN PVD coated SS 253 MA discs were tested under ambient (oxidative) atmospheric conditions using the tribotester *CETR UMT-2* equipped with *S21ME1000* drive according to the innovative method for reliability estimation of AlCrN PVD coating. This method in general combines two tribology related standards. Standard ASTM C1624-05 (or analogue standard ISO EN 20502:2005) is commonly applied to estimate the adhesion strength and mechanical failure modes of ceramic coatings by quantitative single point scratch testing with a help of Rockwell "C" conical diamond indenter with an included angle of 120° and a spherical tip radius of 200 µm. Progressive damage test method along the scratch track was applied with a normal force from 0.98 (0.1 kgf) up to 98.07 N (10 kgf) to determine a minimum normal load at which delamination (buckling spallation) of the coating occurs by decohesion, exhibiting a minimum value of 19.61 N (2 kgf), as demonstrated in Figure 4. A severe delamination (wedging spallation) occurs at applied load of 49 N (5 kgf). Therefore, it was decided to preliminarily scratch of coatings by applying 6 different constant normal loads from 1.96 N (0.2 kgf) - under the limit of the normal load at which first mechanical defects (lateral cracks) in the coating were found; up to 16.67 N (1.7 kgf) – slightly below the limit of the normal load at which delamination (buckling spallation) of the coating occurs, as demonstrated in Table 8 and Figure 5 a.

Another test close to standard ISO 18535:2016(E) or ASTM G99-05 was applied to determine the friction and wear characteristics of the preliminarily scratched AlCrN PVD coating by the ball-on-disc method under dry sliding conditions, as shown in Figure 5 b. The standard test conditions for friction and wear tests were applied with the normal load of 4.9 N (0.5 kgf) to Al_2O_3 counter-body (6 mm in diameter). Wear track radius was 14 mm. Sliding speed of 0.1 $m \cdot s^{-1}$ and sliding distance of 1000 m was set to provide about

11 372 revolutions. The same number of revolutions was applied by keeping the same sliding speed, but different constant normal loads of 1.96 N (0.2 kgf), 2.94 N (0.3 kgf), 7.85 N (0.8 kgf), 11.77 N (1.2 kgf), and 16.67 N (1.7 kgf) to other wear track with the radius of 10, 12, 16, 18 and 20 mm, respectively. This purpose was selected as the objective to determine an evolution of defects in areas where counter-body perpendicularly slides over the scratch track. Space between every two scratches was higher for higher loads to avoid migration of defects from one scratch to another.

Table 8. Selected scratching parameter values.

	Alternate load test	**Constant load test**					
Selected loads, N (kgf)	**0.98 – 98.07 (0.1 – 10.0)**	**1.96 (0.2)**	**2.94 (0.3)**	**4.90 (0.5)**	**7.85 (0.8)**	**11.77 (1.2)**	**16.67 (1.7)**
Loading rate (progressive load), N·min^{-1}	10	10	10	10	10	10	10
Horizontal displacement rate, mm·min^{-1}	2	10	10	10	10	10	10
Total scratch length, mm	20	20	20	20	20	20	20
Space from the first scratch on the disc, degree*	-	0	20	60	120	200	300
Notes: *Scratch with a constant load of 1.96 N (0.2 kgf) is regarded as the first scratch on the disk.							

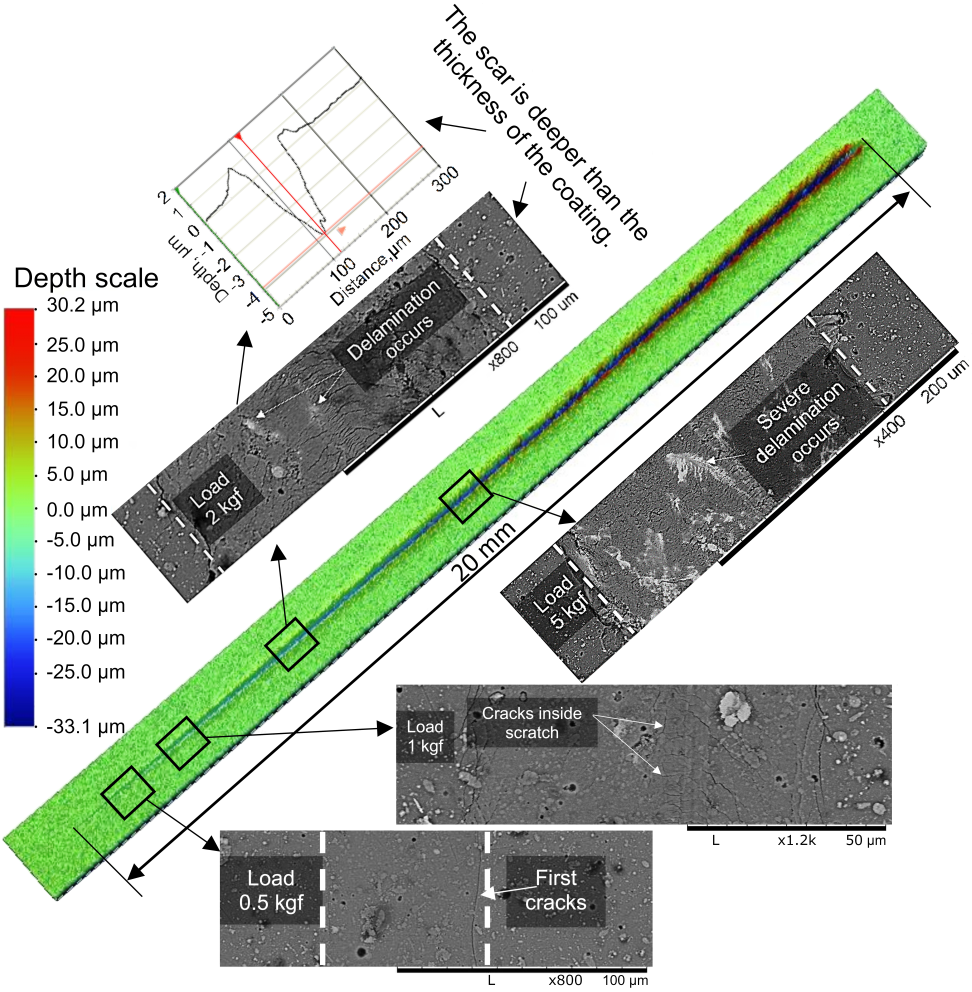

Figure 4. SEM (Hitachi TM1000) and 3D profile analysis (Bruker Contour GT-K0+) of progressive damage along scratch track of AlCrN coating after applying progressive load (from 0.98 up to 98.07 N) during test with Rockwell "C" indenter.

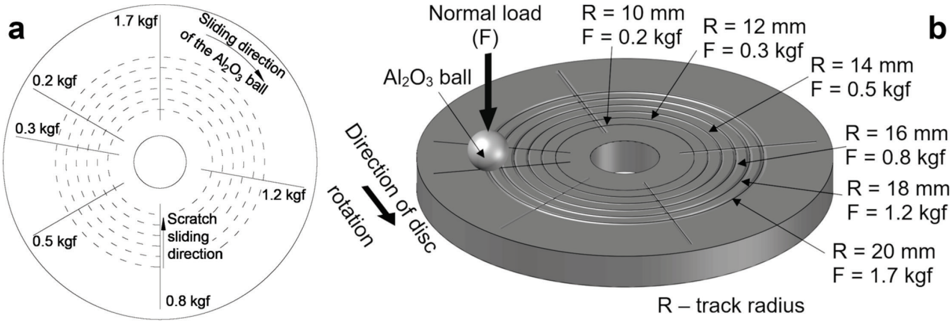

Figure 5. Schematic layouts of scratched disk with Rockwell "C" indenter with indicated tracks (dashed lines) for sliding test (a) and unidirectional sliding tests against Al_2O_3 ball (b) with indicated constant normal loads.

3 RELIABILITY OF TESTED PVD COATINGS UNDERD SLIDING WEAR AND CORROSION CONDITIONS

3.1 Potentiodynamic polarization test of statically corroded uncoated and coated AISI 316L in 3.5 wt% NaCl

Tafel plots and calculated potentiodynamic polarization results of steel substrate and coated specimens are shown in Figure 6 and Table 9, respectively.

It is clearly demonstrated, that the TiAlN PVD coating provides the lowest porosity (about 0.012 %) and highest the protection efficiency (P_i) (about 95 %), as shown in Table 9. The TiCN coating exhibits similar performance to the TiAlN one, confirming the high inertness of a transition metal nitrides and carbonitrides (Ibrahim et al., 2002).

A significant passivation of AlCrN PVD coated sample was found after immersion for 24 h. $E_{corr\ calc}$ significantly shifts toward positive value (-0.153 V vs. SCE) and i_{corr} was found to be 32 times lower (0.05 µA·cm^{-2}) as compared to the same coating after 10 min immersion. A passivation of the AlCrN PVD coating after 24 h immersion also reduces i_{corr} down to 38 and 448 times lower values as compared with the tested substrate SS AISI 316L after 10 min and 24 h immersion, respectively.

Increased duration of the immersion of the AlCrN PVD coated sample leads to decrease in CR down to 4.88·10^{-4} mm·year^{-1} and porosity down to 0.002 %. A significant change in $E_{corr\ calc}$ confirms a hydrolyzation reaction with AlN on the surface and in the pores of the coating. Accordingly, coating reactivity makes calculation results of CR, P_i and P_{open} invalid for estimation of the real coating porosity after immersion for 10 minutes. Corrosion products like amorphous aluminium monohydroxide ($AlOOH_{amorph}$) and crystalline aluminium hydroxide ($Al(OH)_{3crystal}$) form an additional passivation layer (Bowen et al., 1990). Increased protective efficiency up to 99.79 % confirms the inertness of transition metal (e.g. Cr) nitrides (Yang et al., 2013). Selected potentiodynamic polarization test provides the reliable information about the development of the corrosion protectivity of the AlCrN coating.

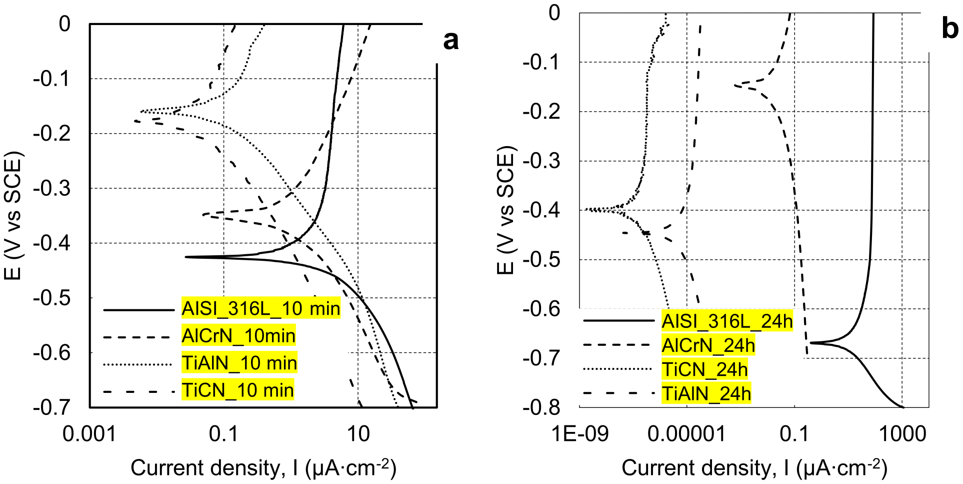

Figure 6. Potentiodynamic polarization curves (Tafel plots) of uncoated and AlCrN PVD coated AISI 316L specimens, (a) – after 10 min immersion, (b) – after 24 h immersion (combined from Paper I, Paper III).

Table 9. Potentiodynamic polarization results of uncoated and TiCN, TiAlN and AlCrN PVD coated AISI 316L specimens tested in 3.5 wt% NaCl aqueous solution after 10 min or 24 h stabilization (combined and updated from Paper I and Paper III).

Material and duration of immersion	**Potentiodynamic polarization measurements (from *NOVA*)**					**Calculation results**		
	i_{corr}, µA·cm^{-2}	**R_{pm}, R_p, Ohm·cm^{-2}**	**$E_{corr\ calc}$, V**	**$\|\beta_a\|$, V·decade^{-1}**	**$\|\beta_c\|$, V·decade^{-1}**	**CR, mm·year^{-1}**	**P_i, %**	**P_{open}, %**
AISI 316L 10 min	1.90	$1.43 \cdot 10^{4}$	-0.423	0.718	0.069	$1.98 \cdot 10^{-2}$	-	-
AlCrN 10 min	1.60	$3.76 \cdot 10^{4}$	-0.340	0.399	0.212	$1.67 \cdot 10^{-2}$	15.92	29.16*
TiCN 10 min	0.19	$1.60 \cdot 10^{5}$	-0.190	0.093	0.303	$8.43 \cdot 10^{-4}$	89.24	0.51
TiAlN 10 min	0.09	$5.27 \cdot 10^{5}$	-0.180	0.159	0.354	$4.94 \cdot 10^{-4}$	94.98	0.01
AISI 316L 24 h	22.14	$1.71 \cdot 10^{3}$	-0.669	0.312	0.121	$2.31 \cdot 10^{-1}$	-	-
AlCrN 24 h	0.05	$2.33 \cdot 10^{6}$	-0.153	0.488	0.517	$4.88 \cdot 10^{-4}$	99.79	0.002
TiCN 24 h	0.15	$1.15 \cdot 10^{5}$	-0.403	0.113	0.254	$1.39 \cdot 10^{-3}$	99.41	0.08
TiAlN 24 h	2.95	$2.24 \cdot 10^{3}$	-0.450	0.105	0.138	$5.11 \cdot 10^{-2}$	80.12	3.79
Note: 10 min, 24 h – after 10 min and 24 h immersion; β_a, β_c – anodic and cathodic slopes in Tafel plot. Deviations E_{corr} not more than ± 0.08 V, i_{corr} – not more than ± 0.10 A. *The result is influenced by the reactivity of the AlN with the water in the AlCrN coating.								

3.2 Tribo-corrosion of uncoated and coated AISI 316L in 3.5 wt% NaCl

Evolution of OCP and coefficient of friction (CoF) before, during and after short tribo-corrosion wear tests of uncoated and coated samples are presented in Figure 7, Paper I and Paper III. No visible passivation was observed after removing the mechanical load. TiCN shows up to three times lower CoF as compared with other specimens in given tribo-corrosion conditions. However, AlCrN PVD deposited onto substrate is the only coating that exhibit no failure, as OCP remains unchanged until the end of the test. Therefore, it was decided to increase test duration up to 12 h, and to compare with a more severe wear regime by applying 29.43 N (3 kgf) load as shown in Figure 8. A surface reactivity and aqueous solution penetration into pores was estimated by 24 h chrono-potentiometry as demonstrated in Figure 9, indicating a passivation of reaction and penetration processes after 45 400 s.

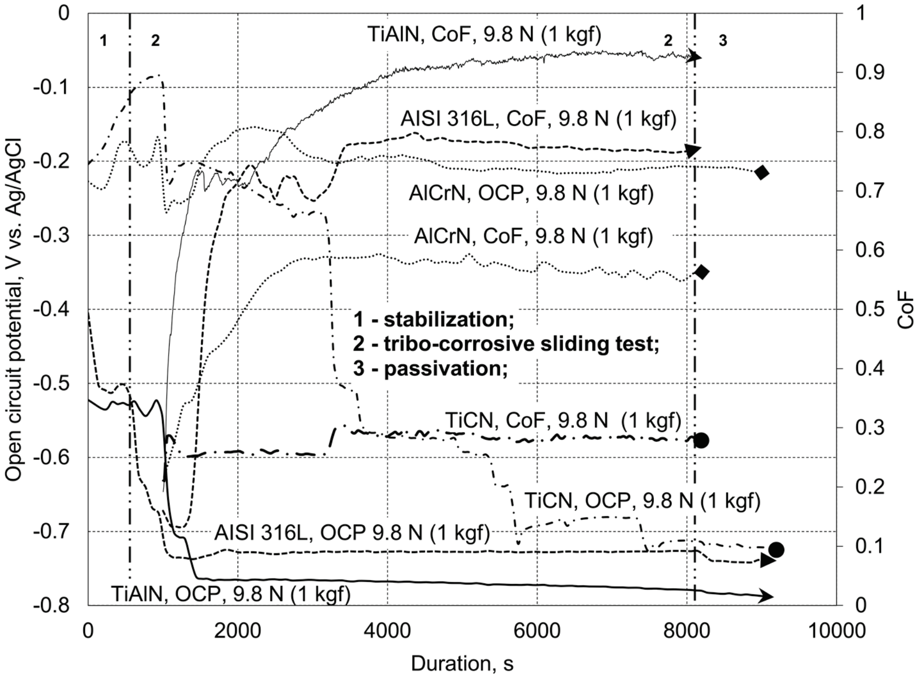

Figure 7. Comparison in evolution of CoF and open circuit potential (vs. Ag/AgCl) of uncoated and coated AISI 316L samples (combined from data in Paper I and Paper III).

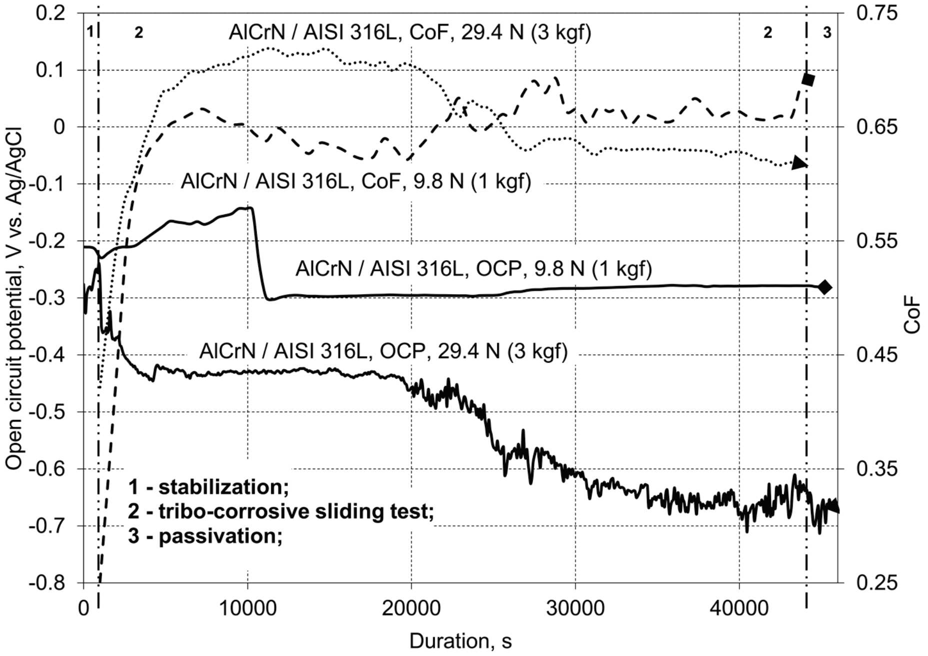

Figure 8. Extended (12 h) tribo-corrosion test of PVD AlCrN coated AISI 316L sample in 3.5 wt% NaCl aqueous solution (combined from data in Paper III).

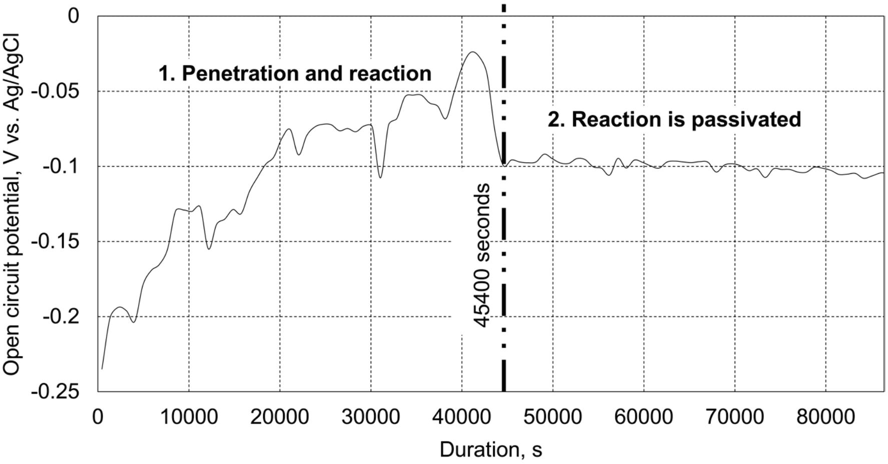

Figure 9. Chrono-potentiometric curve for PVD AlCrN coated AISI 316L sample in 3.5 wt% NaCl aqueous solution (combined from data in Paper III).

A sharp shifting in OCP toward more negative values from about – 0.240 down to – 0.440 V vs. Ag/AgCl was observed in the first 3300 s of the wear test under 29.42 N (3 kgf) load. This value remains stable for about 18 000 s, indicating an inability of corrosion products to create a stable passivation layer under such a load. However, critical failure of the coating was observed after about 18 000 s. OCP was measured to be almost continuously shifting toward negative values from – 0.440 down to about – 0.700 V vs. Ag/AgCl at the end of the test. Simplified schematic illustration of static and dynamic corrosion process is made based on obtained data as shown in Figure 10. Several areas of CrN rich interlayers and microdroplet inclusions uncover during extended tribo-corrosion wear test under 9.8 N (1 kgf) load and several areas of uncovered CrN interlayer, cracks in the coating and even totally removed coating were found after extended tribo-corrosion wear test under 29.42 N (3 kgf) load. EDS results indicate a critically decreased atomic content of Al and the appearance of elements typical for AISI 316L in delaminated areas.

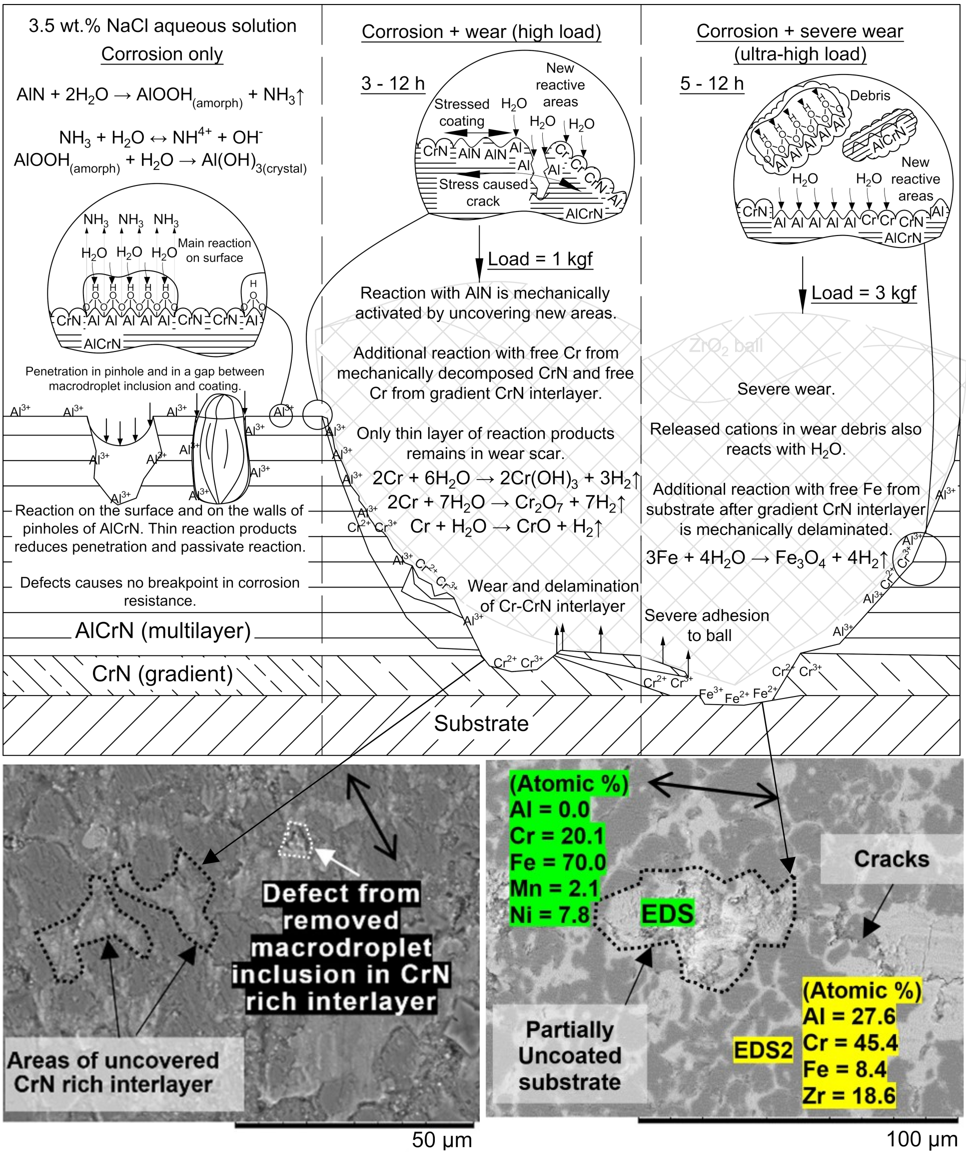

Figure 10. Simplified schematic illustration of the main processes on the surface and in wear scar during static and extended (12 h) tribo-corrosion tests in 3.5 wt.% NaCl solutions, respectively (supported with SEM micrographs and EDS results). A period of observed critical process during sliding test is shown. A ball is shown only for illustration without scale. Mainly released cations are indicated (combined from data in Paper III).

3.3 Raman spectra of statically oxidized materials

Raman spectroscopy of statically oxidized materials is described in detail in Paper II.

Raman spectra on the surface of β-Si_3N_4, Y_2O_3 stabilized tetragonal ZrO_2 and α-Al_2O_3 before and after static oxidation tests at 800 °C for 1 h indicates almost no effect on crystalline phases (McHale, 1997; Platt et al., 2014). These test results indicate the ability of selected counter-bodies to maintain initial crystalline structure at all selected test temperatures up to 800 °C. The influence of the friction caused flash temperature on the crystalline phase is also avoided when other predictable side factors, like vibration or sparks are eliminated or reduced to the minimum at applied environmental temperatures up to 800 °C. Consequently, a possibility to determine a material transfer from counter-body to tested AlCrN coated SS 253 MA and vice versa after sliding tests is enabled.

3.3.1 Static oxidation of stainless steel 253 MA

The appearance and evolution of defects in coatings caused by sliding wear cannot always be determined by the optical and SEM imaging methods. It creates the even great challenge when mechanically mixed layer consisting of a substrate and coating materials is formed and compacted in the wear scar over the substrate. Therefore, a reliable method like Raman spectroscopy for determination of unoxidized and oxidized SS substrate materials becomes preferable not only due to the oxidation caused by environmental conditions but also due to the heat flux and flash caused by friction in sliding contact area as schematically demonstrated in Figure 2 b.

In the present PhD work, almost no significant changes were found in Raman spectra of SS 253 MA after applying the static oxidation temperature up to 500 °C, indicating a formation and development of the thin oxide scales, which consist of α-Fe_2O_3 (hematite). A continuation of oxidation under these oxidative conditions is limited due to the high concentration of Cr (McCarty et al., 1989; Natesan, 2002) in the structure of tested SS.

Partially mild and severe oxidized areas were observed with the optical microscope after static oxidation of SS 253 MA at 800 °C. Temperature increase up to 900 °C leads to the completely severe oxidized surface. A formation of oxide crystals with more clearly separated phases was observed in the spectra after increasing test temperature up to 1000 and 1100 °C. A presence of Cr_2O_3, γ-Fe_2O_3 (maghemite) (Boucherit et al., 1991; de Faria et al., 1997), transition phase of Fe_3O_4 (magnetite) and (Fe, Cr) based oxide spinel phase (Jubb et al., 2010) was determined after static oxidation tests at these temperatures.

3.3.2 Static oxidation of AlCrN PVD coated stainless steel 253 MA

The application of AlCrN PVD coating under environmental or friction initiated elevated temperature under oxidative conditions inevitably required to study the structure, thermal stability and oxidation behaviour of this material.

Raman spectroscopy results of the surface of the tested as-received AlCrN PVD coating indicates typical broad peaks at 236-264 (LA – acoustic transition, related with vibration of Cr ions); 475 (mid-wave number bands 2A/LO and TO, related with vibration of N ions), 712-720 (mid-wave number band A+O – second order transition), 1285 and 1472 cm^{-1} (high-wave number band 2O - second order transition) (Ipaz, 2012). This result indicates a dominating cubic CrN structure (L. Wang, 2008) typical for AlCrN PVD films with a content of Al from 40 up to 60 at. % (Kaindl et al., 2006). It should also be noted that no one typical peak at 249 (E_2, low), 610 (A_1, TO), 669 (E_1, TO), 656 (E_2, high), 891 (A_1, LO) and 912 cm^{-1} (E_1, LO) was observed for hexagonal AlN (Haboeck et al., 2003).

It was found in Raman spectra that CrN decomposes and forms chromium oxide (Cr_2O_3) in the contact with the oxidative atmosphere at all selected elevated temperatures. Elevated temperatures up to 300 and 500 °C leads to the thickening of Cr based oxide layer until the reaction becomes slow due to the reduced oxygen penetration rate. The thickening of the oxide layer intensifies at 800 °C due to the mismatch in thermal expansion between coating and formed oxide layer. Oxygen penetrates through cracked oxide layer and oxidizes the freshly uncovered area of the unoxidized PVD coating or substrate in the case of failure. This factor causes defects in the oxide film and subsequent build-up of the layer by oxygen penetration into defected areas and expansion due to the growth of new oxides. Formation of α-Al_2O_3 or similar structured Al based oxide was found as indicated by the new Raman peak at 553 cm^{-1} after static oxidation at 800 °C. It confirms that the oxidation temperature of AlN is about 700 °C (Lee et al., 2002).

3.4 The effect of the combination of temperature and sliding speed on coefficient of friction, oxidation of AlCrN PVD coated disks and wear rates of counter-bodies

A determination of the reliability of the elevated temperature sliding wear input factors and measured dependent results are demonstrated in this section.

A failure of the coating or enormous high vibrations during relatively short test duration was set as a limit for the determination of the reliable sliding conditions. The detailed description of the results is demonstrated in Paper II. Wear rates were measured on tested ball counter-bodies as it was too complicated to measure wear rates of tested discs. Therefore, wear process was more referred to counter-bodies, but determination of oxides was more referred to tested discs.

3.4.1 The wear mechanism of the tested AlCrN coating against Si_3N_4 counter-body

The effect of sliding speed in a combination with a test temperature on the final CoF, wear rates of the Si_3N_4 counter-bodies and oxidation of coating material is presented in Figure 11. An example of the difference between effects of reliable and unreliable sliding conditions are demonstrated as a failure of the coating shown in Figure 12 a and b. A full range of these results with included unreliable sliding test conditions are demonstrated in maps, as shown in Figure 13 a and b. The test temperature and the applied sliding speed are two reliability influencing varying input factors to be analysed in the present part of this research work.

The highest recorded final CoF values (at the end of the test) from 0.76 up to 0.92 were found at room temperature in the whole range of applied sliding speeds from 0.002 up to 1.458 $m\cdot s^{-1}$ in comparison with results recorded during tests at elevated temperatures as demonstrated in Figure 13 a. Final CoF reaches the lowest values from 0.51 up to 0.60 by increasing test temperature up to 300 °C at selected sliding speeds up to 0.126 $m\cdot s^{-1}$, as shown in Figure 11. The final CoF value tends to increase in the range of coating reliability maintaining sliding speeds by increasing sliding test temperature up to 500 (up to 0.126 $m\cdot s^{-1}$) and 800 °C (up to 0.054 $m\cdot s^{-1}$), reaching maximum values of 0.63 and 0.80, respectively. These results indicate the significant influencing factor of oxidative environmental temperature in the range from 20 up to 800 °C. Results demonstrate down to about 45 % lower final CoF when the test temperature of 300 °C is applied.

Sliding speed becomes a more important factor when the environmental temperature is constant. Generally, an increase in sliding speed leads to a decrease in a final CoF values in a range of lowest sliding speeds at elevated temperatures. This tendency disappears when sliding speeds are higher than 0.006 (at 300 and 500 °C) and 0.018 $m\cdot s^{-1}$ (at 800 °C), as demonstrated in Figure 11. It can be concluded, that the final value of the CoF remains relatively unchanged varying from 0.61 up to 0.63 at 500 °C and sliding speeds up to 1.458 $m\cdot s^{-1}$. However, the CoF increases when applied sliding speed is higher than 0.162 $m\cdot s^{-1}$ at 300 °C. Similar effect occurs at 800 °C when sliding speed exceeds

0.018 m·s^{-1}. Final values of CoF continuously increase up to 0.86 at maximum test sliding speed. Exceptions are recorded CoF values at room temperature. Final values of the CoF remain relatively stable from 0.85 up to 0.92 when sliding speeds up to 0.486 m·s^{-1} are applied. A slight reduction in CoF values occurs when sliding speed exceeds 0.054 m·s^{-1}, reaching lowest final CoF value of 0.76 at maximum applied sliding speed. It should be noted, that running-in (Blau, 2005) period (evolution in CoF) was about the third part of a total duration of the test during lowest sliding speed due to the possible rolling of collected wear debris from removed asperities as demonstrated in Paper II.

Generally, increased test sliding speeds lead to the decrease in wear rates of Si_3N_4 counter-bodies (balls) as demonstrated in Figure 11 (the range of speeds at which coating is reliable) and Figure 13 b (the whole range of test sliding speeds). It is also possible to conclude from the similar study (Antonov et al., 2013), that the wear of Si_3N_4 counter-bodies is several orders of magnitude higher than that of coated disks (see Paper II).

The calculated rise of temperatures for bulk material and flash temperatures of Si_3N_4 counter-bodies sliding against AlCrN PVD coating with applied reliability maintaining sliding speeds during the room temperature test are demonstrated in Figure 11. Calculated temperatures in a full range of applied sliding speeds are demonstrated in Paper II. A quite high bulk temperature was found according to calculations due to the relatively high CoF recorded during tests. It was found that flash temperature theoretically exceeds the maximum service temperature of Si_3N_4 counter-body (1100 °C) when the sliding speed reaches 0.486 m·s^{-1} as shown in Figure 11. However, EDS results in the wear tracks of the worn AlCrN PVD coatings indicate heavily oxidized transfer layer with an increased content of Si (about 5.6 %) after applying sliding speeds of 0.006 and 1.458 m·s^{-1} due to the high CoF and extremely high flash temperature (>3000 °C, see calculations in Paper II) in sliding contact zone, respectively. A visual comparison supported with EDS results between tests after applied reliable and unreliable sliding test conditions is shown in Figure 12 a and b, indicating a transfer of counter-body and failure of the coating when speed exceeds reliability limit of the coating. An increased concentration of Fe indicates a presence of the uncovered SS substrate in wear track and emanation of Fe from the substrate to the surface of the worn AlCrN PVD coating. An increase in the content of oxygen reveals a significant oxidation of the tribolayer.

Raman spectra of the PVD coating before and after static oxidation helps to understand the effect of applied reliable and unreliable combination of the sliding speed and the temperature of an oxidizing environment on the formation of oxides in the wear scar, as shown in Table 10.

The development of oxides at room temperature is strongly dependant on applied sliding speed. A thickness of oxide scales increases in wear scar of the AlCrN PVD coating after tests at lowest applied sliding speed (0.002 m·s^{-1}) but remains too thin to be clearly observed in Raman spectra. Increasing applied sliding speeds up to 0.054 m·s^{-1} lead to a formation of Cr_2O_3 oxide scales in a wear scar, exhibiting the Raman spectra like those of spectra after static oxidation test at 300 °C. An applied sliding speeds from 0.162 up to 0.486 m·s^{-1} lead to a formation of a mixed Cr_2O_3 oxide scales similar to those detected after static oxidation at 300 and 500 °C. The sliding speed of 1.458 m·s^{-1} results in unreliable performance and subsequent failure of the coating as the spinel phase was detected in the spectra. Generally, the similar spectra were found after static oxidation at 800 °C, but it could be concluded that AlN remains unoxidized in wear scar. Similar baselines with a presence of Raman peaks detected from Al_2O_3 were captured after tests at elevated temperatures and exceeded the range of sliding speeds at which the tested coating is reliable.

The range of applied sliding speeds up to 0.162 m·s^{-1} at 300 and 500 °C leads to a formation of similar oxide scales in the wear scar as observed after sliding tests at room temperature and sliding speeds from 0.162 up to 0.486 m·s^{-1}. It should be noted that very similar development of oxide scales occurs at both elevated temperatures at different applied sliding speeds as schematically shown in Figure 11.

Sliding speeds up to 0.054 m·s^{-1} at 800 °C leads to the formation of the similar baseline in Raman spectra captured after static oxidation, indicating almost no effect of applied sliding speed on oxide scales.

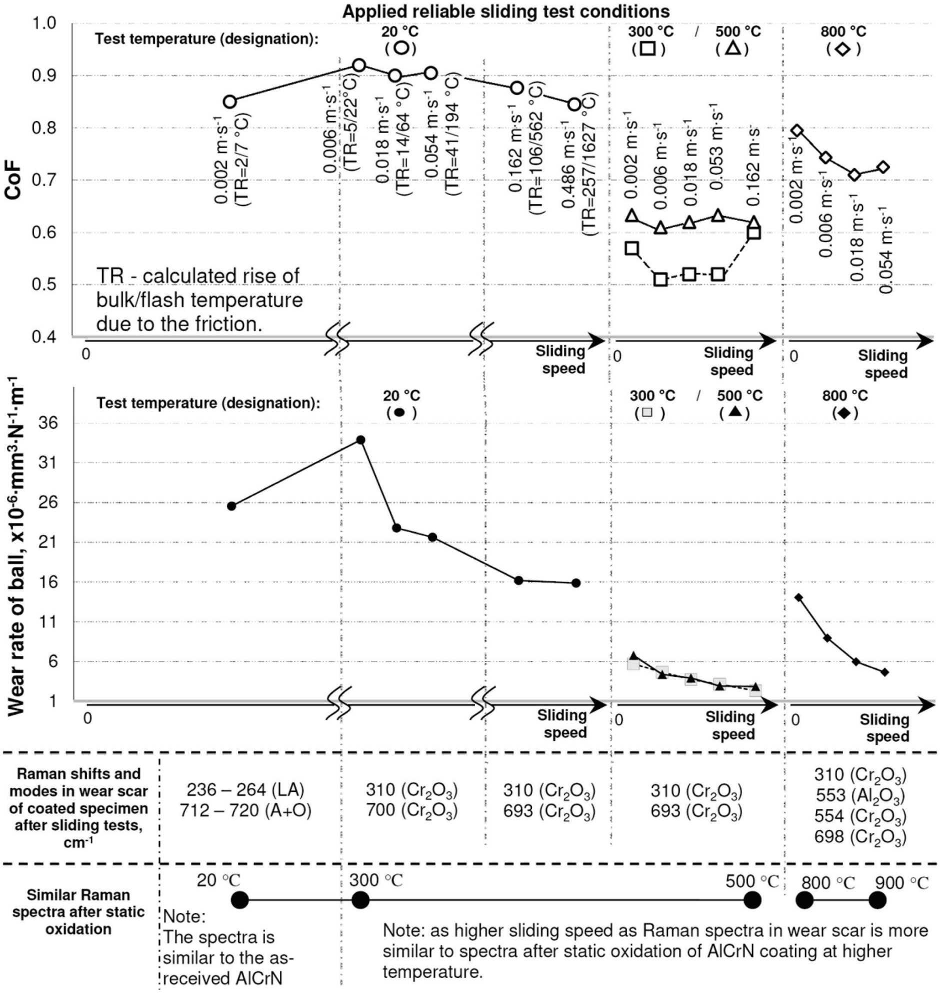

Figure 11. CoF, wear rates of Si_3N_4 counter-bodies, calculated rise of bulk/flash temperature, observed Raman peaks in wear scars of AlCrN coating and indicated similar Raman spectra from static oxidation tests for reliable sliding conditions (data is combined from Paper II).

Table 10. Assignment of Raman peaks after sliding initiated oxidation of AlCrN PVD coated 253 MA stainless steel against Si_3N_4 counter-bodies under room and elevated temperature conditions with indicated reliability of the coating under applied conditions (data is combined from Paper II).

Test temperature, °C					
20		**300 and 500**		**800**	
Sliding speeds, m·s^{-1}	**Raman shift cm^{-1} and assignment**	**Sliding speeds, m·s^{-1}**	**Raman shift cm^{-1} and assignment**	**Sliding speeds, m·s^{-1}**	**Raman shift cm^{-1} and assignment**
0.002	236 – 264 (LA); 712 – 720 (A+O)	0.002; 0.006; 0.018; 0.054; 0.162 **Reliable** ↑	310 (Cr_2O_3); 693 (Cr_2O_3)	0.002; 0.006; 0.018; 0.054 **Reliable** ↑	310 (Cr_2O_3) 553 (Al_2O_3) 554 (Cr_2O_3); 698 (Cr_2O_3)
0.006; 0.018; 0.054	310 (Cr_2O_3) 700 (Cr_2O_3)				
0.162; 0.486 **Reliable** ↑	310 (Cr_2O_3); 693 (Cr_2O_3)	↓ **Unreliable** 0.486; 1.458	310 (Cr_2O_3); 553 (Al_2O_3); 554 (Cr_2O_3); 686 (Fe, Cr-spinel); 693 (Cr_2O_3); 698 (Cr_2O_3)	↓ **Unreliable** 0.162; 0.486; 1.458	310 (Cr_2O_3); 553 (Al_2O_3); 554 (Cr_2O_3); 686 (Fe, Cr-spinel); 693 (Cr_2O_3); 698 (Cr_2O_3)
↓ **Unreliable** 1.458	310 (Cr_2O_3); 693 (Cr_2O_3); 680 (spinel); 1017 (NI); 1323 (NI)				
Note: NI – not identified					

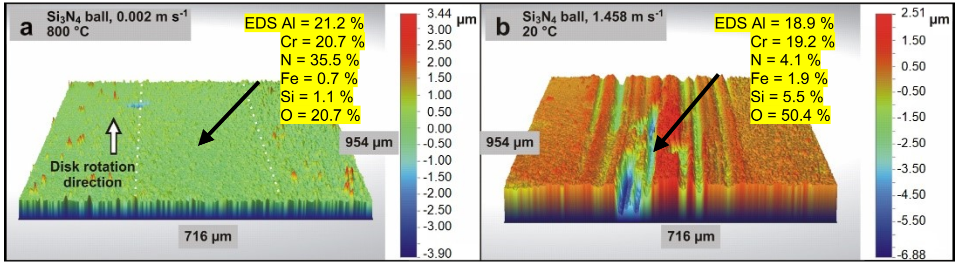

Figure 12. An images of 3D profilometry of the wear tracks on the surface of AlCrN PVD coating after completed test with sliding speeds providing reliability (a) and unreliability of the coating (b) with indicated counter-body material, sliding speed, test temperature and results of EDS analysis (data is combined from Paper II).

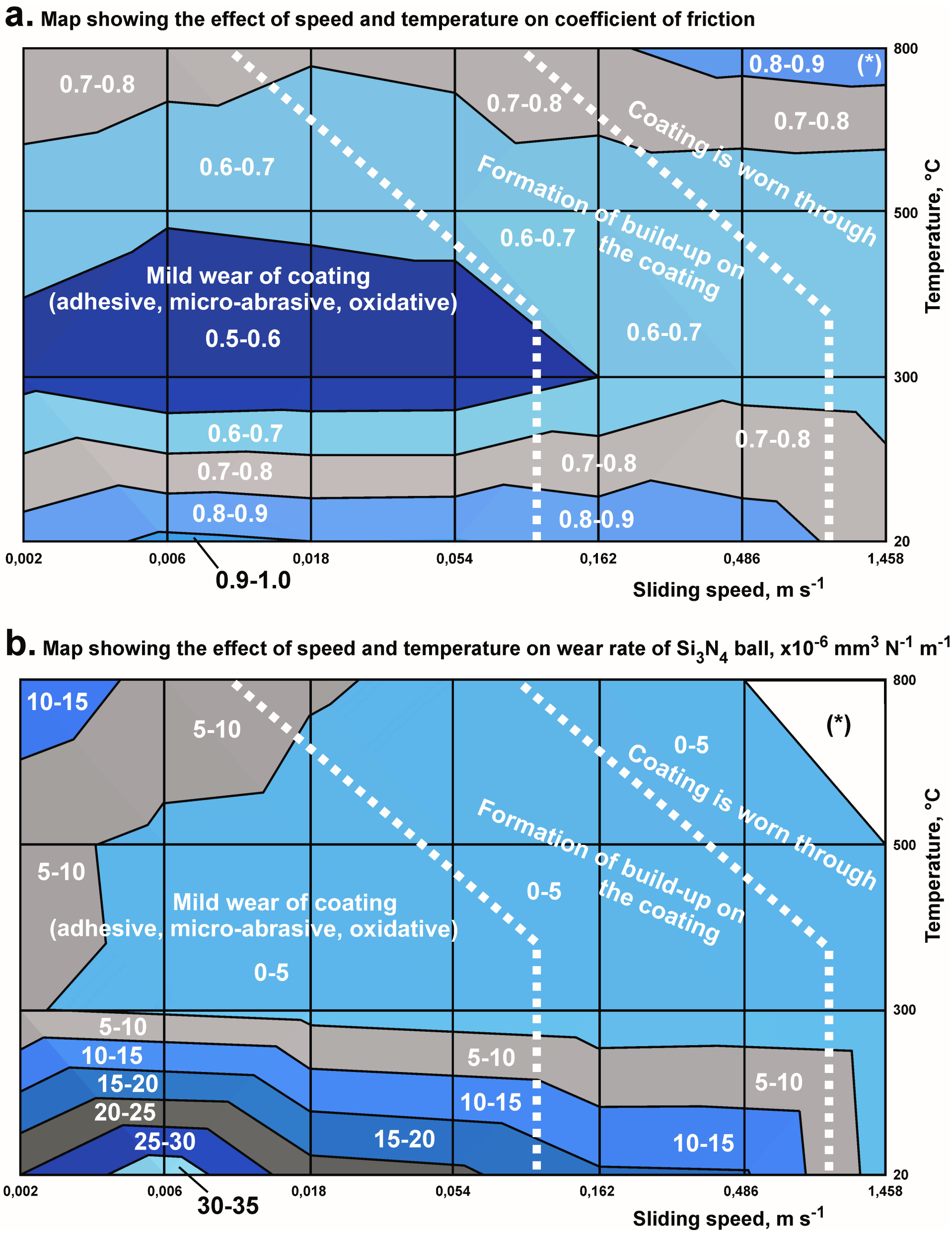

*Figure 13. The maps of the effect of sliding speed and temperature on final CoF during sliding (a) and wear rates of Si_3N_4 counter-bodies measured after sliding (b) against AlCrN coating, constructed according to results demonstrated in Paper II with detailed description. Note: * indicates the test at 800 °C and sliding speed of 1.458 $m\cdot s^{-1}$ stopped after 10 % of total test duration due to the undesirably high vibration and noise (Paper II).*

3.4.2 The wear mechanism of the AlCrN coating tested against Al_2O_3 counter-body

The effect of applied the sliding speed and the temperature on the final CoF and wear rates of Al_2O_3 counter-bodies are represented in Figure 14 a and b. Values of the final CoF at room temperature were varying from 0.64 up to 0.66, as demonstrated in Figure 14 a. Significantly lower values of the final CoF from 0.4 up to 0.46 were recorded during sliding tests at 800 °C. Generally, an increased sliding speed leads to a slightly higher value of the CoF under tested elevated temperature tribo-corrosive conditions. Low wear rates (see Figure 14 b) indicates that the application of the Al_2O_3 counter-body clearly leads to a more pronounced wear of the AlCrN coating in comparison with the Si_3N_4 material applied as a counter-body (Mo et al., 2009a). An oxidation of CrN into Cr_2O_3 also leads to a formation of compacted and smooth flakes located in the tribolayer during wear of the AlCrN PVD coating. Delamination of the AlCrN PVD coating occurs in small areas due to the presence of pinhole defects. The low wear and the small contact area of the alumina ball lead to high stresses at delaminated areas of a coating. Subsequently, this effect causes a catastrophic failure of the AlCrN PVD coating at 800 °C and applied the highest sliding speeds of 0.486 and 1.458 $m \cdot s^{-1}$.

An application of the present tribopair leads to a transfer of un-oxidized and oxidized AlCrN coating material to the wear scar of Al_2O_3 counter-bodies under all applied test conditions. A presence of the same Al atoms in the AlCrN coating and Al_2O_3 counter-body causes complication to determine a transfer of α-Al_2O_3 in any direction by EDS or Raman spectroscopy. Applied sliding speeds from 0.486 up to 1.458 $m \cdot s^{-1}$ causes a formation of thick oxide scales in the tribocontact as detected by the corresponding Raman peaks after wear tests. A formation and a transfer of (Fe, Cr) spinel phase were observed after sliding tests at 800 °C and a speed of 1.458 $m \cdot s^{-1}$. Similar Raman peaks were found after the static oxidation of SS 253 MA (spinel, peak at 682 cm^{-1}) and the static oxidation of AlCrN PVD coating (Cr_2O_3, at 693 cm^{-1}) indicating the development of mechanically mixed layer, which consists of corrosion products from Cr interlayer and uncovered steel substrate.

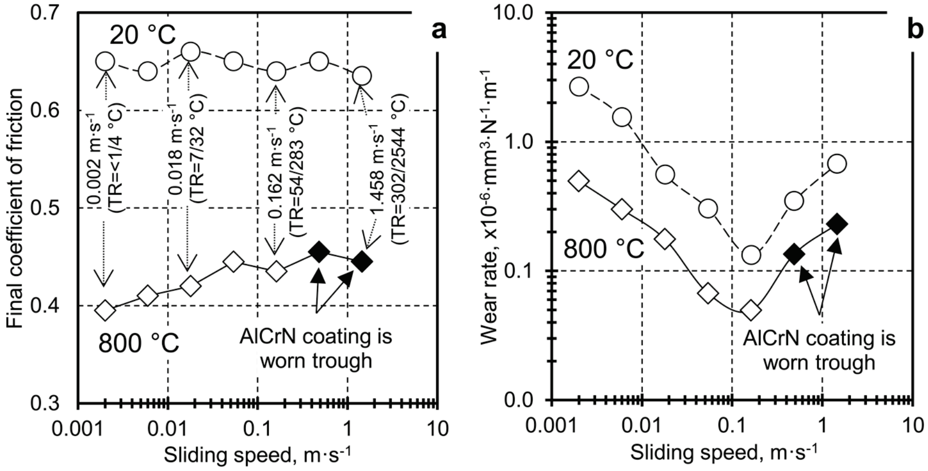

Figure 14. The effect of sliding speed on CoF with indicated calculated rise of bulk/flash temperature (TR) for every second result (a); and the wear rates (b) of tested Al_2O_3 counter-bodies against the AlCrN coating (data is combined from Paper II).

3.4.3 The wear mechanism of the AlCrN coating tested against ZrO_2 counter-body

The effect of the applied sliding speed and the temperature on the final CoF and wear rates of ZrO_2 counter-bodies are represented in Figure 15 a and b. A low hardness and a low thermal conductivity (Schlichting et al., 2001) results in a catastrophically high wear rate of the ZrO_2 counter-body. A melting and a phase transformation from a tetragonal to a monoclinic (Platt, 2014) induces wear rate of the tested counter-body due to a frictional heating (Ashby, 1991). A build-up layer (Podgursky et al., 2014) forms in the wear scar of the AlCrN PVD coating at room temperature and applied low speeds. The larger is the size of the tribological wear contact zone, the higher is frictional heating (see Figure 15 b) and lower thermal conductivity of the ZrO_2 (Samani et al., 2010) counter-body provokes failure of the AlCrN PVD coating when applied sliding speed exceeds threshold values of 0.162 (at room temperature) and 0.006 $m \cdot s^{-1}$ (at 800 °C).

A fracturing of a coating material into fragments leads to a subsequent partial delamination. This process causes an accelerated abrasive wear due to an increased surface roughness in the wear scar of the AlCrN PVD coating. Hard abrasive particles scratch deep grooves in the wear scar of the ZrO_2 ball. EDS and Raman spectroscopy results indicate a critical difference between intensities of material transfer from the ball to the coating (very intensive) and vice versa (almost no transfer).

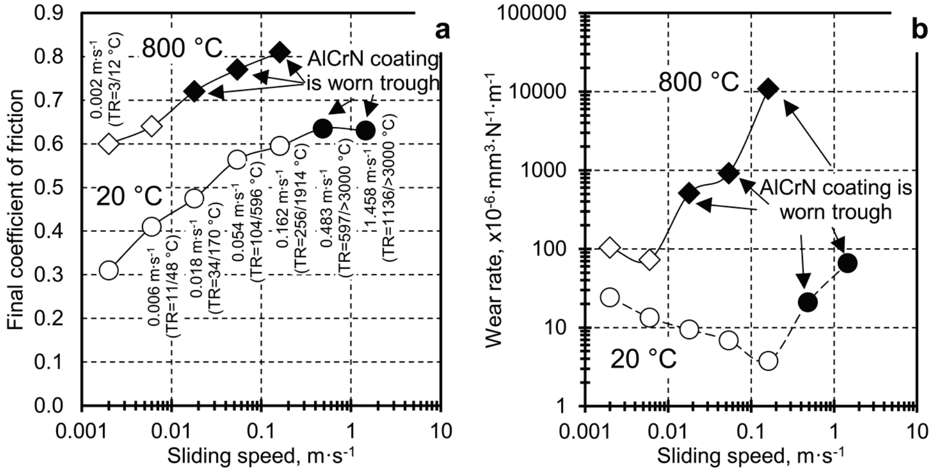

Figure 15. The effect of sliding speed on CoF with indicated calculated rise of bulk/flash temperature (TR) (a) and wear of the tested ZrO_2 counter-bodies (b) against AlCrN coating (data is combined from Paper II).

3.5 Assessment of the reliability of preliminarily scratched coating

The effect of the applied load on Rockwell "C" indenter and Al_2O_3 counter-body and the applied environmental temperature is demonstrated in Figure 16, Tables 11 - 13. The research work performed during development of this method has led to the determination of together 18 events related to wear mechanism. These events occur during sliding of the counter-body over the preliminarily scratched coatings at the test temperature.

An analysis of the combined tribological scratch and sliding caused wear leads to several complications in an expression of the measurement results. It is due to several events which repeat periodically or factors which affects the probability of the occurrence. For example, a cyclic collection, compaction, and removal of the debris material in the scratch track can cause a wrong conclusion about the occurrence of the event, if the observation is done on the tested surface before the collection of debris or the destruction of compacted debris is started. Therefore, a visual observation supported with SEM imaging and collected knowledge from previous publications was selected as the method in this preliminarily research work to make the database for the further investigation with an optical and contact type measurement devices.

Observed and understood events were classified into three parts of favourability:

- Favourable – a tribological event, which leads to increased lifetime and reduces the probability of the failure of the tribosystem;
- Neutral – a tribological event, which occurs and gives no significant effect under applied conditions. Such an event may give some effect if some sliding test parameter (e.g. sliding distance) exceeds some limit;
- Unfavourable – a tribological failure event or an event, which causes a condition at which the coating may critically suffer in future from some exceeded sliding parameter (e.g. sliding distance).

Following events were visually identified in SEM images [a favourability of the event is also shown], as demonstrated in Figure 16 a-f and applied designations (from E1 to E18) were used for indication of the event below:

E1. Counter-body removes asperities on the surface of the PVD AlCrN coating before the edge of the scratch track [favourable].

E2. Counter-body removes asperities on the surface of the PVD AlCrN coating after the edge of the scratch track [favourable].

E3. Counter-body polishes the 1st edge of the scratch track on the PVD AlCrN coating [favourable].

E4. Wear debris collect at the 2nd edge of the scratch track of the PVD AlCrN coating and forms a smooth tribolayer [favourable].

E5. Wear debris collect at the edges of the wear track of the PVD AlCrN coating [neutral].

E6. Coating is removed due to the cracking at the 2nd edge of the scratch track of the PVD AlCrN coating [unfavourable].

E7. Counter-body partially jumps over the small area after the 2nd edge of the scratch track of the PVD AlCrN coating (contact load is locally reduced) and can cause higher stresses in landing areas [neutral].

E8. A severe transfer of Al_2O_3 from the counter-body to the coating after the 2nd edge of the scratch track of the of the PVD AlCrN coating due to high value of inertia of the loading system (contact load becomes higher than applied) [unfavourable].

E9. Coating delaminates inside the scratch track of the PVD AlCrN coating [unfavourable].

E10. Counter-body compresses asperities of the surface of the PVD AlCrN coating and a wear debris into smooth tribolayer with an average surface roughness of $R_a \leq 0.06$ µm [favourable].

E11. Compacted wear debris connects both edges of the scratch track of the PVD AlCrN coating [favourable].

E12. Compacted wear debris partially closes the scratch track of the PVD AlCrN coating [favourable].

E13. Coating fails (the substrate is uncovered) before scratch track of the PVD AlCrN coating [unfavourable].

E14. Coating fails (the substrate is uncovered) after scratch track of the PVD AlCrN coating [unfavourable].

E15. Counter-body mechanically mixes a wear debris of the PVD AlCrN coating and substrate materials [unfavourable].

E16. Counter-body causes ripples (Podgursky, 2014) on the surface of the PVD AlCrN coating [neutral].

E17. Counter-body periodically compacts and removes wear debris in the scratch track due to the too weak adhesion between compacted wear debris and the coating [unfavourable].

E18. Counter-body completely mechanically mixes a layer of the PVD AlCrN coating and the substrate [unfavourable].

Thresholds between reliable and unreliable loads on indenter and counter-body are clearly demonstrated in Table 11, Table 12 and Table 13 for the sliding wear tests at the room temperature, 500 and 800 °C, respectively.

It was found, that, generally, only favourable or neutral events occur at the area of the crossing points of tracks, indicating mild sliding wear conditions under applied load to the counter-body up to 7.85 N (0.8 kgf), if the same maximum load is applied to the indenter at room temperature, as shown in Table 11. Deep scratch track, caused by the indenter leads to a critically reduced maximum reliable load on the counter-body down to 2.94 N (0.3 kgf). Complete failure of the tested AlCrN coating occurs when counter ball slides over the deepest scratch track caused by 16.67 N (1.7 kgf) load, applied to indenter.

The event E15 is the debatable issue. Two possible results could be explained in this case:

- A presence of the substrate material containing mechanically mixed layer (MML) indicates the failure of the coating, therefore, it leads to the exposure of the substrate to the aggressive environment (unfavourable event);
- The formed MML may completely or almost completely recover the substrate, therefore the degradation of the substrate can be reduced (favourable event). Such MML can provide even better tribological properties. However, the formation of the MML is the mostly inhomogeneous process. Therefore, the formed MML may be detached during sliding and may cause a three-body abrasion in the wear contact zone.

Temperature increase up to 500 and 800 °C drastically decreases a range of reliable loads to counter-body and indenter. A set of dominating favourable and unfavourable events also changes to more severe sliding wear conditions. At 500 °C, a reliably applied load to the counter-body generally becomes limited down to 4.9 (0.5 kgf) and 2.94 N (0.3 kgf), when the coating is preliminarily scratched by indenter under maximum load of 7.85 N (0.8 kgf). However, the maximum scratch load of 2.94 N (0.3 kgf) was determined as reliable for sliding wear under 11.77 (1.2 kgf) and 4.9 N (0.5 kgf) loads.

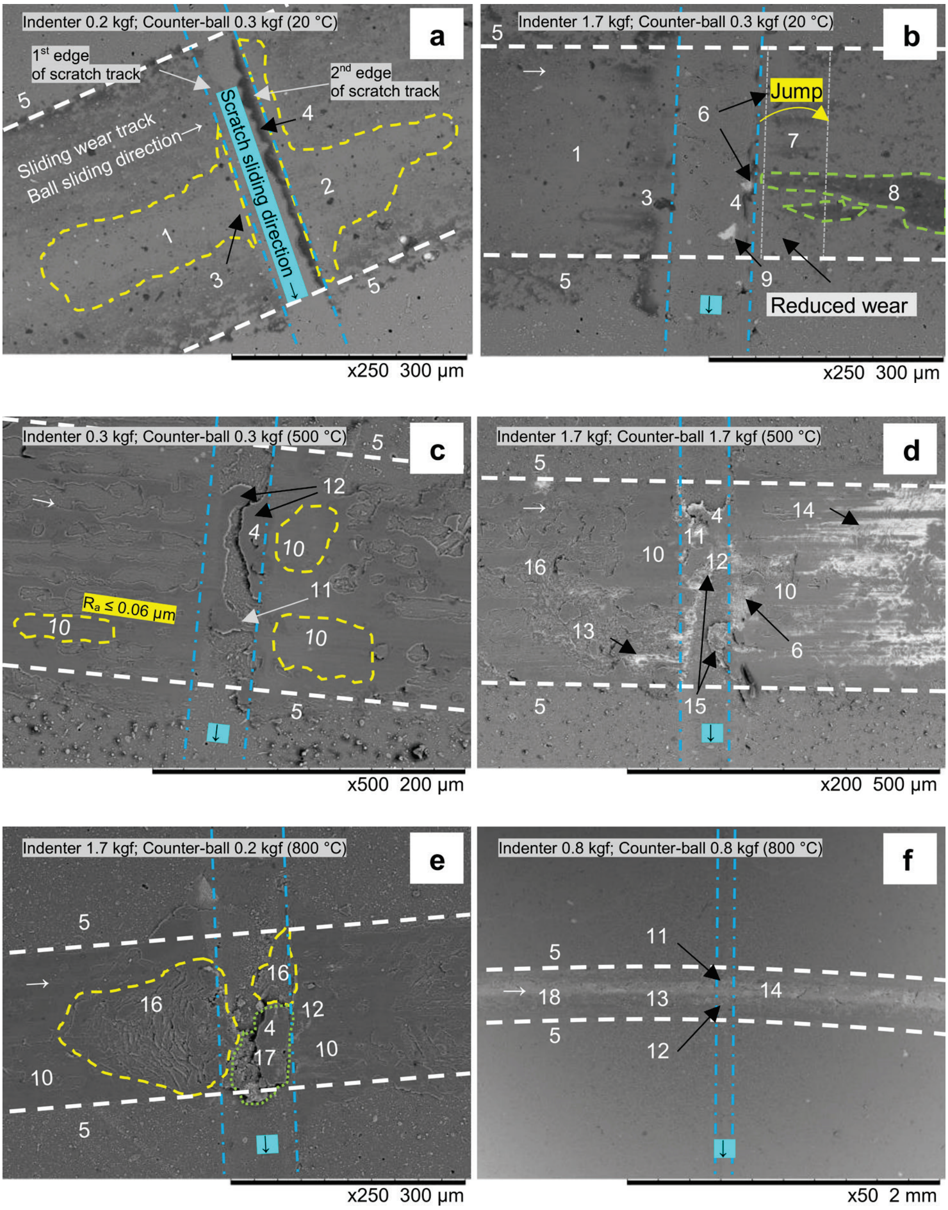

Figure 16. Examples of the SEM images of the observed events (changes) on the surface of the coating at the area of the crossing points of scratch tracks (caused by Rockwell "C" indenter) and wear tracks (caused by Al_2O_3 counter-body) at room temperature (a) and (b); 500 (c) and (d); and 800 °C (e) and (f). An applied load F (kgf) to the indenter and to the counter-body are indicated. Determined events are numbered from 1 to 18 and are explained in the text.

Table 11. Observed events (changes) on the surface of the PVD AlCrN coating at the area of the cross-sections between scratch tracks (caused by Rockwell “C” indenter) and wear tracks (caused by Al_2O_3 ball counter-body) at room temperature.

		The applied load during scratch test, N (kgf)					
		1.96 (0.2)	**2.94 (0.3)**	**4.9 (0.5)**	**7.85 (0.8)**	**11.77 (1.2)**	**16.67 (1.7)**
The applied load during sliding wear test, N (kgf)	**1.96 (0.2)**	1_F, 2_F, 3_F, 4_F, 5_N	1_F, 2_F, 3_F, 4_F, 5_N, 12_F	1_F, 2_F, 3_F, 4_F, 5_N, 12_F	1_F, 2_F, 3_F, 4_F, 5_N, 12_F	1_F, 2_F, 3_F, 4_F, 5_N, 12_F	5_N, 9_U, 18_U
	2.94 (0.3)	1_F, 2_F, 3_F, 4_F, 5_N	1_F, 2_F, 3_F, 4_F, 5_N, 12_F, 16_N	1_F, 2_F, 3_F, 4_F, 5_N, 12_F	1_F, 2_F, 3_F, 4_F, 5_N, 12_F	3_F, 4_F, 5_N, 11_F, 12_F, 16_N	5_N, 9_U, 18_U
	4.9 (0.5)	1_F, 2_F, 3_F, 4_F, 5_N	1_F, 2_F, 3_F, 4_F, 5_N, 12_F	1_F, 2_F, 3_F, 4_F, 5_N, 12_F	1_F, 2_F, 3_F, 4_F, 5_N, 12_F	1_F, 2_F, 3_F, 4_F, 5_N, 6_U, 12_F	5_N, 9_U, 18_U
	7.85 (0.8)	1_F, 2_F, 3_F, 4_F, 5_N	1_F, 2_F, 3_F, 4_F, 5_N, 12_F	1_F, 2_F, 3_F, 4_F, 5_N, 12_F	1_F, 2_F, 3_F, 4_F, 5_N, 12_F	1_F, 2_F, 3_F, 4_F, 5_N, 12_F, 13_U, 15_U, 16_N	5_N, 9_U, 18_U
	11.77 (1.2)	1_F, 2_F, 3_F, 4_F, 5_N, 16_N	1_F, 2_F, 3_F, 4_F, 5_N, 7_N, 9_U, 12_F, 13_U	1_F, 2_F, 3_F, 4_F, 5_N, 7_N, 8_U, 9_U, 12_F, 13_U	1_F, 2_F, 3_F, 5_N, 6_U, 9_U, 12_F, 13_U, 14_U	1_F, 2_F, 3_F, 4_F, 5_N, 9_U, 12_F	5_N, 9_U, 18_U
	16.67 (1.7)	1_F, 4_F, 5_N, 7_N, 8_U, 12_F, 13_U	1_F, 3_F, 4_F, 5_N, 6_U, 7_N, 8_U, 9_U	1_F, 2_F, 3_F, 4_F, 5_N, 7_N, 8_U, 9_U, 10_F, 12_F, 13_U	1_F, 2_F, 3_F, 5_N, 6_U, 7_N, 8_U, 9_U, 12_F, 13_U, 14_U	1_F, 4_F, 5_N, 6_U, 13_U, 14_U, 15_U, 16_N	5_N, 9_U, 18_U
Notes: X_F – favourable event; X_N – neutral event; X_U – unfavourable event.							

Table 12. Observed events (changes) on the surface of the PVD AlCrN coating at the area of the cross-sections between scratch tracks (caused by Rockwell “C” indenter) and wear tracks (caused by Al_2O_3 ball counter-body) at 500 °C.

		The applied load during scratch test, N (kgf)					
		1.96 (0.2)	**2.94 (0.3)**	**4.9 (0.5)**	**7.85 (0.8)**	**11.77 (1.2)**	**16.67 (1.7)**
The applied load during sliding wear test, N (kgf)	**1.96 (0.2)**	4_F, 5_N, 10_F, 12_F	4_F, 5_N, 10_F, 11_F, 12_F	4_F, 5_N, 10_F, 11_F, 12_F	4_F, 5_N, 10_F, 11_F, 12_F	4_F, 5_N, 10_F, 11_F, 12_F, 16_N, 17_U, 18_U	4_F, 5_N, 10_F, 11_F, 12_F, 14_U
	2.94 (0.3)	4_F, 5_N, 10_F, 12_F	4_F, 5_N, 10_F, 11_F, 12_F	4_F, 5_N, 10_F, 11_F, 12_F	4_F, 5_N, 10_F, 11_F, 12_F	4_F, 5_N, 10_F, 11_F, 12_F, 13_U, 16_N, 17_U, 18_U	4_F, 5_N, 11_F, 12_F, 13_U, 14_U, 15_U, 16_N
	4.9 (0.5)	4_F, 5_N, 10_F, 12_F	4_F, 5_N, 10_F, 11_F, 12_F	4_F, 5_N, 10_F, 12_F, 14_U, 16_N	4_F, 5_N, 10_F, 12_F, 16_N	4_F, 5_N, 9_U, 10_F, 11_F, 12_F, 17_U, 18_U	4_F, 5_N, 10_F, 11_F, 12_F, 14_U, 16_N
	7.85 (0.8)	4_F, 5_N, 10_F, 12_F	4_F, 5_N, 10_F, 11_F, 12_F, 13_U	4_F, 5_N, 6_U, 10_F, 12_F, 13_U, 14_U, 15_U, 16_N	4_F, 5_N, 6_U, 10_F, 12_F, 13_U, 14_U, 15_U, 16_N	4_F, 5_N, 6_U, 9_U, 10_F, 11_F, 12_F, 13_U, 14_U, 15_U, 17_U, 18_U	4_F, 5_N, 6_U, 10_F, 11_F, 12_F, 13_U, 14_U, 15_U, 16_N
	11.77 (1.2)	4_F, 5_N, 9_U, 10_F, 12_F, 13_U	4_F, 5_N, 7_N, 9_U, 10_F, 12_F, 13_U, 14_U, 15_U, 16_N	4_F, 5_N, 6_U, 9_U, 10_F, 12_F, 13_U, 14_U, 15_U, 16_N	4_F, 5_N, 6_U, 11_F, 12_F, 14_U, 15_U, 16_N	4_F, 5_N, 6_U, 9_U, 10_F, 11_F, 12_F, 13_U, 14_U, 15_U, 17_U, 18_U	4_F, 5_N, 6_U, 10_F, 11_F, 12_F, 13_U, 14_U, 15_U, 16_N
	16.67 (1.7)	4_F, 5_N, 6_U, 7_N, 9_U, 10_F, 12_F, 13_U, 14_U	4_F, 5_N, 7_N, 9_U, 10_F, 12_F, 13_U, 14_U, 15_U, 16_N	4_F, 5_N, 6_U, 9_U, 10_F, 12_F, 13_U, 14_U, 15_U, 16_N	4_F, 5_N, 6_U, 11_F, 12_F, 15_U, 16_N	4_F, 5_N, 6_U, 10_F, 11_F, 12_F, 13_U, 14_U, 15_U, 17_U, 18_U	4_F, 5_N, 6_U, 10_F, 11_F, 12_F, 13_U, 14_U, 15_U, 16_N
Notes: X_F – favourable event; X_N – neutral event; X_U – unfavourable event.							

Table 13. Observed events (changes) on the surface of the PVD AlCrN coating at the area of the cross-sections between scratch tracks (caused by Rockwell "C" indenter) and wear tracks (caused by Al_2O_3 ball counter-body) at 800 °C.

		The applied load during scratch test, N (kgf)					
		1.96 (0.2)	**2.94 (0.3)**	**4.9 (0.5)**	**7.85 (0.8)**	**11.77 (1.2)**	**16.67 (1.7)**
The applied load during sliding wear test, N (kgf)	**1.96 (0.2)**	$4_F, 5_N, 10_F, 11_F, 12_F$	$4_F, 5_N, 10_F, 11_F, 12_F$	$4_F, 5_N, 9_U, 10_F, 11_F, 12_F, 13_U, 18_U$	$5_N, 11_F, 12_F, 13_U, 14_U, 15_U$	$5_N, 11_F, 12_F, 13_U, 14_U, 15_U, 18_U$	$5_N, 11_F, 12_F, 13_U, 14_U, 15_U, 18_U$
	2.94 (0.3)	$4_F, 5_N, 10_F, 11_F, 12_F$	$4_F, 5_N, 10_F, 11_F, 12_F$	$4_F, 5_N, 6_U, 7_N, 9_U, 10_F, 11_F, 12_F, 13_U, 14_U, 15_U, 16_N, 17_U, 18_U$	$5_N, 11_F, 12_F, 13_U, 14_U, 15_U, 18_U$	$5_N, 11_F, 12_F, 13_U, 14_U, 15_U, 18_U$	$5_N, 11_F, 12_F, 13_U, 14_U, 15_U, 18_U$
	4.9 (0.5)	$4_F, 5_N, 10_F, 11_F, 12_F$	$4_F, 5_N, 10_F, 11_F, 12_F, 16_N$	$4_F, 5_N, 10_F, 11_F, 12_F, 14_U, 15_U$	$5_N, 11_F, 12_F, 13_U, 14_U, 15_U, 18_U$	$5_N, 11_F, 12_F, 13_U, 14_U, 15_U, 18_U$	$5_N, 11_F, 12_F, 13_U, 14_U, 15_U, 18_U$
	7.85 (0.8)	$4_F, 5_N, 10_F, 12_F$	$4_F, 5_N, 11_F, 12_F, 15_U, 16_N$	$4_F, 5_N, 6_U, 7_N, 10_F, 11_F, 12_F, 14_U, 15_U, 16_N$	$5_N, 11_F, 12_F, 13_U, 14_U, 15_U$	$5_N, 11_F, 12_F, 13_U, 14_U, 15_U, 18_U$	$5_N, 11_F, 12_F, 13_U, 14_U, 15_U, 18_U$
	11.77 (1.2)	$4_F, 5_N, 10_F, 12_F$	$4_F, 5_N, 7_N, 10_F, 12_F, 15_U, 16_N$	$4_F, 5_N, 6_U, 7_N, 10_F, 11_F, 12_F, 13_U, 14_U, 15_U$	$5_N, 6_U, 10_F, 11_F, 12_F, 15_U$	$5_N, 11_F, 12_F, 13_U, 14_U, 15_U, 18_U$	$5_N, 11_F, 12_F, 13_U, 14_U, 15_U, 18_U$
	16.67 (1.7)	$4_F, 5_N, 10_F, 11_F, 12_F, 16_N, 17_U$	$4_F, 5_N, 7_N, 10_F, 12_F, 15_U, 16_N$	$4_F, 5_N, 6_U, 7_N, 10_F, 11_F, 12_F, 13_U, 14_U, 15_U, 18_U$	$5_N, 11_F, 12_F, 14_U$	$5_N, 6_U, 11_F, 12_F, 13_U, 14_U, 15_U, 18_U$	$5_N, 11_F, 12_F, 13_U, 14_U, 15_U, 18_U$

Notes: X_F – favourable event; X_N – neutral event; X_U – unfavourable event.

3.6 Discussion

The characterization of properties of a PVD coating is closely tied to applied characterization method of a selected substrate and a deposition process (Ding et al., 2008). In the present work, a *Platit π-80* unit offers automatic bias control of deposition with a high control speed of the closed loop for bias control (Kimmari et al., 2013; Yaldiz et al., 2009). It leads to low single peaks in the plot caused by the transmission of the voltage from the power supply to the rotating substrate as demonstrated in Figure 17 a. Such instability can be additionally responsible for defected areas in the PVD coating of several samples from the same booth, as the example is demonstrated in Figure 17 b. It is clear, that the purity of the SS substrate and working chamber are two main factors which lead to such defects. The condition of electrodes also should be considered. Instabilities in bias voltage and position of the substrate also lead to deviation in the total thickness of the PVD coating as demonstrated in Figure 17 c. Specimens with defected coatings were as possible excluded from testing in the present work, however, a more automatic SEM scanning method should be applied to make the selection process more accurate.

AlCrN PVD coating performs significantly better in the corrosive (Figure 6 and Table 9) and tribo-corrosive (3.5 wt% NaCl aqueous solution) conditions than tested TiCN or TiAlN PVD coatings with the similar thickness deposited on the SS AISI 316L substrate. A formation of a thin and mainly amorphous $AOOH_{(amorph)}$ layer occurs due to the well-known reaction between AlN and H_2O (Barshilia et al., 2006). Corrosion film leads to a slow penetration of an aqueous solution, therefore a corrosion rate of the AlCrN PVD coating becomes slow.

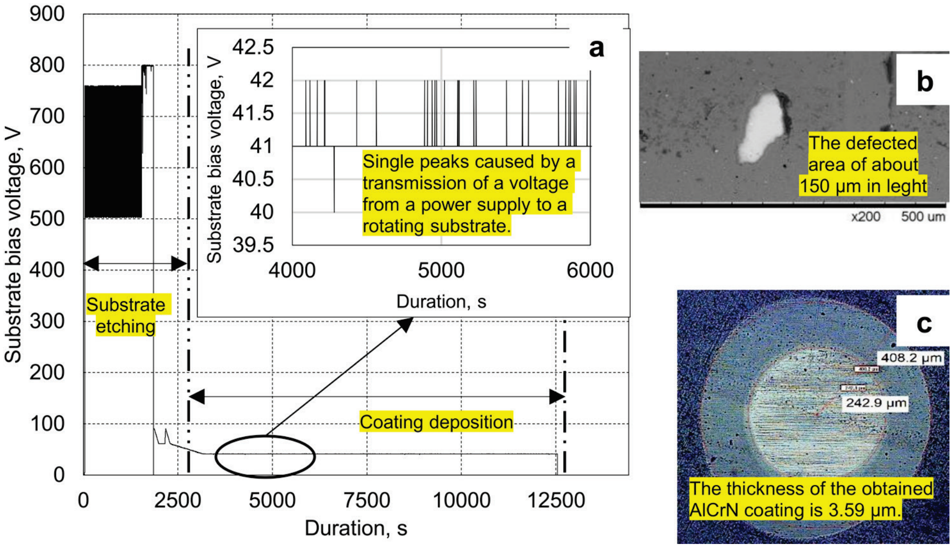

Figure 17. Recorded hidden process instability in substrate bias voltage determined during AlCrN PVD process on SS 253 MA substrate in Platit π-80 unit (a); and thickness of obtained AlCrN (measured by KaloMax ball cratering method) in present PhD study (b).

A reliability estimation scheme and a fault analysis critically require the characterization of a coating. Properly applied relevant test parameters allows to determine and to estimate important irregularities and deviations in properties (Liqin Wang et al., 2017) of a coating. The dominating phase of a face-centered cubic CrN changes to a dominating hexagonal wurtzite AlN phase in an $Al_xCr_{1-x}N$ PVD coating when the ratio of Al exceeds $x = 0.71$ (L. Wang, 2008). Clearly dominating inversion symmetry of the tested AlCrN PVD coating distinguishes groups of bands in the acoustic and optical ranges of Raman spectra (Barshilia et al., 2004), indicating a ratio of Al less than 0.71 as demonstrated in Figure 18 a and supported by the data from literature (Ipaz, 2012) and by the result of the XRD analysis for the same coating from the same PVD booth (Paper II and Paper III).

An estimation of the reliability of a PVD coating in sliding applications commonly refers to tribological problems detected in a commercially available tool in service. It leads to a required research work on problems that commonly starts with a collection of an information about exact service conditions. Subsequently, this data leads to a selection of an appropriate experimental method. A preliminarily investigation is a usual first step in understanding the applicability of a selected method that gives required information for the selection of varying input factors to support preliminarily obtained data.

A lower roughness of an SS substrate and a coating is usually required to reduce a CoF and a wear rate of materials in sliding contact. Here it should be noted that more aggressive conditions, like higher applied normal load or higher sliding speed, may accelerate a polishing of a coating and an arrangement of tribopair in a sliding contact.

Static oxidation tests of the SS 253 MA substrate indicate the good oxidation resistance up to 500 °C. High oxidation resistance of a Cr and a dense Fe based oxide scales leads to a sufficiently protected metal in the oxidative environment. Raman spectroscopy indicates the presence of Cr_2O_3, Fe_3O_4, γ-Fe_2O_3 and a (Fe, Cr) based spinel on the surface of the oxidized SS. It is well known, that Cr_2O_3 is one of a most widely applied compound as a coating in tribological applications, due to a high hardness of about 2300 HV and a good high temperature wear resistance up to about 1000 °C. The discovered iron-based oxides and the spinel are commonly applied as coatings to protect a steel substrate from a further oxidation. However, enormous high corrosion rate can occur, when such coating experiences mechanical damages or a direct contact to a corrosive aqueous solution like saltwater.

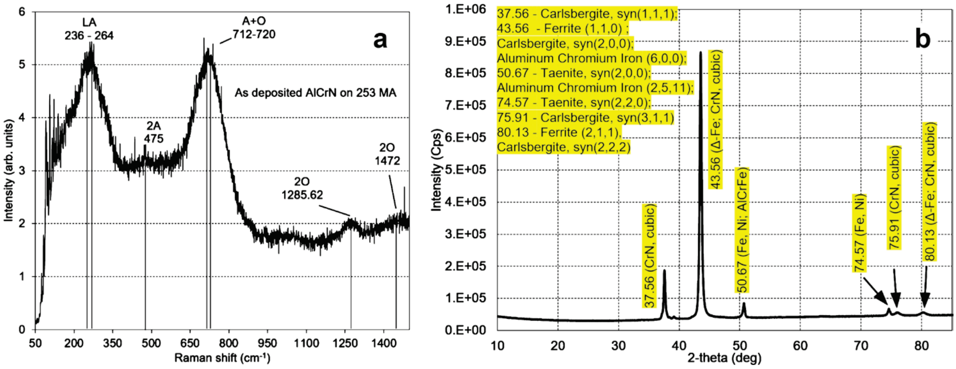

Figure 18. The Raman spectra of AlCrN PVD coated SS 253 MA (a) and the XRD pattern of AlCrN PVD coated AISI 316L (b) with indicated determined possible crystalline phases. It should be noted that selected XRD method was scanning in depth of about 30 µm and signals from substrate and interlayer may interact (data is combined from results described in Paper II and Paper III).

It is well known from theory that Gibbs free energy determines whether the process is advantageous, and the product is more stable ($\Delta G° < 0$) or a process is not advantageous, and a product is less stable ($\Delta G° > 0$). It also well known, that AlN is more thermodynamically stable than CrN due to a fact, that $\Delta G°_{AlN} = -287.4$ kJ·mol^{-1} is more negative value than $\Delta G°_{CrN} = -92.80$ kJ·mol^{-1}. These values inevitably lead to dominating decomposition of CrN and oxidation into Cr_2O_3 as observed in Raman spectra after static oxidation of the AlCrN PVD coating at all elevated temperatures. This effect can lead to and exceeded Al ratio of 0.71, causing dominating hexagonal wurtzite AlN phase in the AlCrN structure at the surface where the oxidation process reduces a concentration of CrN. It means that in tribo-corrosive conditions at elevated temperatures a counter-body slides in direct and apparent contact with dominating AlN in the AlCrN PVD coating structure with embedded or mechanically removed Cr_2O_3 particles. This situation occurs until applied tribo-corrosive sliding conditions exceed some limit, like AlN decomposition at the too high temperature or applied sliding speed. AlN is stable at room temperature due to a presence of a surface oxide layer with the thickness from 5 up to 10 nm. The oxidation rate of an AlN in air critically increases at temperatures above 700 °C, but the formation of not defective oxide layer leads to a protection of a bulk AlN at temperatures up to 1370 °C (Berger, 1996). However, this protection ability is limited in a case of the tested AlCrN PVD coating due to the presence of decomposing CrN, which leads to the formation of defects due to a growth of a Cr based oxides. Static oxidation of the AlCrN coating at 800 °C leads to a formation of α-Al_2O_3, as observed in the Raman spectra. It is well known, that it is complicated to determine a formation temperature of an α-Al_2O_3 phase due to many influencing factors like a crystalline phase of raw alumina, size of crystals, pH value, etc. Commonly, a formation of an α-Al_2O_3 occurs at about 1050 °C via kappa (κ-Al_2O_3), theta alumina (θ-Al_2O_3) (Ptáček, 2014) or at about 800 °C via diaspore (α-AlO(OH)). However, particle sizes of released free metallic Al from AlN due to the thermal or mechanical impact can induce a direct oxidation into α-Al_2O_3 phase at lower temperatures as well. Gibbs free energy of α-Al_2O_3 ($\Delta G°_{\alpha\text{-}Al2O3}$ = -1581 kJ·mol^{-1}) is more negative than $\Delta G°_{Cr2O3}$ = -1053 kJ·mol^{-1}. It leads to improved stability of an alumina over a wide range of temperatures under oxidative conditions. Significant microstructural modifications on the surface of the multilayered AlCrN PVD coating become induced at elevated temperatures from 800 up to 1100 °C causing changes in mechanical properties like hardness and wear resistance (Vancoille et al., 1994).

A hardness of a substrate and a thickness of a coating significantly influences the reliability of a given coating system under normal loading conditions due to a possible bending and a subsequent brittle fracturing. The indentation test was done on the AlCrN PVD coated SS 253 MA as demonstrated in Paper II. The indentation test result indicates the only deformation caused by Al_2O_3 counter-body at temperatures up to 900 °C and applied normal loads up to 10 N. It could be concluded that the selected SS 253 MA insignificantly affects the reliability of the selected AlCrN PVD coating in sliding wear applications under applied selected tribo-corrosive conditions. A high risk of the possible deformation of the SS 253 MA substrate during sliding was causing a great challenge for authors of Paper II in the selection of applied load to provide the measurable wear rate and to avoid a catastrophic failure of the AlCrN PVD coating at the same time.

Si_3N_4 and Al_2O_3 counter-bodies exhibit a highest CoF values at room temperature, while this value is highest for ZrO_2 at 800 °C. ZrO_2 exhibits a high sensitivity to environmental temperature and frictional heating. The final CoF was recorded relatively unchanged in a whole range of tested sliding speeds against Al_2O_3 counter-bodies at selected constant temperature, as demonstrated in Figure 14 a. However, initial roughness of the surfaces of the AlCrN PVD coating causes high values of CoF during the relatively short running-in period (up to 10 % of the beginning of the total applied test duration) of sliding against ZrO_2 and Al_2O_3 counter-bodies at 20 and 800 °C, respectively. A "smoothing" of the surface in the wear track or a development of a low-shear transfer film (Blau, 2005) leads to the decrease in CoF values by 15 % during the steady-state period. The lowest hardness of the ZrO_2 counter-body leads to more intensive abrasive wear in this study. Transformations and fracturing of the ZrO_2 lead to an accelerated wear of counter-body due to the higher hardness of fragments from the AlCrN coating. Generally, a continuous contact of the small area of counter-bodies causes an overheating and subsequent several orders of magnitude higher specific wear rate as compared with the long wear track of the AlCrN PVD coating.

Insignificant wear rates of the AlCrN PVD coating during sliding with low speeds from 0.002 up to 0.018 m·s^{-1} indicates removal of the asperities from the surface of the coating due to the micro-abrasion and adhesive wear. A presence, a formation, and properties of these asperities depends on the applied oxidative environmental temperatures and sliding speeds as demonstrated in Paragraph 3.3.2. (about static oxidation), Figure 11 and in Table 10 (about the effect of sliding on oxidation). An effect of the sliding speeds and temperatures on oxidation of the AlCrN PVD coating material in wear track was detected with a help of Raman spectroscopy and compared with the data after static oxidation. Results indicate maximum sliding speeds against Si_3N_4 counter-bodies of 0.486, 0.162 and 0.054 m·s^{-1} at 20, 300/500 and 800 °C, respectively at which coating is reliable. These ranges of tribo-corrosive conditions cause a formation of thermodynamically unstable (CrO_2, Cr_2O_5 and CrO_3) and stable (Cr_2O_3) oxides in wear tracks of the tested AlCrN PVD coating (Sánchez-López et al., 2014), even when lowest sliding speed (0.002 m·s^{-1}) at room temperature was applied. A presence of embedded Cr based oxides in the wear track of the AlCrN PVD coated SS 253 MA provides favourable solid lubrication.

The set of unlubricated sliding tests at room and elevated temperature oxidative conditions were done in present PhD work using the tribotester *CETR UMT-2* equipped with the high temperature sliding module *S21ME1000* (in use at TalTech since 2015). According to practical experience by using this equipment author of the thesis would like to highlight that undesirable difference in height of the surface of the disc can be measured after installation of the specimen in the tribotester as demonstrated in Figure 19 a. It is evident that the normal load in tribo-contact point increases when counter-body slides closer to the highest point on the disc causing increased wear rate of coating and vice versa. Usually, maximum difference is determined before the beginning of the test and testing with difference higher than 20 µm (with spring suspension) is not performed. The tribotester *CETR UMT-2* is equipped with the PID controller that collects data of measured changes in normal load from the load sensor and removes or add additional load during sliding to reduce the effect of height maximums. However, this parameter is useful when the disc rotates with a speed lower than 10 RPM and the system has enough time to react to changes in actual normal load as shown in Figure 19 b.

A failure of the tested AlCrN PVD coating (partial delamination) occurs, when applied sliding speeds exceed the reliable values under given tribo-corrosive conditions. A wear intensity of an SS may change from a mild to a severe wear regime when dominating oxidation mode (build-up layer) turns into a dominating adhesive wear due to an uncovered SS substrate. Mild wear condition can cause accelerated formation and thickening of oxide films due to the frictional heat and a wear rate of a coated material lower than oxide growth rate. A formation and growing of oxide scales evidently lead to an increased surface roughness of a coating and an SS due to an inhomogeneous structure, shapes, and sizes of oxide scales, especially in defected areas of a surface.

The formation of α-Al_2O_3 occurs in wear tracks during all sliding tests at 800 °C due to the oxidation similarly as it was determined by Raman spectroscopy after static oxidations tests at the same temperature. However, sliding speeds above reliable values were also causing a formation of α-Al_2O_3 at 300 and 500 °C due to the mechanically and frictional heating-initiated decomposition of AlN and oxidation of free Al into α-Al_2O_3. The result indicates that decomposed AlN and released Al particles become small enough to be directly subjected to the flash caused the temperature increase in combination with applied oxidative environment temperature of 300 and 500 °C, while a rise of bulk temperature of the AlCrN PVD coating is not so critically high.

When sliding speed exceeds the threshold of corresponding to reliable test conditions, the presence of α-Al_2O_3 causes unfavourable abrasive wear and the high CoF due to the lowest wear resistance in dry and lubricated conditions in comparison with Cr based oxides. It should be noted that oxidation of an AlN and fracturing of α-Al_2O_3 into particles initiates a release of hard Cr based oxides embedded or located between asperities of unoxidized and oxidized coating material during sliding. It leads to a presence of a large number of hard and an abrasive wear debris in a sliding contact responsible for vibration and high CoF.

Thermal and mechanical properties of oxide scales and a substrate influences the critical oxide scale thickness in a case of a mild sliding wear conditions. A bending of formed oxide scales may lead to a fracturing these scales parallel to a strong enough bonded interface and subsequent delamination. A fatigue of this interface leads to a dominating fracturing along a metal-oxide coating or oxide free ceramic coating-oxide layer interfaces. Heat flux in the sliding contact area can cause predictable delamination of formed oxide scales on the surface of the AlCrN PVD coating or at areas of an uncovered substrate due to the formation of thermal loading that causes critical thermal stress distribution. It should be noted that Cr oxidizes to Cr(VI) in an oxidizing environment (Johnson et al., 2007). A presence of Cr(VI) causes a formation of toxic and cancerogenic chromates in the soil, for example. Therefore, a formation and a durability of oxide scales may significantly influence not only the reliability of a coating in applied tribo-corrosive conditions, but also may cause environmental problems. Properly selected sliding speeds, applied loads and environmental conditions may lead not only to an increased lifetime of a coating but also can help to provide a reliability of a tool with a partially defected coating in a case of operation during common or unpredictable situations.

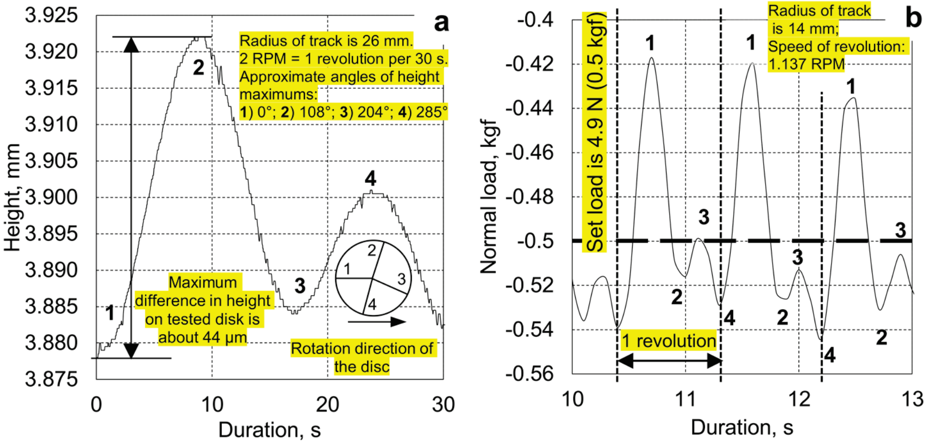

Figure 19. Example of the height measurement result on AlCrN PVD coated SS 253 MA disc done with the tribotester CETR UMT-2 equipped with S21ME1000 drive and the Al_2O_3 counter ball with the diameter of 6 mm (a); and fragment of measured fluctuation around applied normal load during sliding test against the same type of ball (b) with indicated height maximums and minimums on the tested disc.

3.7 Remarks about the standard ISO 18535:2016(E)

The recently published standard ISO 18535:2016(E) was applied for testing the amorphous tetrahedral carbon (ta-C) coated high speed steel received from the Faculty of Technology and Education, Koszalin University of Technology (Poland) to determine its suitability for testing at elevated temperatures and minimum thickness of the coating that is possible to test. The production method (deposition using the electromagnetic venetian blind plasma filter) and mechanical properties (Young's modulus and hardness) have been demonstrated in (Zavaleyev et al., 2017). The tested coating of ta-C is the type of the diamond-like carbon (DLC) film with the different thicknesses from 0.05 up to 1 µm.

Two different testing conditions are proposed by the standard for the determination of the friction and wear characteristics of DLC films at room temperature by a ball-on-disc method:

- Friction test – applied load of 3 N; sliding speed of 0.05 m·s^{-1}; and sliding distance of 200 m;
- Friction and wear test – applied load of 5 N; sliding speed of 0.1 m·s^{-1}; and sliding distance of 1000 m.

Friction and wear test (Al_2O_3 ball with the diameter of 6 mm was used as counter-body) conditions were applied at room temperature for testing the selected DLC coatings starting from the thickest one. The DLC coating with the thickness of 0.2 µm worn through during the test. It indicates the threshold thickness at which the selected type of the coating fails. A complete failure of the selected DLC coating with any tested thickness occurs during friction and wear tests at elevated temperatures (200 and 400 °C). Therefore, it was decided to apply a milder standardized friction test condition. Unfortunately, the standardized friction sliding test leads to a too small wear of the selected DLC coating at room temperature to be detected by the selected contact profilometer *Mahr Perthometer*. Thus, the minimum thickness of the coatings should be specified or the conditions for testing of ultra-thin coatings and coatings at elevated temperatures should be added.

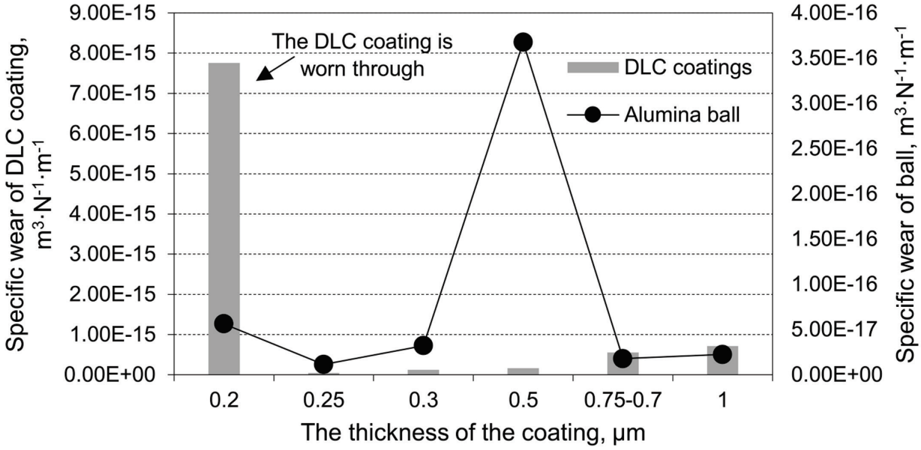

Figure 20. The specific wear of the DLC coating and Al_2O_3 counter-body measured by contact profilometer Mahr Perthometer (friction and wear test at the room temperature).

4 Conclusions

The main goal of the present PhD thesis was to apply and to develop reliability estimation methods for PVD coatings under corrosive and tribo-corrosive conditions and to improve the understanding about influencing factors arising from the production process, handling of parts and the laboratory testing.

Gradient TiCN and TiAlN, and multilayered AlCrN PVD coatings were studied in detail and the following conclusions can be drawn:

1. The multilayered AlCrN PVD coating exhibits the highest reactivity characteristic of the AlN and subsequent the highest protection efficiency (P_i = 99.79 %) after 24 h immersion in 3.5 wt% NaCl solution, due to the formation of the $AlOOH_{amorph}$ containing the passivating layer on the surface of the coating. Penetration of the aqueous solution and subsequent reaction passivates in about 13 h under static conditions. AlCrN PVD coating performs sufficiently better and indicates no failure even during extended (12 h) sliding test as compared with tested gradient TiCN or TiAlN coatings deposited onto the same SS AISI 316L substrate and under the same applied tribo-corrosive conditions (3.5 wt% NaCl solution and the normal load of 9.8 N or 1 kgf). Therefore, AlCrN PVD coating was selected for reliability estimation in high temperature applications.
2. The presence of surface defects on the multilayered AlCrN PVD coating causes no failure in static corrosive conditions (3.5 wt% NaCl aqueous solution). A reaction of AlN with the aqueous solution not only forms $AlOOH_{amorph}$ based protective layer, which passivates a penetration and a reaction, but also leads to the formation of effective lubricating particles in the sliding contact zone and works even more effective as CoF reducer under high 29.42 N (3 kgf) applied load and partially uncovered substrate (effectively detected during tests by OCP measurements) in the wear scar, as observed after tests by Raman spectroscopy and SEM.
3. The SS 253 MA substrate does not significantly oxidize up to 500 °C due to the oxidation resistance of thin Cr based oxide on the surface and due to the formation of the dense iron containing oxide scales. Cr_2O_3, Fe_3O_4, γ-Fe_2O_3 and (Fe, Cr) based spinel (detected by Raman spectroscopy after tests) form at higher temperatures up to 1100; these oxides can provide additional protection of the SS from oxidation (Fe_3O_4, γ-Fe_2O_3 and (Fe, Cr) based spinel) and the resistance to wear (Cr_2O_3).
4. Static oxidation of the AlCrN PVD coating mainly leads to the formation of the Cr_2O_3 at temperatures up to 800 °C due to the high stability of AlN. Severe microstructural modifications occur at temperatures from 800 up to 1100 °C. A part of the AlN turns into thermodynamically stable α-Al_2O_3 at 1100 °C, as determined by Raman spectroscopy.
5. The threshold sliding speeds against Si_3N_4 counter-bodies under applied normal load of 3 N at 20, 300/500 and 800 °C are 0.486, 0.162 and 0.054 $m\cdot s^{-1}$, respectively. The behaviour of the sliding tribopair is unreliable at higher sliding speeds, due to the failure of the coating. The presence of oxides from the oxidized SS substrate can be easy detected by Raman spectroscopy. Wear maps were made according to the obtained results.

6. The novel test method for reliability estimation of preliminarily scratched AlCrN PVD coating on SS 253 MA under high temperature sliding tribo-corrosive conditions was successfully developed on the base of two available testing standards ASTM C1624-05 and ISO 18535:2016(E). The scratch load (for Rockwell "C" indenter; progressive load test) until which the fracturing (buckling spallation) of the coating was avoided was found to be 19.61 N (2 kgf). Coated discs were subsequently preliminarily scratched with six different loads below the critical value. Sliding tests against Al_2O_3 counter ball results in:
   a. Occurrence of the favourable, neutral and unfavourable events were determined by SEM imaging and subsequently applied the load to Al_2O_3 counter ball was defined as an unfavourable in the case of the occurrence of any unfavourable event;
   b. The maximum reliable applied loads during sliding test for the loads applied during preliminary scratching by Rockwell "C" indenter determined during testing at room temperature are as follows: $F_{alumina}/F_{Rockwell\ “C”}$ of 11.77/1.96; 7.85/2.94; 7.85/4.9; 7.85/7.85; and 2.94/11.77 N/N;
   c. The maximum reliable applied loads during sliding test for the loads applied during preliminary scratching by Rockwell "C" indenter determined during testing at 500 °C are as follows: $F_{alumina}/F_{Rockwell\ “C”}$ of 7.85/1.96; 4.9/2.94; 2.94/4.9; and 2.94/7.85 N/N;
   d. The maximum reliable applied loads during sliding test for the loads applied during preliminary scratching by Rockwell "C" indenter determined during testing at 800 °C are as follows: $F_{alumina}/F_{Rockwell\ “C”}$ of 11.77/1.96; and 4.9/2.94 N/N.

References

Antonov, M., Hussainova, I., Adoberg, E., Effect of loading system inertia on tribological behaviour of ceramic–ceramic, ceramic–metal and metal–metal dry sliding contacts. *Tribology International*, 2013, 65, 207–214.

Antonov, M., Hussainova, I., Sergejev, F., Kulu, P., Gregor, A., Assessment of gradient and nanogradient PVD coatings behaviour under erosive, abrasive and impact wear conditions. *Wear*, 2009, 267 (5–8), 898–906.

Antonov, M., Michalczewski, R., Pasaribu, R., Piekoszewski, W., Comparison of a tribological model and real component test methods for lubricated contacts. *Estonian Journal of Engineering*, 2009, 15 (4), 349–358.

Ashby, M. F. *Materials selection in mechanical design* (4 ed.), 2011. Oxford, UK: Butterworth-Heinemann.

Ashby, M. F., Abulawi, J., Kong, H. S., Temperature maps for frictional heating in dry sliding. – *Tribology Transactions*, 1991, 34 (4), 577–587.

ASTM G59 - 97e1 Standard test method for conducting potentiodynamic polarization resistance measurements. In *Annual Book of ASTM Standards,* 1997, (p. 4). West Conshohocken.

ASTM G102 – 89 (2015) e1 - Standard practice for calculation of corrosion rates and related information from electrochemical measurements. In *Annual Book of ASTM Standards,* 2015, (p. 7). West Conshohocken.

Barshilia, H. C., Rajam, K. S., Raman spectroscopy studies on the thermal stability of TiN, CrN, TiAlN coatings and nanolayered TiN/CrN, TiAlN/CrN multilayer coatings. *Journal of Materials Research*, 2004, 19 (11), 3196–3205.

Barshilia, H. C., Selvakumar, N., Deepthi, B., Rajam, K. S., A comparative study of reactive direct current magnetron sputtered CrAlN and CrN coatings. *Surface and Coatings Technology*, 2006, 201 (6), 2193–2201.

Beake, B. D., Fox-Rabinovich, G. S., Progress in high temperature nanomechanical testing of coatings for optimising their performance in high speed machining. *Surface and Coatings Technology*, 2014, 255, 102–111.

Berger, L. I. *Semiconductor Materials* (1 ed.), 1996. Boca Raton, Florida, USA: CRC Press.

Blau, P. J., On the nature of running-in. *Tribology International*, 2005, 38 (11–12), 1007–1012.

Boucherit, N., Hugot-Le Goff, A., Joiret, S., Raman studies of corrosion films grown on Fe and Fe-6Mo in pitting conditions. *Corrosion Science*, 1991, 32 (5–6), 497–507.

Bowen, P., Highfield, J. G., Mocellin, A., Ring, T. A., Degradation of aluminum nitride powder in an aqueous environmet. *Journal of the American Ceramic Society*, 1990, 73 (3), 724–728.

Bull, S. J., Davidson, R. I., Harvathova, K., Mitchell, D., White, J. R., Preliminary investigation into the application of scratch testing to marine coatings. *Journal of Materials Science*, 2002, 37 (22), 4937–4943.

Chim, Y. C., Ding, X. Z., Zeng, X. T., Zhang, S., Oxidation resistance of TiN, CrN, TiAlN and CrAlN coatings deposited by lateral rotating cathode arc. *Thin Solid Films*, 2009, 517 (17), 4845–4849.

de Faria, D. L. A., Venâncio Silva, S., de Oliveira, M. T., Raman microspectroscopy of some iron oxides and oxyhydroxides. *Journal of Raman Spectroscopy*, 1997, 28 (11), 873–878.

Ding, X., Zeng, X. T., Liu, Y. C., Fang, F. Z., Lim, G. C., $Cr_{1-x}Al_xN$ coatings deposited by lateral rotating cathode arc for high speed machining applications. *Thin Solid Films*, 2008, 516 (8), 1710–1715.

Dinu, M., Mouele, E., Parau, A., Vladescu, A., Petrik, L., Braic, M., Enhancement of the corrosion resistance of 304 stainless steel by Cr–N and Cr(N, O) coatings. *Coatings*, 2018, 8 (4), 132–150.

Dwivedi, G., Wentz, T., Sampath, S., Nakamura, T., Assessing process and coating reliability through monitoring of process and design relevant coating properties. *Journal of Thermal Spray Technology*, 2010, 19 (4), 695–712.

Fenker, M., Balzer, M., Kappl, H., Corrosion protection with hard coatings on steel: Past approaches and current research efforts. *Surface and Coatings Technology*, 2014, 257, 182–205.

Fernández-Abia, A. I., Barreiro, J., Fernández-Larrinoa, J., Lacalle, L. N. L. de, Fernández-Valdivielso, A., Pereira, O. M., Behaviour of PVD coatings in the turning of austenitic stainless steels. *Procedia Engineering*, 2013, 63, 133–141.

Fischer, A., Mischler, S., Tribocorrosion: fundamentals, materials and applications. *Journal of Physics D: Applied Physics*, 2006, 39 (15), 3120–3219.

Friedrich, C., Berg, G., Senf, J., Broszeit, E., Reliable PVD coatings on components: aspects of deposition and characterization for quality management. *Surface and Coatings Technology*, 1999, 112 (1–3), 152–161.

Haboeck, U., Siegle, H., Hoffmann, A., Thomsen, C., Lattice dynamics in GaN and AlN probed with first- and second-order Raman spectroscopy. *Physica Status Solidi (C)*, 2003, (6), 1710–1731.

Holmberg, K., Reliability aspects of tribology. *Tribology International*, 2001, 34 (12), 801–808.

Ibrahim, M. A. M., Korablov, S. F., Yoshimura, M., Corrosion of stainless steel coated with TiN, (TiAl)N and CrN in aqueous environments. *Corrosion Science*, 2002, 44 (4), 815–828.

IEEE standard computer dictionary: a compilation of IEEE standard computer glossaries: 6101990. Inst of Elect & Electronic., 1990.

Ipaz, L., Aperador, W., Caicedo, J., Esteve, J., Zambrano, G., A practical application of x-ray spectroscopy in Ti-Al-N and Cr-Al-N thin films. In *X-Ray Spectroscopy*, 2012, (pp. 1–38).

ISO 13372:2012 - Condition monitoring and diagnostics of machines - Vocabulary. In *International Organization for Standardization*, 2012, (p. 15).

Jiang, J., Stack, M. M., Neville, A., Modelling the tribo-corrosion interaction in aqueous sliding conditions. *Tribology International*, 2002, 35 (10), 669–679.

Johnson, D. F., Jiang, D. E., Carter, E. A., Structure, magnetism, and adhesion at Cr/Fe interfaces from density functional theory. *Surface Science*, 2007, 601 (3), 699–705.

Joordens, J. C. A., D'Errico, F., Wesselingh, F. P., Munro, S., de Vos, J., Wallinga, J., Ankjærgaard, C., Reimann, T., Wijbrans, J. R., Kuiper, K. F., Mücher, H. J., Coqueugniot, H., Prié, V., Joosten, I., van Os, B., Schulp, A. S., Panuel, M., van der Haas, V., Lustenhouwer, W., Reijmer, J. J. G., Roebroeks, W., Homo erectus at Trinil on Java used shells for tool production and engraving. – *Nature*, 2015, 518 (7538), 228–231.

Jost, H. P., *Lubrication (tribology), education and research: a report on the present position and industry's needs.*, 1966. London, UK: H. M. Stationery Off.

Jubb, A. M., Allen, H. C., Vibrational spectroscopic characterization of hematite, maghemite, and magnetite thin films produced by vapor deposition. *ACS Applied Materials & Interfaces*, 2010, 2 (10), 2804–2812.

Kaindl, R., Franz, R., Soldan, J., Reiter, A., Polcik, P., Mitterer, C., Sartory, B., Tessadri, R., O'Sullivan, M., Structural investigations of aluminum-chromium-nitride hard coatings by Raman micro-spectroscopy. *Thin Solid Films*, 2006, 515 (4), 2197–2202.

Kawate, M., Kimura Hashimoto, A., Suzuki, T., Oxidation resistance of $Cr_{1-x}Al_xN$ and $Ti_{1-x}Al_xN$ films. *Surface and Coatings Technology*, 2003, 165 (2), 163–167.

Kimmari, E., Podgursky, V., Simunin, M., Adoberg, E., Surženkov, A., Viljus, M., Hartelt, M., Wäsche, R., Sildos, I., Kulu, P., Tribological behavior of carbon nanofibers deposited on hard nanocomposite (nc-$Ti_{1-x}Al_xN$)/(α-Si_3N_4) coating. *Surface and Coatings Technology*, 2013, 225, 21–25.

Laroudie, F., Tassin, C., Pons, M., Laser surface alloying of 316L stainless steel: different hardening routes and related microstructures. *Le Journal de Physique IV*, 1994, 04 (C4), C4-77-C4-80.

Lee, J. W., Radu, I., Alexe, M., Oxidation behavior of AlN substrate at low temperature. *Journal of Materials Science: Materials in Electronics*, 2002, 13 (3), 131–137.

Liew, W. Y. H., Jie, J. L. L., Yan, L. Y., Dayou, J., Sipaut, C. S., Madlan, M. F. Bin, Frictional and wear behaviour of AlCrN, TiN, TiAlN single-layer coatings, and TiAlN/AlCrN, AlN/TiN nano-multilayer coatings in dry sliding. In *Procedia Engineering,* 2013.

McCarty, K. F., Boehme, D. R., A Raman study of the systems $Fe_{3-x}Cr_xO_4$ and $Fe_{2-x}Cr_xO_3$. *Journal of Solid State Chemistry*, 1989, 79 (1), 19–27.

McHale, J. M., Surface energies and thermodynamic phase stability in nanocrystalline aluminas. *Science*, 1997, 277 (5327), 788–791.

Mo, J. L., Zhu, M. H., Sliding tribological behaviors of PVD CrN and AlCrN coatings against Si_3N_4 ceramic and pure titanium. *Wear*, 2009a, 267 (5–8), 874–881.

Mo, J. L., Zhu, M. H., Tribological oxidation behaviour of PVD hard coatings. *Tribology International*, 2009, 42 (11–12), 1758–1764.

Natesan, K., *Study of metal dusting phenomenon and development of materials resistant to metal dusting.* 2002. Argonne, IL.

Nirmal, U., Hashim, J., Megat Ahmad, M. M. H., A review on tribological performance of natural fibre polymeric composites. *Tribology International*, 2015, 83, 77–104.

Platt, P., Frankel, P., Gass, M., Howells, R., Preuss, M., Finite element analysis of the tetragonal to monoclinic phase transformation during oxidation of zirconium alloys. *Journal of Nuclear Materials*, 2014, 454 (1), 290–297.

Podgursky, V., Hantschel, T., Bogatov, A., Kimmari, E., Antonov, M., Viljus, M., Tsigkourakos, M., Vandervorst, W., Buijnsters, J. G., Raadik, T., Kulu, P., Rippling on wear scar surfaces of nanocrystalline diamond films after reciprocating sliding against ceramic balls. *Tribology Letters*, 2014, 55 (3), 493–501.

Ptáček, P., *Strontium aluminate - cement fundamentals, manufacturing, hydration, setting behaviour and applications* (P. Ptáček, Ed.), 2014. InTech.

Ramalho, A., A reliability model for friction and wear experimental data. *Wear*, 2010, 269 (3–4), 213–223.

Ricker, R. E., Can corrosion testing make the transition from comparison to prediction? *JOM*, 1995, 47 (9), 32–35.

Ricker, R. E., Papavinasam, S., Berke, N., Brossia, S., Dean, S. W., On using laboratory measurements to predict corrosion service lives for engineering applications. *Journal of ASTM International*, 2008, 5 (7), 101–350.

Roy, M., Pauschitz, A., Wernisch, J., Franek, F., Effect of mating surface on the high temperature wear of 253 MA alloy. *Materials and Corrosion*, 2004, 55 (4), 259–273.

Saeidi, K., Neikter, M., Olsen, J., Shen, Z. J., Akhtar, F., 316L stainless steel designed to withstand intermediate temperature. *Materials & Design*, 2017, 135, 1–8.

Saketi, S., Olsson, M., Influence of CVD and PVD coating micro topography on the initial material transfer of 316L stainless steel in sliding contacts A laboratory study. – *Wear*, 2017, 388–389, 29–38.

Samani, M. K., Chen, G. C. K., Ding, X. Z., Zeng, X. T., Thermal conductivity of CrAlN and TiAlN coatings deposited by lateral rotating cathode arc. *Key Engineering Materials*, 2010, 447–448, 705–709.

Sánchez-López, J. C., Contreras, A., Domínguez-Meister, S., García-Luis, A., Brizuela, M., Tribological behaviour at high temperature of hard CrAlN coatings doped with Y or Zr. *Thin Solid Films*, 2014, 550, 413–420.

Schlichting, K. W., Padture, N. P., Klemens, P. G., Thermal conductivity of dense and porous yttria-stabilized zirconia. *Journal of Materials Science*, 2001, 36 (12), 3003–3010.

Schütze, M., Mechanical properties of oxide scales. *Oxidation of Metals*, 1995, 44 (1–2), 29–61.

Sheikh-Ahmad, J., Morita, T., Tool Coatings for Wood Machining. In *15th International Wood Machining Seminar At: Los Angeles, CA*2001, (pp. 109–120).

Silverman, M., *How Reliable is Your Product?: 50 Ways to Improve Product Reliability.* 2012. Silicon Valley, California, USA: Super Star Press.

Stack, M. M., Antonov, M. M., Hussainova, I., Some views on the erosion–corrosion response of bulk chromium carbide based cermets. *Journal of Physics D: Applied Physics*, 2006, 39 (15), 3165–3174.

Tan, C. M., Goh, T. N. (Eds.), *Theory and practice of quality and reliability engineering in Asia industry,* 2017. Singapore: Springer Singapore.

Tomala, A., Ripoll, M. R., Badisch, E., Tool – solid lubricant – workpiece interactions in high temperatures applications. *Procedia Engineering*, 2013, 68, 626–633.

Tzanakis, I., Hadfield, M., Thomas, B., Noya, S. M., Henshaw, I., Austen, S., Future perspectives on sustainable tribology. *Renewable and Sustainable Energy Reviews*, 2012, 16 (6), 4126–4140.

Vancoille, E., Blanpain, B., Xingpu, Y., Celis, J.-P., Roos, J. R., Tribo-oxidation of a TiN coating sliding against corundum. *Journal of Materials Research*, 1994, 9 (04), 992–998.

VDI - The Association of German Engineers, *VDI 3198 - Coating (CVD, PVD) of cold forging tools.* 2013, (p. 8). VDI-Gesellschaft Produktion und Logistik.

Wang, L., Li, Y., Boundary for aviation bearing accelerated life test based on quasi-dynamic analysis. *Tribology International*, 2017, 116, 414–421.

Wang, L., Nie, X., Housden, J., Spain, E., Jiang, J. C., Meletis, E. I., Leyland, A., Matthews, A., Material transfer phenomena and failure mechanisms of a nanostructured Cr–Al–N coating in laboratory wear tests and an industrial punch tool application. *Surface and Coatings Technology*, 2008, 203 (5), 816–821.

Wood, R. J. K., Tribo-corrosion of coatings: a review. *Journal of Physics D: Applied Physics*, 2007, 40 (18), 5502–5521.

Wood, R. J. K., Marine wear and tribocorrosion. *Wear*, 2017, 376–377, 893–910.

Yaldiz, C. E., Veinthal, R., Gregor, A., Georgiadis, K., Mechanical properties of thin hard coatings on TiC-NiMo substrates. *Estonian Journal of Engineering*, 2009, 15 (4), 329–339.

Yang, M., Allen, A. J., Nguyen, M. T., Ralston, W. T., MacLeod, M. J., DiSalvo, F. J., Corrosion behavior of mesoporous transition metal nitrides. *Journal of Solid State Chemistry*, 2013, 205, 49–56.

Yoo, Y. H., Le, D. P., Kim, J. G., Kim, S. K., Vinh, P. Van, Corrosion behavior of TiN, TiAlN, TiAlSiN thin films deposited on tool steel in the 3.5 wt.% NaCl solution. *Thin Solid Films*, 2008, 516 (11), 3544–3548.

Zavaleyev, V., Walkowicz, J., Kuznetsova, T., Zubar, T., The dependence of the structure and mechanical properties of thin ta-C coatings deposited using electromagnetic venetian blind plasma filter on their thickness. *Thin Solid Films*, 2017, 638, 153–158.

Acknowledgements

First, I would like to express my gratitude to my supervisor’s professor Irina Hussainova and senior research scientist PhD Maksim Antonov from Department of Mechanical and Industrial Engineering for involving me in PhD research studies at TalTech and for their support, guidance and encouragement. A successful submission of together 13 publications in 4 study years would be impossible without share of energy.

I wish to express my sincere thanks to technician Heinar Vagiström for providing PVD coatings on stainless steel samples.

I also wish to express my gratitude to many people who helped me during my PhD research. Special thanks to PhD Mart Viljus, PhD Rainer Traksmaa, senior scientist PhD Valdek Mikli and associate professor Arvo Mere for the help and sometimes for their effort in emergency assistance with SEM and XRD scanning measurements.

I also want to thank every single one of my teachers at TalTech, especially to professor Priit Kulu. I’m very thankful for the time and effort you put into teaching and training me. For this, I am very grateful.

This journey to Tallinn and subsequent PhD would not have been possible without the support of my family and friends, especially from my friend Andrejs Šiškins.

My research was funded by the **Government** of the **Republic of Estonia** with the scholarship from Department of Mechanical and Industrial Engineering projects B56 "Innovative polycrystalline diamond (PDC) drag bit for soft ground tunnel boring machines (1.05.2016−30.04.2019)", and ETF8850 "Self-organisation of minerals based adaptive tribomaterials (1.01.2011−31.12.2014)".

This research was additionally supported by the Estonian Research Council under the personal grant PUT1063, Estonian Ministry of Higher Education and Research under project IUT19-29 and R&D project ETAG18012.

This work has been partially supported by ASTRA “TUT Institutional Development Program for 2016-2022” Graduate School of Functional Materials and Technologies (2014-2020.4.01.16-0032).

Abstract

Reliability Aspects of PVD Coatings Sliding under Wear and Corrosive Conditions

Complicated shaped steel parts have a good potential as replacements in the automotive and aerospace industries, however, they are severely affected by reliability related issues like decreased wear and corrosive resistance attracting much research interest. Physical vapour deposited (PVD) coatings deposited onto stainless steel (SS) substrate are known as having positive influence on a sliding wear resistance in tribopair with a ceramic counter-body. The coating was deposited by the lateral rotating cathode arc PVD technology on selected SS substrate.

In this study, the gradient layered TiCN and TiAlN, and multilayered AlCrN coatings have been employed as the protective layers for the austenitic SS AISI 316L used in aqueous tribo-corrosive conditions. Tribo-corrosive resistance was determined in 3.5 wt % NaCl aqueous solution by Raman spectroscopy and a potentiodynamic polarization scan. Static corrosion experiments were done to support the correlation between sliding contact surface chemistry, other properties, and measured tribological properties of the tested material. The description of the corrosion mechanisms responsible for surface degradation is presented. Results indicate the highest protection efficiency up to 99.79 % of AlCrN PVD coating after 24 h immersion in 3.5 wt% NaCl solution. That effect occurs due to the formation of the $AlOOH_{amorph}$ containing passivation layer with a solid lubrication effect in the sliding contact zone even under 29.4 N (3 kgf) applied normal load.

Raman spectroscopy was used to determine the sliding wear resistance of the SS 253 MA protected with the AlCrN PVD coating under high temperature oxidative conditions (25–800 °C). A correlation between physicochemical processes in the sliding contact surface and measured tribological properties of material was supported by static corrosion experiments. Results indicate an occurrence of severe microstructural modifications at static oxidation temperatures occurs from 800 up to tested 1100 °C mainly due to the formation of Cr_2O_3. Thermodynamically stable AlN in AlCrN structure provides the threshold sliding speeds against Si_3N_4 counter-bodies under applied normal load of 3 N at 20, 300/500 and 800 °C is 0.486, 0.162 and 0.054 $m \cdot s^{-1}$, respectively.

The corrosion mechanisms responsible for surface degradation are reported in detail and wear maps were made according to the obtained results. The presented results can be helpful for prediction of the reliable conditions in tribological sliding applications of AlCrN coating.

An innovative method was also proposed and assessed for estimation of the reliability of mechanically influenced (scratched) PVD coatings for high temperature tribo-corrosive sliding applications. Maps of the dependence of wear related events on the applied preliminarily scratch and subsequent sliding test normal load were made, revealing reliable regimes at room and elevated (500 and 800 °C) temperatures.

Lühikokkuvõte
PVD pinnete töökindluse aspektid liughõõrdumise ja korrosiooni tingimustes

Keerulise kujuga terasdetailide kasutamisel autotööstuses ja kosmosetööstuses on suur potentsiaal, kuid seda mõjutavad oluliselt töökindlusega seotud probleemid, nagu madal kulumis- ja korrosioonikindlus. Siit ka suur huvi antud uurimistöö järele. On teada, et füüsikaline aursadestus (PVD, ingl. k) tõstab oluliselt roostevaba terase kulumiskindlust ja nad töötavad paremini hõõrdepaaris keraamilise pindega liughõõrde tingimustes.

Antud uuringus kasutati kaitsepinnetena TiCN ja TiAlN gradientpindeid ning mitmekihilisi AlCrN pindeid AISI 316L roostevabal terasel tööks tribo-söövitavates vedelikes. Pinded sadestati katoodlahendusega kaarleekaursadestusmeetodil seadmel Platit π80. Pinnete paksus oli 3.3 µm. Vastupanu tribo-korrosioonile määrati NaCl vesilahuses (3.5 massi %) Raman-spektroskoopia abil ja potentsiodünaamilise polarisatsiooni meetodiga. Staatilised korrosioonikatsed kinnitasid libiseva kontaktpinna keemilise omapära ja katsetatud materjali mõõdetud triboloogiliste omaduste vahelist korrelatsiooni. Selgitati välja pinnete hävimise tribo-korrosioonimehhanismid. Tulemused näitasid, et mitmekihilistel AlCrN pinnetel on suurim kaitsetõhusus (kuni 99.79 %) 24-tunnise katsetuse jooksul NaCl 3.5 massi % vesilahuses. See on põhjustatud libisevas kontaktsoonis passiivse (amorfse) AlOOH kihi moodustumisega, mis toimib tahke määrdeainena (see tuvastati isegi 29.4 N (3 kgf) normaalkoormusel).

Raman-spektroskoopia abil uuriti AlCrN pinde kulumiskindlust 253 MA roostevabal terasel toa- ja kõrgel temperatuuril (25-800 °C) oksüdeerivates liughõõrde tingimustes. Staatiliste korrosioonikatsetel leidis kinnitust korrelatsioon libiseva kontaktpinna füüsikalis-keemiliste protsesside ja materjali mõõdetud triboloogiliste omaduste vahel. Tulemused viitavad märgatavatele mikrostruktuursetele muutustele staatiliste oksüdeerumiskatsete jooksul temperatuuridel 800 kuni 1100 °C, ja mis on põhjustatud peamiselt Cr_2O_3 moodustumisega. Termodünaamiliselt stabiliilne AlN AlCrN pinde struktuuris liughõõrdel vastu räninitriid (Si_3N_4) kontrakeha normaalkoormusega 3 N temperatuuridel 20, 300/500 ja 800 °C tagab töökindluse piirkiirustel vastavalt kuni 0.486, 0.162 ja 0.054 $m{\cdot}s^{-1}$.

Pinde hävimise vastutavad korrosioonimehhanismid on üksikasjalikult kirjeldatud ja saadud tulemuste põhjal on koostatud kulumisdiagrammid. Saadud tulemused võivad olla kasulikud AlCrN-pinnete töökindluse prognoosimiseks triborakendusvaldkondades.

Pinnete töökindluse seisukohalt pakuti ka uuenduslik meetod mehaaniliselt mõjutatud (kriimustatud) PVD-pinnete triboloogilistes rakendustes sobivuse hindamiseks tööks toa- ja kõrgetel temperatuuridel. Töökindluse ja kulumisega seotud nähtuste tuvastamiseks ja hindamiseks eelnevalt kriimustatud ja hiljem katsetatud pinnete jaoks koostati kulumisdiagrammid toa- ja kõrgel (500 ja 800 °C) temperatuuridel liughõõrde tingimustes.

Appendix

PAPER I

Baronins, J., Podgursky, V., Antonov, M., Bereznev, S., Hussainova, I., Electrochemical behaviour of TiCN and TiAlN gradient coatings prepared by lateral rotating cathode arc PVD technology. *Key Engineering Materials*, 2016, 721, 414–418.

Key Engineering Materials
ISSN: 1662-9795, Vol. 721, pp 414-418
doi:10.4028/www.scientific.net/KEM.721.414
© 2017 Trans Tech Publications, Switzerland

Submitted: 2016-05-31
Revised: 2016-07-23
Accepted: 2016-08-02
Online: 2016-12-01

Electrochemical Behaviour of TiCN and TiAlN Gradient Coatings Prepared by Lateral Rotating Cathode arc PVD Technology

Janis Baronins[1,a *], Vitali Podgursky[1,b], Maksim Antonov[1,c], Sergei Bereznev[2,d] and Irina Hussainova[1,3,e]

[1]Department of Materials Engineering, Tallinn University of Technology, Estonia

[2]Department of Materials Science, Tallinn University of Technology, Estonia

[3]ITMO University, Kronverksky 49, St. Petersburg, 197101, Russian Federation

[a]Janis.Baronins@ttu.ee, [b]Vitali.Podgurski@ttu.ee, [c]Maksim.Antonov@ttu.ee,
[d]Sergei.Bereznev@ttu.ee, [e]Irina.Hussainova@ttu.ee

Keywords: PVD, gradient coating, electrochemical corrosion, protection, tribocorrosion

Abstract. TiCN and TiAlN gradient coatings were deposited on the AISI 316L stainless steel substrates by lateral rotating cathode arc (LARC) physical vapour deposition (PVD) technology. Corrosion and tribocorrosion behaviour was studied in 3.5 wt. % NaCl solution. The thickness of coatings was about 3 μm. For both coatings the corrosion potential shifted to more positive values as compared to the uncoated substrate. The corrosion current density decreased for TiCN and TiAlN coatings indicating up to 40 folds higher polarization resistance. The coefficient of friction value of TiCN coating is three times lower and durability is six times higher than that of TiAlN coating under the same tribocorrosion conditions.

Introduction

It is well known that in the corrosive medium the breakdown of the films occurs due to crevice corrosion, pitting, galvanic corrosion, inter-granular corrosion, selective leaching, erosion-corrosion and chemical stress corrosion [1]. In addition to water, steel corroding chlorides (e.g. NaCl, KCl, $CaCl_2$, etc.) are the most common chemicals in nature, thus stress corrosion caused by chlorides (expansion caused cracking) requires careful examination [1–3].

Transition metal nitrides hard coatings are widely used in industry due to high hardness, high electrically conductivity and good corrosion resistance [4]. However, coatings are often affected by corrosion due to chemicals used in aggressive environments. Therefore corrosion resistance of coatings is important topic nowadays [2,3]. Merl et al. [3] have proposed that the corrosion takes place on the macro- and micro-defects (pinholes, porous structure, etc.) in physical vapour deposited (PVD) coatings, where solution can reach substrate. However, macrodefects like inclusions on the coating surface is not always a place of the breakdown in corrosion resistance tests [3]. In a case of non-voluntary or limited voluntary wetting [5] it takes longer time for water intrusion and for corroding chloride ions to penetrate into pores and other types of defects.

Antonov et al. [6] have investigated gradient and non-gradient PVD coatings (TiCN, TiAlN, etc.) on cemented carbide substrate. The gradient deposition technology allows improving the adhesion between coating and substrate. PDV coatings could be applied to various substrates like metals, ceramics, cermets, polymers, and diamonds influencing the performance of final product.

Despite the fact, that TiCN and TiAlN coatings are tested against tribocorrosion, there are much less available publications about tribocorrosion of gradient type TiCN and TiAlN hardcoatings.

Depending on microstructure defects, the corrosion resistance of hard coatings like TiN and TiAlN can protect steel, leading to trans-passive state exhibition in NaCl solution [7]. Tribocorrosion is a combined surface degradation process in corrosive medium where tribological and electrochemical actions take place simultaneously [8,9]. The aim of the preliminary study is to find the PVD gradient coating (deposited onto stainless steel AISI 316L) with a highest protective efficiency against corrosion and tribocorrosion in 3.5 wt. % NaCl solution to assist the selection and development of coatings for wear applications in corrosive medium, e.g. as a hard coating for drilling equipment for use in marine or similar conditions with a presence of water.

Experimental methods

Preparation of samples. The flat samples of stainless steel AISI 316L (25×15×5 mm) were polished with SiC sandpaper down to 0.5 µm. Substrates were cleaned with isopropanol for 50 min by using ultrasonic bath. The samples were sputter-cleaned in argon plasma with the bias voltage -850 V at 425 °C for 1h. TiCN and TiAlN (with the Al content of 60 at. %) coatings were deposited onto substrates in nitrogen atmosphere using a lateral rotating cathode arc (LARC) technology (Platit π-80 unit). The deposition temperature for both coatings was 450 °C.

Specimens are marked as following: uncoated (bare) stainless steel AISI 316L as reference (*R*), samples coated with TiCN (*A*) and TiAlN (*B*). All tests were repeated at least three times.

Structural characterization of coatings. A scanning electron microscope (SEM) *Hitachi TM1000* equipped with energy-dispersive X-ray spectroscopy (EDS) was used for investigation of the surface morphology. The thickness of coating was measured by kalotest method with the *kaloMAX* tester in accordance with ball cratering technique developed by *BAQ* (Germany).

Potentiodynamic polarization test. Potentiodynamic polarization measurements were performed in 3.5 wt. % NaCl solution in the three electrode cell using a saturated calomel reference electrode (SCE) and platinum (Pt) counter electrode (CE) with a working surface area of 2 cm^2. Specimens, isolated with a non conductive silicone, leaving an exposed surface area of about 1 cm^2 were used as working electrodes (WE). *Autolab PGSTAT30* galvanostat - potentiostat system with *General Purpose Electrochemical System* (*GPES*) software (*Metrohm Autolab B.V.*, Netherlands) was used for data recording and processing. After the open circuit potential (OCP) stabilization the limits of linear sweep voltammetry were set as -0.7 and 0 V (except for reference sample after 24 h immersion a range was from -0.8 to 0 V) by selecting a scan rate 5 mV·s^{-1}.

Penetration rate *CR* (the thickness loss per unit of time [mm·year^{-1}]), protective efficiency P_i [%], porosity *F* [%] of coating, the polarization resistances of the substrate and coating-substrate systems R_{pm} and R_p were calculated according with methods described in standard [10] and research work by Yoo et al [11].

Tribocorrosion test at open circuit potential. Tribocorrosion experiments were carried out with a Universal Micro Materials Tester (*UMT-2*) from *CETR* (*Bruker*) in a reciprocating mode (amplitude $1 \cdot 10^{-3}$ m, frequency 1 Hz) with a stationary ball located above specimen (wear debris may remain in wear scar). All tests were done at ambient atmosphere environment (23±2 °C, relative humidity 30±5 %). Specimen was fixed to a reciprocating table equipped with an electrochemical cell as shown in Fig.1 a. Electrochemical cell was filled with 50 ml 3.5 wt. % NaCl solution, ensuring 1 cm level of liquid above the specimen connected to potentiostat as WE. Standard Ag/AgCl as RE and Pt as CE were used to provide a three electrode setup. *EmStat*$^{3+}$ potentiostat with *PSTrace* software (*PalmSens BV*, Netherlands) was used for data recording and processing. Specimen was isolated with a non conductive silicone, leaving 1 cm^2 of exposed surface area. Prior to the wear test, sample was cleaned step by step with acetone, ethanol and then dried. Created system was stabilized for 1 h before starting the test. Recorded test was divided into three periods: (1) stabilization (1000 seconds), (2) tribocorrosion (7200 s) and passivation (1000 s). A zirconia (ZrO_2) ceramic ball with a diameter of 1 cm, made of high purity yttria-stabilized zirconia (YSZ, 95 % ZrO_2, 5 % Y_2O_3) manufactured by *Tosoh/Nikkato* corporation (Japan) with a surface roughness R_a = 0.03 µm (measured by *Mahr* perthometer, *PGK 120*, contact mode, according to DIN EN ISO 4287) was used as counter-body. Applied load was 9.8 N (1 kg).

Results and discussion

Microstructural characterization. SEM image of the as-deposited TiAlN coating surface morphology is shown in Fig.1 b. Defects including macroparticles (inclusions), voids and pinholes with sizes mostly less than 10 µm were observed on the surfaces of coated specimens. Therefore, a relatively slow water and chloride ions intrusion in the coating can be expected due to limited pore wetting and chloride ions diffusion. The cross-section SEM images (not shown) of about 3 μm thick coatings (measured by kalotest method) show that TiAlN is more defected (containing more cracks, pores, etc., mainly due to the inclusions in the middle of a dense coating) as compared to TiCN one.

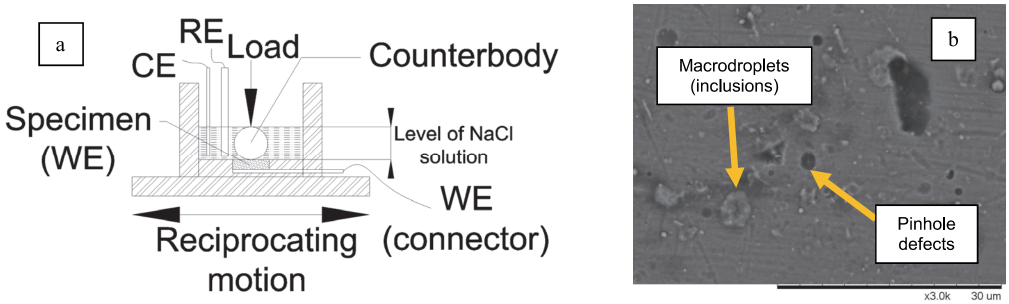

Fig.1. Schematic drawing of tribocorrosion test (a) and SEM micrograph of as-deposited coating TiAlN (b)

Potentiodynamic polarization test. Tafel plots, obtained for steel substrate and coated specimens, are shown in Fig.2 (after 10 min. and after 24 h immersion). Potentiodynamic polarization data from *GPES* is shown in Table 1. The corrosion potential (E_{corr}) of the steel substrate is about -0.357 V vs. SCE and corrosion current i_{corr} is 1.793 μA·cm^{-2}. TiCN and TiAlN coatings after 10 min. immersion show that E_{corr} shift towards the positive values (-0.185 and -0.177 V vs. SCE) with up to 20 folds lower i_{corr} as compared to AISI 316L. After 24h immersion in 3.5 wt. % NaCl solution, E_{corr} shift towards the negative side for all samples, indicating a loss of oxide layer protection for bare steel (sample *R*) and more intensive penetration of corrosive solution toward substrate for TiCN and TiAlN coatings, remaining one to three folds better pore resistance (see Table 1) as compared to AISI 316L. After 24 h immersion, the TiCN coating with E_{corr} = -0.40 V vs. SCE shows a higher pore resistance ($1.15 \cdot 10^5$ Ω·cm^{-2}) as compared to TiAlN coating ($2.24 \cdot 10^3$ Ω·cm^{-2}).

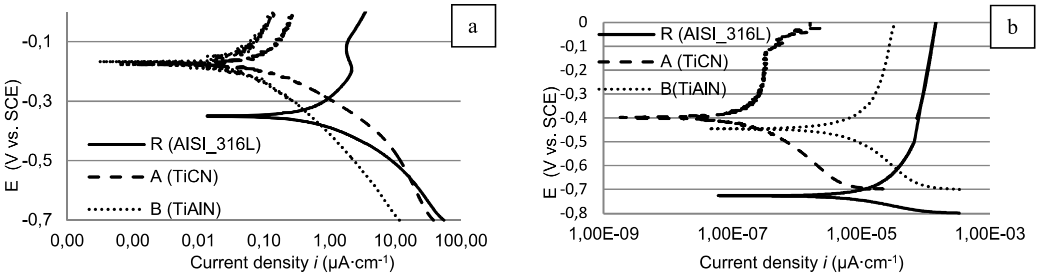

Fig.2. Potentiodynamic polarization curves (Tafel plots) of tested specimens, (a) – after 10 min. immersion, (b) – after 24 h immersion

In contrast to the SEM results (Fig. 1b), a lowest porosity (about 0.012 %) and highest protection efficiency (P_i) (about 95 %) are obtained for TiAlN (sample *B*) as shown in Table 1. The TiCN coating shows similar performance to TiAlN one, conforming the high inertness of transition metal nitrides and carbonitrides [4,7,12].

Tribocorrosion test. Evolution of OCP before, during and after wear tests of reference sample *R* (AISI 316L) sample *A* (TiCN) and sample *B* (TiAlN) is presented in Fig.3 a. The graph shows a significant drop in OCP of coated specimens from a moment when load was applied and reciprocating motion was started. OCP of bare steel (sample *R*) already reached close to maximum negative OCP during stabilization period. For all samples, there was no visible passivation after removal of mechanical load. TiCN shows best performance in given tribocorrosion conditions.

Table 1. Potentiodynamic polarization data of specimens tested in 3.5 wt. % NaCl solution after 10 min and 24h immersion. Penetration rate (*CR*), protective efficiency (P_i) and porosity (*F*) are also shown

	Potentiodynamic polarization measurements					**Calculation results**		
	E_{corr}	i_{corr}	β_a	β_c	R_{pm}, R_p	*CR*	P_i	*F*
	[V]	[μA·cm^{-2}]	[V·decade^{-1}]	[V·decade^{-1}]	[Ω·cm $^{-2}$]	[mm·year^{-1}]	[%]	[%]
R_{10m}	-0.36	1.79	0.079	0.147	$1.23\cdot10^4$	$3.746\cdot10^{-3}$	-	-
R_{24h}	-0.73	4.26	0.064	0.047	$3.25\cdot10^2$			
A_{10m}	-0.19	0.19	0.093	0.303	$1.60\cdot10^5$	$8.432\cdot10^{-4}$	89.24	0.510
A_{24h}	-0.40	1.15	0.113	0.254	$1.15\cdot10^5$			
B_{10m}	-0.18	0.09	0.159	0.354	$5.27\cdot10^5$	$4.94\cdot10^{-4}$	94.98	0.012
B_{24h}	-0.45	2.95	0.105	0.138	$2.24\cdot10^3$			

Note: X_{10m}, X_{24h} – after 10 min and 24 h immersion; *R* – reference; A – TiCN; B – TiAlN; β_a, β_c – anodic and cathodic slopes in Tafel plot. Deviations E_{corr} not more than ± 0.08 V, i_{corr} – not more than ± 0.10 A.

Three times lower and more stable coefficient of friction (COF) (0.25-0.30) for TiCN coating was found after 1300 s as compared to TiAlN coating and bare steel. A OCP shifting toward negative side with a simultaneous small increase in COF for TiCN (sample *A*) is observed after about 3500 s; removed macro droplets from coating during sliding led to loss of corrosion protective efficiency (Fig.3 b). TiAlN coating significantly lost protective efficiency at the same time when load and sliding was applied; after 1200 s substrate has become unprotected in wear zone, reaching OCP -0.78 V vs. Ag/AgCl due to significantly removed TiAlN coating and created micron sized cracks as shown in Fig.3c. It could be concluded that TiCN coating exhibits three times lower COF value and six times longer protection of substrate as compared with TiAlN coating under the same tribocorrosion conditions mainly due to less defective structure.

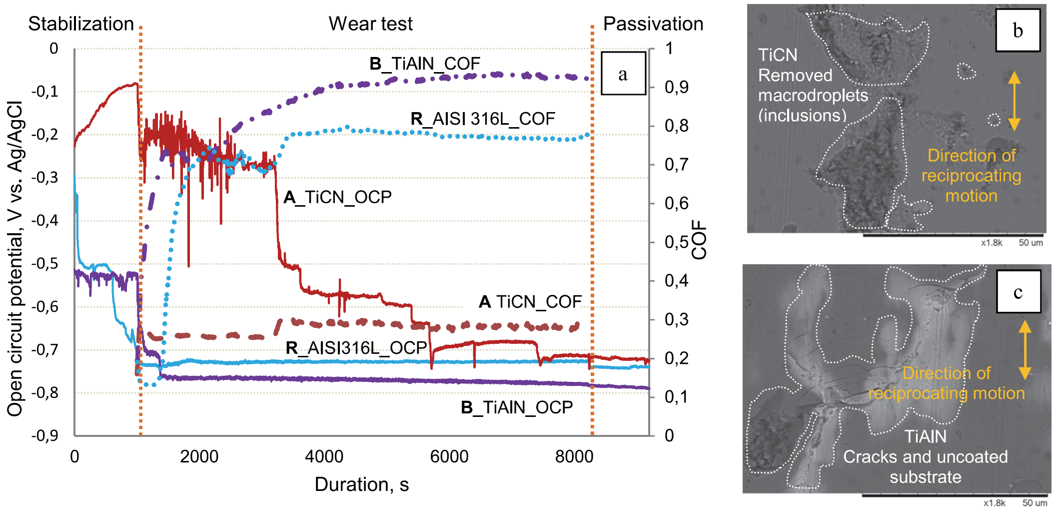

Fig.3. Evolution of COF and open-circuit potential (vs. Ag/AgCl) (a), SEM images of wear tracks after tribo-corrosion tests on TiCN (b) and TiAlN (c) coatings

Conclusions

It was found that in case of gradient PVD coatings with thickness of 3 μm:

1) TiAlN coating ensure best performance during short (10 min.) immersion in the 3.5 wt. % NaCl solution, providing up to almost 95 % higher protective efficiency as compared to the bare steel grade 316L;
2) TiCN coating is providing higher pore resistance ($1.15 \cdot 10^5\ \Omega \cdot cm^{-2}$) due to less shifting corrosion potential toward more negative potential (reaching -0.40 V vs. SCE) after long time (24 h) immersion as compared to TiAlN and bare steel;
3) COF of TiCN coating is three times lower (0.25-0.30) and durability (corrosion protective efficiency) is six times longer than for TiAlN coating and bare steel under the same tribocorrosion conditions;
4) TiCN coating is mainly losing only embedded particles, remaining from PVD process, while TiAlN coating is partially lost and damaged in tribocontact (wear scar).

Acknowledgements

This work was supported by base funding provided to R&D institutions by the Estonian Ministry of Education and Research, project number B56. Additionally this work was supported by the Estonian Research Council under PUT1063 (I. Hussainova) and the Estonian Ministry of Education and Research under target financing projects IUT 19-29 and IUT 19-28.

References

[1] M.M.C. and A.E. Claudia Marcela Méndez, Ares, Developments in Corrosion Protection, InTech, 2014.

[2] L. Zhang, Y. Chen, Y. Feng, S. Chen, Q. Wan, J. Zhu, Electrochemical characterization of AlTiN, AlCrN and AlCrSiWN coatings, Int. J. Refract. Met. Hard Mater., 53 (2015) 68–73.

[3] D.K. Merl, P. Panjan, M. Panjan, M. Čekada, The Role of Surface Defects Density on Corrosion Resistance of PVD Hard Coatings, Plasma Process. Polym., 4 (2007) 613–617.

[4] M. Yang, A.J. Allen, M.T. Nguyen, W.T. Ralston, M.J. MacLeod, F.J. DiSalvo, Corrosion behavior of mesoporous transition metal nitrides, J. Solid State Chem., 205 (2013) 49–56.

[5] S.H. Yoon, Membrane Bioreactor Processes: Principles and Applications, CRC Press, 2015.

[6] M. Antonov, I. Hussainova, F. Sergejev, P. Kulu, A. Gregor, Assessment of gradient and nanogradient PVD coatings behaviour under erosive, abrasive and impact wear conditions, Wear, 267 (2009) 898–906.

[7] M.A.M. Ibrahim, S.F. Korablov, M. Yoshimura, Corrosion of stainless steel coated with TiN, (TiAl)N and CrN in aqueous environments, Corros. Sci., 44 (2002) 815–828.

[8] S. Mischler, Triboelectrochemical techniques and interpretation methods in tribocorrosion: A comparative evaluation, Tribol. Int., 41 (2008) 573–583.

[9] D. Landolt, S. Mischler, M. Stemp, Electrochemical methods in tribocorrosion: a critical appraisal, Electrochim. Acta, 46 (2001) 3913–3929.

[10] ASTM, ASTM G59 - 97e1 Standard Test Method for Conducting Potentiodynamic Polarization Resistance Measurements, ASTM International, West Conshohocken, 1997.

[11] Y.H. Yoo, D.P. Le, J.G. Kim, S.K. Kim, P. Van Vinh, Corrosion behavior of TiN, TiAlN, TiAlSiN thin films deposited on tool steel in the 35 wt% NaCl solution, Thin Solid Films, 516 (2008) 3544–3548.

[12] R. Marchand, F. Tessier, F.J. DiSalvo, New routes to transition metal nitrides: and characterization of new phases, J. Mater. Chem., 9 (1999) 297–304.

PAPER II

Antonov, M., Afshari, H., **Baronins, J.**, Adoberg, E., Raadik, T., Hussainova, I., The effect of temperature and sliding speed on friction and wear of Si_3N_4, Al_2O_3, and ZrO_2 balls tested against AlCrN PVD coating. *Tribology International*, 2018, 118, 500–514.

Tribology International 118 (2018) 500–514

Contents lists available at ScienceDirect

Tribology International

journal homepage: www.elsevier.com/locate/triboint

The effect of temperature and sliding speed on friction and wear of Si_3N_4, Al_2O_3, and ZrO_2 balls tested against AlCrN PVD coating

M. Antonov [a,*], H. Afshari [a], J. Baronins [a], E. Adoberg [a], T. Raadik [b], I. Hussainova [a,c,d]

[a] *Department of Mechanical and Industrial Engineering, Tallinn University of Technology, Ehitajate Tee 5, 19086, Tallinn, Estonia*
[b] *Department of Materials and Environmental Technology, Tallinn University of Technology, Ehitajate Tee 5, 19086, Tallinn, Estonia*
[c] *ITMO University, Kronverksky 49, St. Petersburg, 197101, Russian Federation*
[d] *University of Illinois at Urbana-Champaign, Department of Mechanical Science and Engineering, Urbana, IL, 61801, USA*

ARTICLE INFO

Keywords:
PVD coating
Coefficient of friction
Sliding
Wear map
High temperature
3D printing

ABSTRACT

Advanced modern materials are required to operate at challenging conditions including mutual interactions under pressure and at elevated temperatures. In the present work, unidirectional sliding tests were performed to evaluate the wear behaviour of tribo-couple of AlCrN PVD coating deposited onto a stainless steel substrate and Si_3N_4, Al_2O_3, and ZrO_2 ceramic balls counterbodies at different speeds ranged from as low as 0.002 up to as high as 1.458 m s^{-1} and temperatures from 20 up to 800 °C. The wear scars were studied with the help of 3D optical surface profilometry, scanning electron microscopy, energy-dispersive and Raman spectroscopy. Bulk and flash temperatures conditioned by sliding were analytically calculated. The wear mechanisms responsible for surface degradation are detailed.

1. Introduction

The developments toward uncompromising efficiency in nowadays industry are mainly constrained by the availability of suitable high performance materials that can withstand extreme conditions such as combined effect of elevated temperatures, oxidative or corrosive environment, wear related issues, etc. During the last 30 years there has been a growing interest to 3D printing (class of additive manufacturing) of objects made out of plastic, metallic, ceramic and/or composite materials due to efficient spending of resources with close to zero wastage, ability to produce complex shapes especially those that cannot be produced by subtractive manufacturing processes [1,2]. The 3D printed parts have already been used in aerospace, automotive, biomedical, energy and other fields [2]. The tools working at high temperature corrosive wear conditions that could be produced by 3D printing are, for example, stop and control valves for chemical, petrochemical and power generation industry, jet engine parts, sliding bearings with complicated shape, piston rings, etc. [3,4]. Stainless steels are typically used for such kind of applications due to relatively easy process of machining into precision components. The widespread of ceramic components, however, is greatly limited due to brittleness and associated high risk of unpredictable failure. As an alternative to ceramic components, the 3D printed stainless steel parts protectively coated by a thin ceramic layer can improve the performance (reducing the risk of galling) of a tool [4,5]. The final component produced usually possesses sufficient toughness, wear resistance, durability and easy handling.

In many unlubricated or lubricated tribological application the dissimilar materials of tribocouple are showing better performance if compared to self-mated sliding materials [6–10]. Self-mated metals can suffer from extremely high adhesion while self-mated ceramics can suffer from abrasion due to formation of wear debris [6,7]. Thus, it is reasonable to pay attention to the tribocouple composed of solid ceramic sliding against a coated metal. The development of highly efficient internal combustion engines (reciprocating or rotary) made predominantly from ceramics can be closer to realization when some parts (piston rings, for example) are substituted by 3D printed parts enhanced by coatings. A cylinder lining has to be made from ceramics due to their low weight (density) and low thermal conductivity to provide higher efficiency of fuel burning and minimize heat losses and exclude the necessity of water-cooling [11,12]. The most studied materials candidates for ceramic engine applications are Si_3N_4, ZrO_2 and Al_2O_3 [11,12]. The speed of piston movement is not constant but cyclic including all speeds from idle to maximum.

The main failure of cutting tools at high cutting speeds is caused by cracking of a thermal origin due to a high level of thermal shock caused by high speeds and high degree of temperature variations in and at close

---

* Corresponding author.
E-mail address: Maksim.Antonov@ttu.ee (M. Antonov).

http://dx.doi.org/10.1016/j.triboint.2017.05.035
Received 30 September 2016; Received in revised form 25 May 2017; Accepted 26 May 2017

proximity to a cutting contact area [13]. To increase reliability of cutting and metal forming tools, hard protective coatings are widely used. Important requirements are sufficient hardness, high wear-, corrosion-, and oxidation resistance as well as good thermal stability [14,15]. It was demonstrated that in high speed cutting applications, the temperature in a contact area can rise over 900 °C [16]. Therefore, a physical vapour deposition (PVD) of CrN coating, which has been extensively used for cutting tools, is not the best candidate suitable for these applications due to lack of tolerance to the relatively high temperatures (above 600 °C) [17,18]. Different materials have recently been tested in order to find the best solution for this issue. One of such solutions is AlCrN PVD coating successfully applied for high speed cutting tools and other industries due to a high wear resistance, an improved oxidation resistance, a relatively high hot hardness and a low heat conductivity combined with an enhanced thermal stability at elevated temperatures up to 900 °C [15,17–23].

The PVD AlCrN coatings have been studied in many ways to understand their tribological behaviour in a contact with a different counterpart sliding materials [15,17,21–24]. However, the most of the studies have been performed at the conditions of relatively low temperatures and sliding speeds. Therefore, there is the need for the more comprehensive studies at higher temperatures and in the wide range of sliding speeds.

In a present work, a commercial PVD AlCrN coated stainless steel 253 MA discs sliding against Si_3N_4, Al_2O_3 and ZrO_2 balls at temperatures from 20 °C to 800 °C were tested. Sliding speeds in a range between 0.002 and 1.458 m s^{-1} were selected to analyse the effect of a frictional heat (and flash temperatures generated) on the coefficient of friction, wear rate and mechanisms of material degradation. Rise of bulk and flash temperatures was calculated to provide some hints on the mechanism of wear. Based on the results of the tests, the wear and coefficient of friction graphs and maps were constructed. The data obtained is of special importance for further research and industrial needs. Further research (focused ion beam micromachining for transmission electron microscopy, X-ray diffraction at various temperatures, Auger spectroscopy, elevated temperature indentation and scratch testing, etc.) can help to provide deeper understanding of tribolayer formation.

2. Experimentals

2.1. Materials

The micro-alloyed high temperature oxidation resistant stainless steel 253 MA (EN 1.4835, supplied by *Outokumpu*) discs were coated by multilayered AlCrN PVD coating with the help of the arc ion plating technique in Platit π80 unit. The selected 253 MA stainless steel has sufficiently high Young's modulus to provide support for the coating even at high temperatures (200, 155 and 120 kN mm^{-2} at 20, 600 and 1000 °C, respectively) and can be used in tribological applications at 800 °C [25,26]. It was concluded in Ref. [27] that the doubling of the hardness of PVD coating steel substrate (by laser hardening) provides only 5–25% decrease in wear rate depending on type of coating investigated. The substrates were cleaned in ultrasonic bath with an alcohol and then sputter-cleaned in argon plasma inside a coating chamber. The Cr adhesion and gradient CrN interlayers were used in order to provide the sufficient adhesion of AlCrN coating to the substrate. The multi-layered structure of alternated layers with 0.6 and 0.5 aluminium content was produced by varying the Cr cathode arc current as specified in Table 1. The adhesion of coating was graded as class 1 according to VDI 3198 (cracking without adhesive delamination of the coating). The thickness of AlCrN coating was 3 μm while thickness of Cr + CrN layers was about 0.3 μm (determined by *BAQ GmbH* KaloMAX ball cratering device according to EN1071-2007). The selected deposition conditions are given in Table 1. The thickness of one layer (with Al content being either 0.6 or 0.5) were calculated to be around 25 nm based on the total thickness and number of layers specified in the deposition receipt. The ratio of Al/(Al + Cr) in the coating and use of alternated layers was selected to provide the optimum combination of hardness and fracture toughness [20,28]. The coating has face-centered cubic (CrN) structure while transition to hexagonal (AlN) structure is possible in coating with higher Al content (when Al content is more than 0.6, according to at. %) [29].

Table 1
Details of deposition conditions for AlCrN PVD coating.

Parameter	Value
Substrate temperature, °C	450
Substrate bias voltage, V	−40 to −120
Cathode arc current, A	130 (Al) 65-80 (Cr)
Theoretical Al content acc. to at. % of metals in coating (Al/(Al + Cr))	0.6–0.5
Processing time, minutes	120

The discs tested were of 60 mm in diameter and 5 mm thick. The parallelism of flat surfaces was obtained by automatic grinding. Subsequently, the required roughness was reached using a Phoenix 4000 (*Buehler*) sample preparation system by applying SiC sandpaper. The samples were rotated to obtain multidirectional grinding pattern. The surface roughness (Ra), measured according to DIN EN ISO 4287 (by *Mahr* perthometer, PGK 120, contact mode) was 0.03 μm for Si_3N_4, Al_2O_3, ZrO_2 balls and 0.06 μm for AlCrN hard coating. Low roughness of surfaces (Ra 0.005 μm) is required for convenient measurement of wear rates of materials [30] while real components have significantly higher roughness (Ra 0.05–2.00 μm) to provide adequate lubrication, due to limitations of technological equipment or in order to provide cost effectiveness [31,32]. The roughness of tested samples was selected to be closer to that found for the industrially used devices. Silicon nitride (β-Si_3N_4 - 92.2, Y-3.5, Al-3.5, Ti-0.8 wt. %) and alumina balls (α-Al_2O_3 - 99.5 wt. %) with indication of their main properties were supplied by *Redhill Precision*, Czech Republic. Zirconia ball was made of high purity yttria-stabilized tetragonal zirconia (YSZ, 95% ZrO_2, 5% Y_2O_3, *Tosoh/Nikkato corporation,* Japan). Main properties of the coating and the balls are listed in Table 2. The hardness and modulus of elasticity of the AlCrN coating were measured by *Micro Materials* NanoTest NTX nano-indentation device with the help of diamond Berkovich tip calibrated with fused silica reference sample. The additional sample with the AlCrN coating was deposited (with the same settings as for 253 MA substrate) onto WC-10 wt. % Co substrate to provide adequate support during testing. The load was 30 mN with indentation depth around 200 nm. The depth of indentation was selected to constitute about 7% of the coating thickness (to reduce the influence of the substrate) while to penetrate about 8 layers with varied Al content (to provide averaged properties of the multi-layered structure). The hardness and modulus of elasticity of deposited AlCrN coating (Table 2) are very similar to those of the same coating produced by the same technology (hardness - 33.5 GPa; modulus of elasticity - 610 GPa [23]). Most of the properties for balls were taken from their batch datasheets provided by suppliers. The hardness of AlCrN coating with Al content of 0.5 is almost not influenced by annealing up to temperatures of 800 °C [33]. The AlCrN coating and zirconia have the highest and the lowest hardness, respectively, among all materials studied. The materials have relatively low fracture toughness as compared to metals. AlCrN and zirconia have the lowest thermal conductivity that provide conditions for high thermal gradients and overheating along the contact areas. All balls have higher maximum service temperature than coating (900 °C) or substrate (due to softening at these temperatures).

The particular attention was paid to tribological testing of silicon nitride balls while alumina and zirconia balls were tested only at 20 and 800 °C for comparison. Silicon nitride has the average wear rates (among selected balls) that could be measured with a high precision and was suitable for estimation of the effect of both variables (test temperature and sliding speed). No polishing of the coating was performed.

Table 2
Main properties of tested materials (coating and balls).

	fcc-AlCrN	β-Si_3N_4	α-Al_2O_3	Tetragonal ZrO_2 (YSZ)
Hardness at 20 °C, GPa	30.6 ± 2.8	15	15	10.5
Fracture toughness K_{IC}, MPa $m^{0.5}$	6.4 [19]	6.9	3.9	6.0
Young's modulus of elasticity, GPa	585 ± 54.7	308	370	210
Poisson's ratio	0.30 [23]	0.29	0.24 [36]	0.32 [36]
Thermal conductivity at 20 °C, W m^{-1} K^{-1}	1.5 [34]	21	31	3 [37]
Maximum service temperature, °C	900 [23]	1100 [35]	1200 [35]	1200 [35]
Density, kg m^{-3}	–	3240	3860	6000
Thermal diffusivity, x 10^{-6} m^2 s^{-1}	–	8.0 [36]	8.5 [36]	0.9 [36]

2.2. Flash and bulk temperature calculations

For better understanding of conditions during sliding test, the analytical equations detailed in Ref. [38] were used to estimate the rise of bulk and flash temperatures of balls. The "bulk temperature" means the temperature on the surfaces when frictional heat is injected uniformly across the apparent contact area. In reality, however, the frictional heat is injected over the real contact area that is usually much smaller than an apparent contact area. Therefore, the temperature at the actual contact areas can be considerably higher; and it is referred to as a "flash temperature" [38]. These temperatures were calculated for room temperature sliding tests by applying the data provided in Table 2 and by using the friction coefficients and size of wear scars obtained during the current work. The size of contact area in the beginning of the test was calculated according to conventional Hertzian contact stress theory while results of real measurements of wear scars were used for calculation of temperatures at the end of test.

2.3. Experimental

Tests were performed in an ambient atmospheric condition (with oxygen) using the tribological device setup CETR/Bruker - UMT2 equipped with S21ME1000 drive (Fig. 1) according to ASTM G99-05. Before each test, the surface of disk and ball was cleaned with ethanol and acetone and then dried. The ball diameter was 10 mm; load was 3 N to provide initial maximum contact pressure close to 1 GPa. Disc with AlCrN coating was fixed on a rotational table in a chamber equipped with resistive heaters. Stationary ball was located above the disk that reduce the possibility of the wear debris to escape from wear scar [39,40]. In systems where the debris can more easily escape, once they are generated (ball is located below the specimen) the tribological results can vary from those observed in present work. A heating rate of 6 °C min^{-1} was used to avoid possible thermal shock to test materials and equipment. Test temperatures were selected to be 20 °C, 300 °C, 500 °C and 800 °C. Intermediate temperatures should provide some softening (reduction of brittleness) of the balls while the highest test temperature is close to maximum service temperature for AlCrN and substrate. However, the temperature of the contact point for the balls is also influenced by the sliding speed (Tables 3 and 4). The range of sliding speeds (from 0.002 to 1.458 m s^{-1}) was selected to provide the minimum and an extreme heating due to sliding. The speed of each next step is 3 times higher than that of the previous step. This somehow compensates the fact that various radiuses of wear tracks are used for testing. When two nearest tracks are compared then the difference in radius is only 10–20% while the difference in speed is 300%. That is why the testing with track of varied radius should not influence the wear mechanism (generation of wear debris, growth of tribolayer, etc.) to great extent. Duration of the test was selected to ensure that the running-in period is less than 30% of the total test duration. Stabilized coefficients of friction at the end of test were stated and used for calculation of rise in bulk and flash temperatures. The tests were repeated at least twice and the average values are stated.

The diameter of ball's wear scars was measured by using optical microscope *Zeiss* Discovery. V20 equipped with AxioVision software. It was confirmed by 3D optical profilometer *Bruker* ContourGT-K0+ that wear scars of balls are flat. The volume loss of the ball was calculated according to ASTM G99-05 by using diameter of wear scar and diameter of the ball as input variables. The same 3D profilometer was used for investigation of wear rates (scan of the 3D topography of the portion of the wear track, setting of the zero plane and automatic volumetric wear calculation) and topography of wear scars of AlCrN coating.

Microstructural examination of specimens was conducted by a scanning electron microscope (SEM) *Hitachi* TM-1000 (Japan) and *Zeiss* EVO MA15 scanning electron microscopes equipped with energy dispersive spectroscopy (EDS) module.

Raman spectral measurements were made at room temperature (after static oxidation or sliding test) with a help of a high resolution micro-

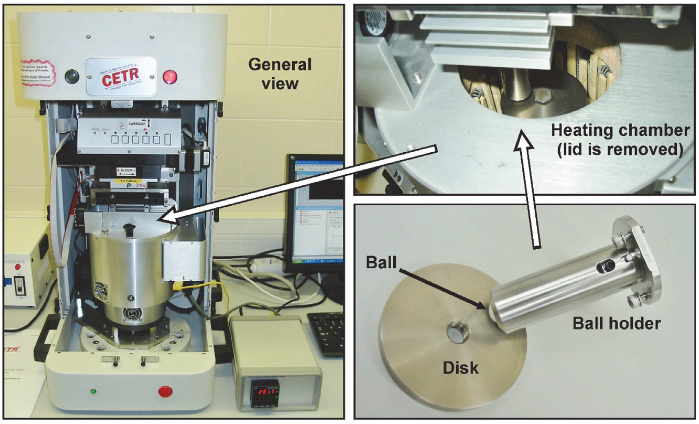

Fig. 1. Universal tribometer CETR/Bruker – UMT2 equipped with S21ME1000 heating chamber.

Table 3
Test parameters.

Sliding speed, m s^{-1}	Track radius, mm	Time, min	Sliding distance, m	Number of revolutions
0.002	10	180.0	21.6	343
0.006	12	133.5	48.1	637
0.018	14	99.1	107.0	1217
0.054	16	73.5	238.1	2369
0.162	18	54.5	529.7	4684
0.486	20	40.4	1178.1	9375
1.458	22	30.0	2624.4	18986

Table 4
Calculated rise of temperatures for bulk material and flash temperature of balls sliding against AlCrN coating during room temperature tests.

Sliding speed, m s^{-1}	Si_3N_4			Al_2O_3			ZrO_2		
	Rise of bulk temp. (°C)		Rise of flash temp. (°C)	Rise of bulk temp. (°C)		Rise of flash temp. (°C)	Rise of bulk temp. (°C)		Rise of flash temp. (°C)
	Start	End	From start till end	Start	End	From start till end	Start	End	From start till end
0.002	2	<1	7	<1	<1	4	3	<1	12
0.006	5	<1	22	2	<1	10	11	1	48
0.018	14	1	64	7	2	32	34	3	170
0.054	41	2	194	20	4	96	104	5	596
0.162	106	3	562	54	9	283	265	11	1914
0.486	257	5	1627	137	11	861	597	8	>3000
1.458	514	11	>3000	302	14	2544	1136	7	>3000

Raman spectrometer (*Horiba Jobin Yvon* HR800) equipped with a multichannel Charge-coupled device (CCD) detection system set in the backscattering configuration. An Nd-YAG induced laser (λ = 532 nm) with a spot size of 10 μm in diameter was used for excitation. Laser beam power was changed with a help of filters D1 (2.8 mW; factor was 0.0912; used for Si_3N_4, Al_2O_3, ZrO_2) and D0.3 (15.8 mW; factor was 0.5147; used for 253 MA, AlCrN, Si_3N_4) to obtain a clear Raman spectra at different reflection intensities from different surfaces. The same material before and after experiment was usually investigated with the same laser beam power (if effect of transfer layer was not significant). The samples

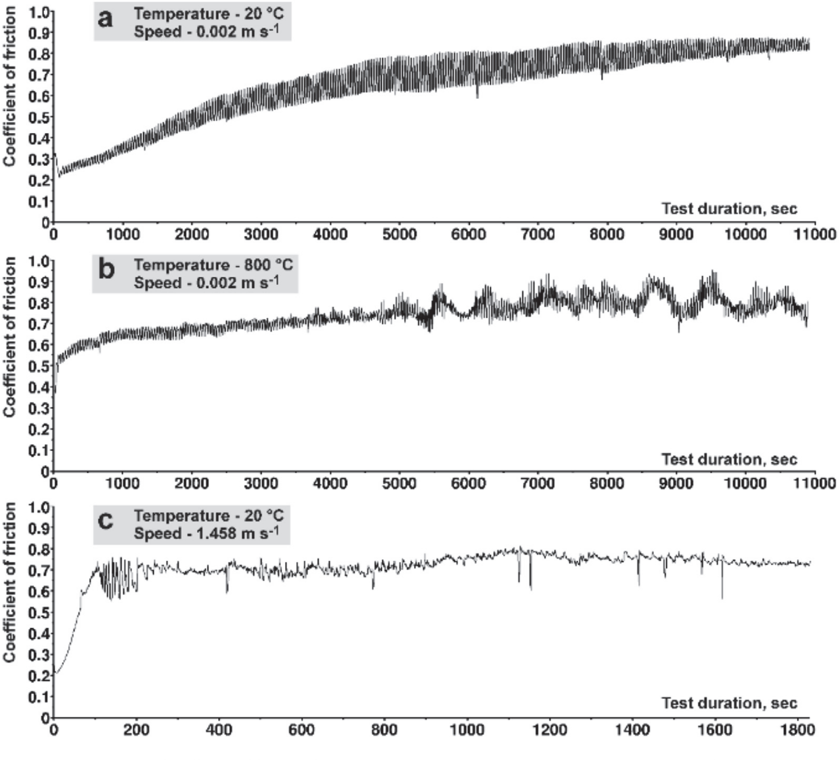

Fig. 2. Representative graphs of coefficient of friction of Si_3N_4 ball tested against AlCrN coating. Test temperature and sliding speed are indicated.

subjected to static oxidation (2 h at 300 °C, 500 °C and 800 °C) were also investigated in addition to those tested by sliding.

3. Results

3.1. Effect of temperature and sliding speed on coefficient of friction and wear rate of balls

Fig. 2 represents the typical variation of coefficient of friction (CoF) as a function of the test duration and temperature for AlCrN coating sliding against Si_3N_4 ball at all temperatures, Al_2O_3 ball at 20 °C and ZrO_2 ball at 800 °C. The curves are characteristic of a dry couple having a small amount of surface oxide or adsorbed species that is quickly worn away to cause a rise in friction [41]. The ZrO_2 ball at 20 °C and Al_2O_3 ball at 800 °C have slightly higher (max 15%) CoF value during running-in period for a short period of time (max 10% of test duration after starting) that is conditioned by an initial roughness of the surface. A high value of CoF is keeping until “smoothing” of the surface or development of a low-shear transfer film [41].

The longest duration of running-in period was exhibited by Si_3N_4 ball tested at room temperature with the lowest speed (0.002 m s^{-1}). Increase in temperature or sliding speed usually leads to shortening of the

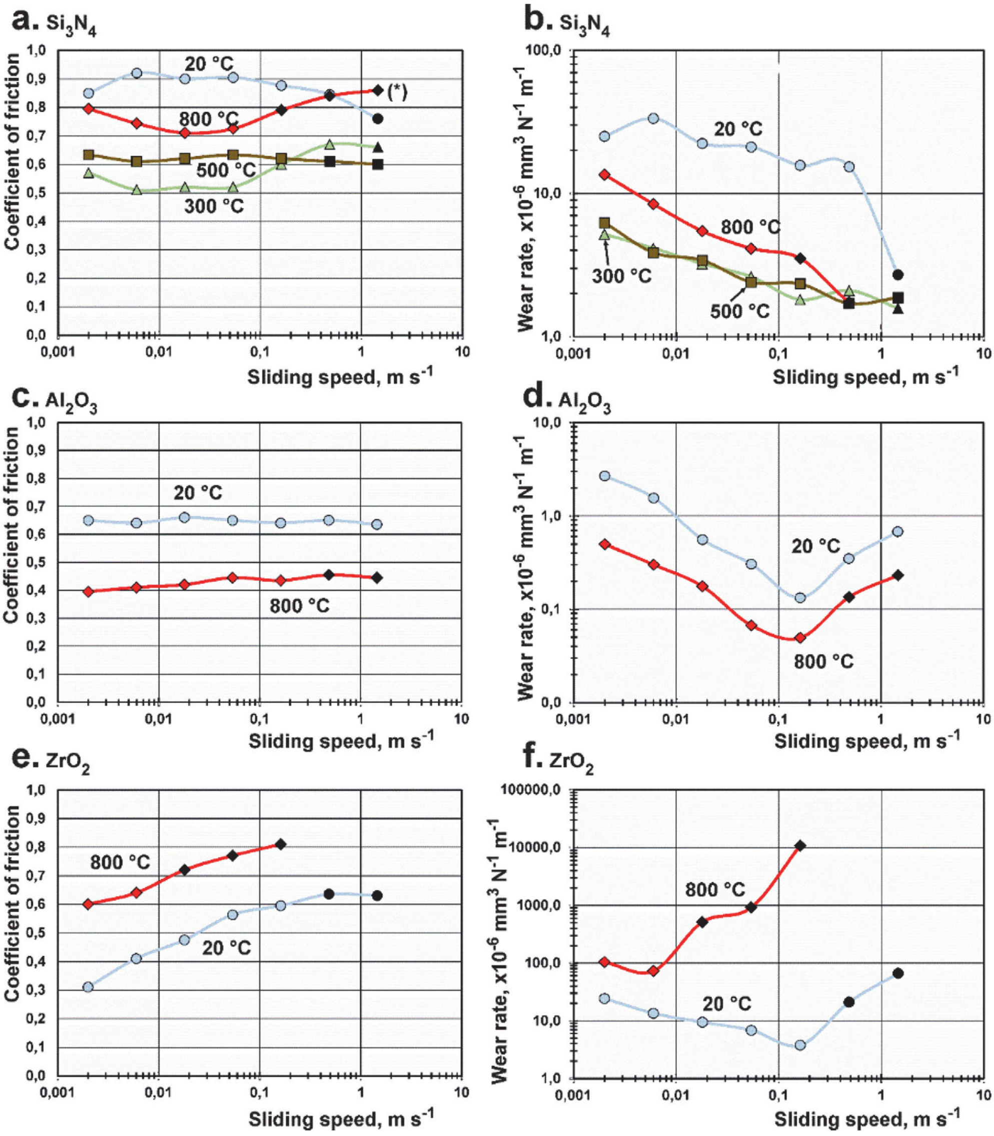

Fig. 3. Curves showing the effect of sliding speed and temperature on CoF and wear of tested balls sliding against AlCrN coating. The markers filled with black colour are indicating that the AlCrN coating was partially or substantially worn through. (*) The test at 800 °C with speed of 1.458 m s^{-1} was run for only 10% of test duration and was stopped due to undesirably high vibration and noise.

duration of running-in period.

The wear rate of AlCrN coatings in the range from 0.002 to 0.018 m s^{-1} was insignificant and is attributed to removal of the asperities from an untouched surface due to micro-abrasion and/or adhesive wear [42]. Precise repeatable measurements of wear rates of AlCrN coating (even with the help of high-precision optical 3D profilometer) was unattainable that is in accordance with the previous studies of the same coating [23]. In the current study, the authors were trying to avoid overloading of the tribocouple (i.e. to make accelerated test enabling the measurable wear rate) due to a high risk of substrate deformation and accompanied change of wear mechanisms. Taking into consideration wear rates of the similar PVD coated disks studied by authors (0.2–20.0 × 10^{-15} mm^3 N^{-1} m^{-1}), it is possible to conclude that wear of balls is several orders of magnitude higher as compared to the coated disks [39]. It can be explained by the fact that ball is always in a contact with material and, therefore, experiences continuous overheating while the coating has some time for cooling between the subsequent sliding events. At various speeds the transfer of ball material to the AlCrN coating was observed (material gain or build-up). The absence of transfer film at mean sliding speed of 0.01 m s^{-1} was observed in case of diamond film testing with same types of balls [43]. Tests with speed of 0.486 and 1.458 m s^{-1} (especially at elevated temperatures) were accompanied by undesirably high vibration and noise and usually were leading to the partial or substantial fracturing of the AlCrN coating. Transition from mild-to-severe wear is expected for the same speed and pressure for alumina [36].

The effect of sliding speed and temperature on coefficient of friction and wear rate of the balls is presented in Fig. 3. The ball of Si_3N_4 exhibits the highest CoF at room temperature in the whole range of speeds tested; alumina has the average and zirconia shows the lowest CoF similarly to [44]. At 800 °C, the lowest CoF is provided by alumina while the CoF of zirconia is approaching that of silicon nitride. The low CoF of alumina balls can be attributed to development of Cr_2O_3 and Al_2O_3 oxide passivation layers on the surface of coating [23,24]. The lowest

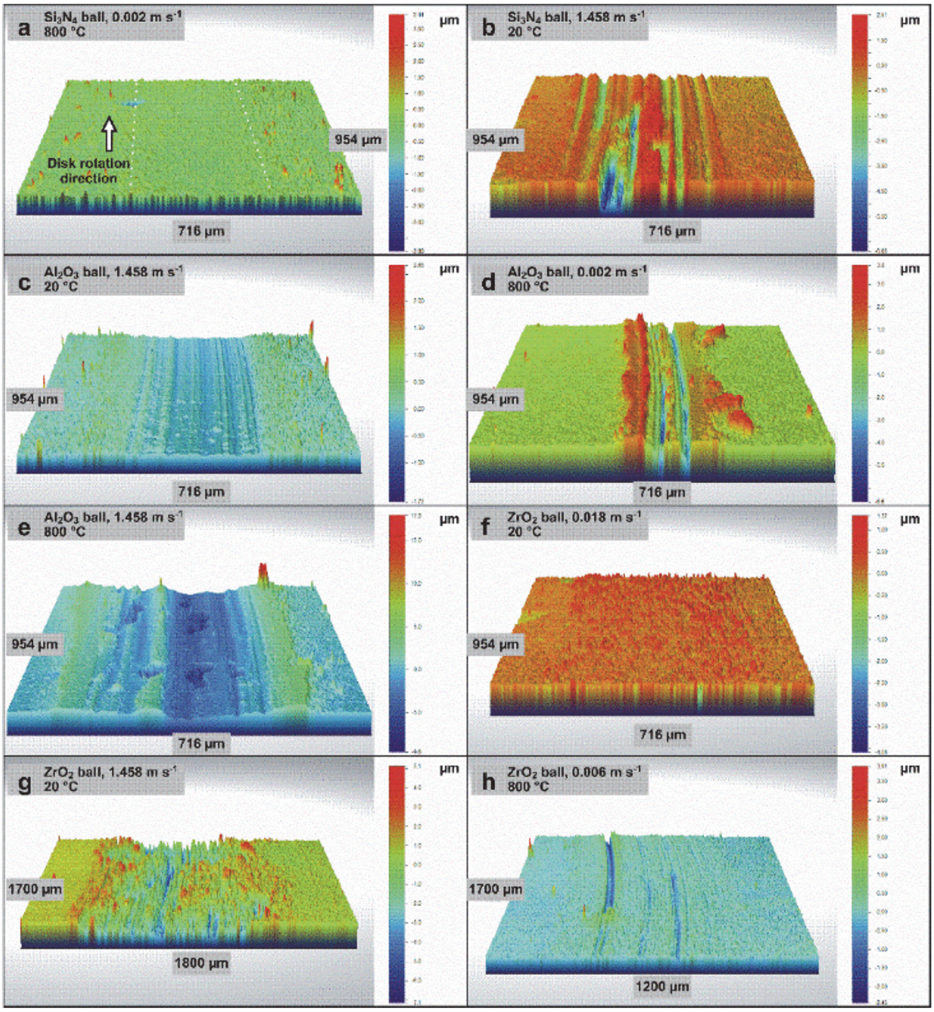

Fig. 4. 3D optical images of AlCrN coating wear tracks after completed tests. Ball material, sliding speed and test temperature are indicated.

coefficients of friction for silicon nitride were observed during tests at 300 or 500 °C. Generally, the CoF of Si_3N_4 decreases with an increase in sliding speed while at the highest speeds (when fracturing of AlCrN coating is initiated) the tendency does not follow the general trend any longer, Fig. 3a. The low CoF at room temperature and the lowest speed is associated with collection of wear debris providing possibility for rolling and due to insufficient test duration and significant effect of running-in period (Figs. 3a and 2a). Silicon nitride and alumina show the highest CoF when tested at room temperature, while zirconia has the highest CoF at 800 °C. The CoF of zirconia is higher at high sliding speeds and temperatures. This allows to make conclusion that zirconia is very sensitive to the temperature and both, a test temperature or a heat generated by frictional heating, are responsible for the rise in the coefficient of friction. Besides, zirconia has the lowest hardness among the materials studied and an abrasive wear takes place.

The high CoF usually results in the high wear rates. In general, all balls show some decrease in the wear rate with an increase in the sliding speed from 0.002 to 0.162 $m\ s^{-1}$ (Fig. 3). This is valid for wear rate units expressed as “$mm^3\ N^{-1}\ m^{-1}$“; however, when the sliding distance is not taken into consideration and the units of wear rate are expressed as “$mm^3\ s^{-1}$”, the wear rate increases with an increase in sliding speed as it was shown in Ref. [42]. Silicon nitride usually demonstrates a decrease in wear rate at the highest speed in contrast to alumina and zirconia, which show an increase in the wear rates. In the case of alumina, this behaviour is associated with a brittle fracture due to increased vibration (mechanical shocks). The accelerated wear of zirconia is conditioned by transformations and fracture of the counterbody coating because hard fragments of a damaged coating can cause the abrasive wear.

Partial or substantial failure of coating (Fig. 3, black markers) at higher temperatures is initiated at lower speeds (than at room temperature) due to the frictional heating (Table 4). The coefficient of friction and the wear of alumina ball tested at 800 °C are comparable to results obtained by other researchers [23]; however, the CoF and wear rate obtained during current study at room temperature is somewhat higher as compared to previously reported that can be explained by difference in a substrate material (WC-Co in Ref. [23]) or roughness of coating (polished by 0.05 μm alumina suspension). Results shown in Refs. [17,18] are similar to those obtained during current study at room temperature for Si_3N_4 ball.

3.2. Analytical calculations of bulk and flash temperatures

The result of bulk and flash temperature calculations are presented in Table 4. The highest flash temperature is experienced by ZrO_2 that is caused by its low thermal conductivity. On the other hand, Si_3N_4 balls have quite high bulk temperature due to high coefficients of friction experienced during the test. These indicative values are mainly given to illustrate how essential is the effect of balls scar heating when the maximum service temperatures of materials is considered (Table 2). Based on the flash temperature values, possible melting of ball material asperities or phase transformation (of ZrO_2) is expected even during the tests at room temperature and at the sliding speeds over 0.486 $m\ s^{-1}$. However, these are only indicative values since change of properties (hardness, modulus of elasticity, thermal conductivity) influenced by temperature rise is not considered [38].

3.3. Wear mechanisms

The 3D images of the wear scars on the surface of AlCrN coating tested against different balls are shown in Fig. 4. SEM images of coating and balls are provided in Figs. 5–8.

The results of EDS measurements of the wear tracks of the coating are presented in Table 5. The iron (emanating from substrate) content indicates the presence of damaged areas on the surface of coating under consideration. The silicon content indicates the transfer of material from Si_3N_4 ball into the surface of counterbody. The high oxygen content reveals significant oxidation of the tribolayer.

The summary of results obtained by Raman spectroscopy is given in Table 6. Characteristic Raman spectra are given in Fig. 9. The main conclusion that are drawn from Raman investigation (Table 6, Fig. 9) could be summarized as following: (1) The structure of as-received materials was confirmed (Tables 2, 6). It was also found that the β-Si_3N_4 and α-Al_2O_3 are stable at all test temperatures (20–800 °C) while transformation of ZrO_2 from tetragonal to monoclinic is activated with rise of temperature. (2) The formation of oxides and spinel phases of iron and chromium (the exact composition is hard to determine due to similar peaks) is activated at high temperatures and high sliding speeds (Fig. 9a, b, d, e). (3) The Al_2O_3 is formed on AlCrN coating at higher temperatures and sliding speeds than Cr_2O_3 (Table 6, Fig. 9b, f). (4) The determination

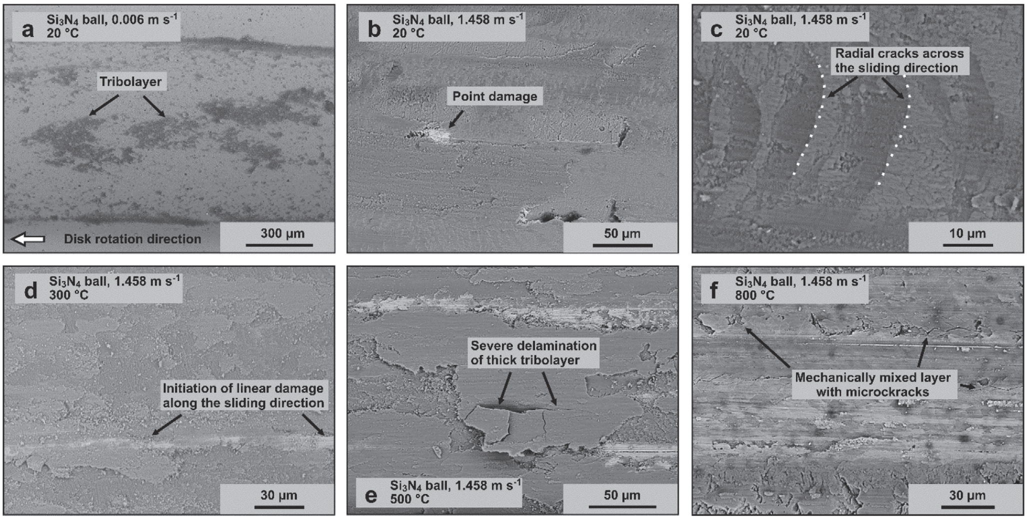

Fig. 5. SEM images of AlCrN wear tracks after completed testing against Si_3N_4 ball. Sliding speed and test temperature are indicated.

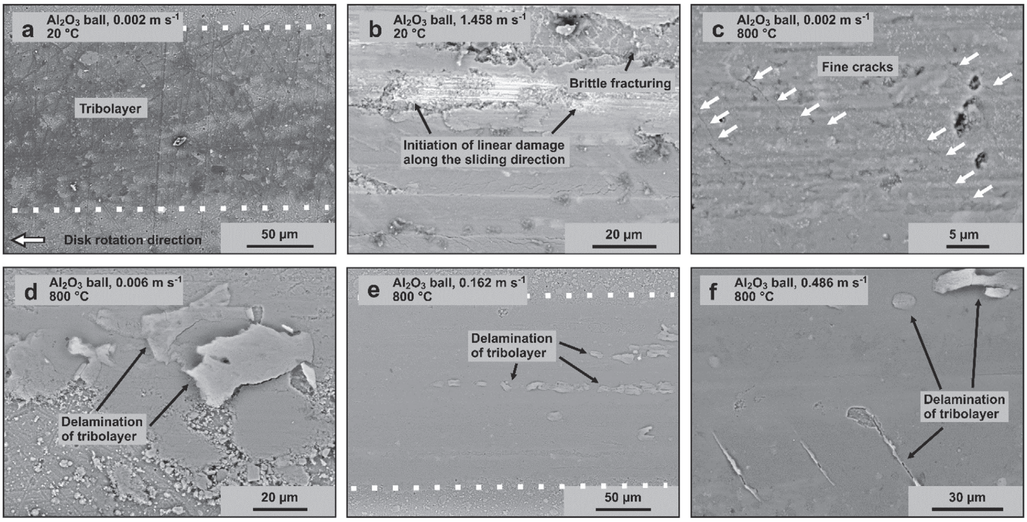

Fig. 6. SEM images of AlCrN wear tracks after completed testing against Al_2O_3 ball. Sliding speed and test temperature are indicated.

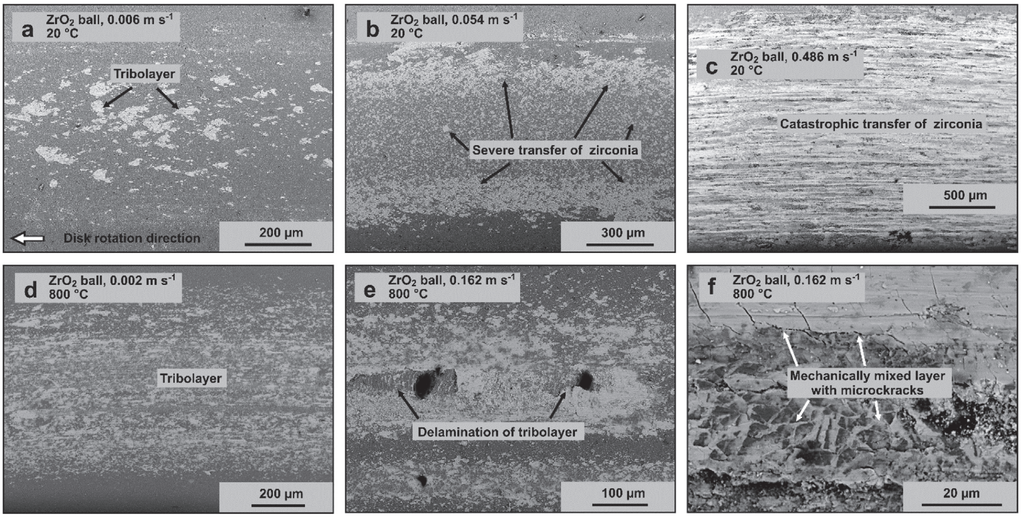

Fig. 7. SEM images of AlCrN wear tracks after completed testing against ZrO_2 ball. Sliding speed and test temperature are indicated.

of the exact composition of the tribolayer is complicated due to formation of mixed oxides, mechanical mixing of components (from coating, ball, substrate, environment) at high sliding speeds and similarity in position of peaks (Cr_2O_3 and Cr_3Si, for example), Fig. 9f.

3.3.1. *Wear mechanism of Si_3N_4 ball tested against AlCrN coating*

The wear of Si_3N_4 ball tested against AlCrN coating at low speeds is insignificant ; however, the initiation of failure is more likely at the high speed due to vibration and frictional heating (Fig. 3b, Table 4). There is a minor ball material transfer onto the coating even at the lowest speed at room temperature (Fig. 5a, Table 5). However, this was hard to prove by Raman spectroscopy (Table 6). At room temperature and the highest speed, the shifting (relocation or re-deposition) of coating material, transversal and longitudinal cracks are observed inside the coating (Fig. 5b and c). There is minor and preferential removal of the coating material at 300 and 500 °C during testing with the highest speed (Fig. 5d and e). At 800 °C and the highest speed, the coating turns into an oxidized mechanically mixed layer, combining both substrate and ball materials (Fig. 5f). In general, the defects shown in Fig. 5b–h are observed mainly at the highest tested speed (1.458 m s^{-1}). According to Table 5, the thickness of a transfer layer from the ball material onto the AlCrN coating at room temperature and the lowest speeds is quite thin since it can hardly be found by EDS (less than 1 µm), (Fig. 5a). At higher temperatures, the Si and O content is usually higher indicating intensified transfer and build-up of the oxidized Si-containing tribolayer on the top of coating (Table 5). The damage of the coating is usually originating from defects and the extent of damage is higher at higher temperatures and higher speeds. The rise of intensity of corrosive processes during

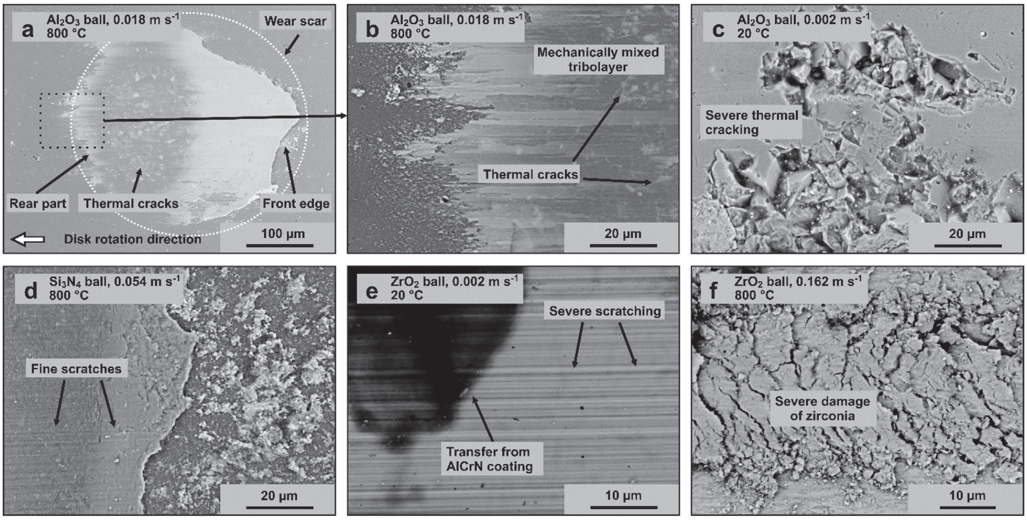

Fig. 8. SEM images of balls after completed tests against AlCrN coating. Ball material, sliding speed and test temperature are indicated.

sliding tests of PVD coatings due to damages initiated from defects was confirmed in Ref. [51]. High iron content coming from substrate (1.9 at.%) indicates the loss of coating integrity for the track analysed after room temperature test with a speed of 1.458 m s^{-1} (Table 5). The analysis of other part of track tested under the same conditions shows that there is significantly lower Fe, Si and O content that point to the conclusion that structure of track is inhomogeneous. Similar situation can be observed when EDS results of two track zones tested at 0.006 m s^{-1} at room

Table 5
Effect of test temperature and sliding speed on concentration of main elements (EDS analysis; concentration is given in at %.) of worn AlCrN coating tested against Si_3N_4 ball. The maximum errors for elements are as follows: Al – 1.1%; Cr – 1.2%; N – 4.1%; Fe – 0.1%; Si – 0.1%; O – 2.9%.

Temp., °C	Speed, m s^{-1}	Al	Cr	N	Fe	Si	O	Al/(Al + Cr)	N/(Al + Cr)	Description
20	0.002	24.0	25.5	49.0	0.4	0.2	0.9	0.48	0.99	Smooth tribolayer (low Si content)
	0.006	23.9	24.7	49.2	0.5	0.3	1.4	0.49	1.01	Smooth tribolayer (without protruding asperities)
	0.006	23.6	24.7	19.7	0.4	5.7	26.0	0.49	0.41	Heavily oxidized transfer layer area (protruding above the surface)
	0.018	23.2	24.0	48.1	0.5	0.3	3.8	0.49	1.02	Smooth tribolayer (low Si content)
	0.054	23.5	25.8	47.0	0.6	0.3	2.8	0.48	0.95	Smooth tribolayer (low Si content)
	0.162	24.2	25.1	46.4	0.4	0.2	3.7	0.49	0.94	Smooth tribolayer (low Si content)
	0.486	22.5	24.7	48.0	0.3	0.2	4.3	0.48	1.02	Smooth tribolayer (low Si content)
	1.458	18.9	19.2	4.1	1.9	5.5	50.4	0.50	0.11	Heavily oxidized transfer layer area with some damage of coating (protruding above the surface)
	1.458	24.2	24.5	37.1	0.5	0.6	13.2	0.50	0.76	Oxidized coating (without protruding asperities)
300	0.002	23.9	25.0	38.0	0.4	1.2	11.5	0.49	0.78	Oxidized transfer layer
	0.006	20.5	22.9	42.2	0.4	1.0	13.1	0.47	0.97	Oxidized transfer layer
	0.018	22.5	23.7	35.3	0.4	1.5	16.6	0.49	0.77	Oxidized transfer layer
	0.054	20.8	22.2	37.8	0.4	1.5	17.3	0.48	0.88	Oxidized transfer layer
	0.162	21.2	23.9	38.8	0.4	0.6	15.1	0.47	0.86	Oxidized transfer layer
	0.486	20.5	20.5	36.7	1.1	0.5	20.7	0.50	0.90	Area with some exfoliation of tribolayer (low Si content)
	1.458	21.8	21.9	48.3	0.4	0.1	7.6	0.50	1.11	Smooth area with smooth tribolayer (low Si content) without exfoliation is analysed
500	0.002	26.3	26.3	45.2	0.4	0.3	1.6	0.50	0.86	Area with mild wear
	0.006	21.8	23.2	45.5	0.5	0.4	8.6	0.48	1.01	Oxidized coating
	0.018	21.1	21.8	45.7	0.5	0.5	10.5	0.49	1.06	Oxidized coating
	0.054	23.4	23.3	34.3	0.5	1.5	16.9	0.50	0.73	Oxidized transfer layer
	0.162	21.1	22.4	42.5	0.6	0.7	12.7	0.48	0.98	Oxidized transfer layer
	0.486	23.3	25.5	44.3	0.5	0.2	6.2	0.48	0.91	Slightly worn area is analysed
	1.458	24.4	23.8	43.4	0.5	0.2	7.8	0.51	0.90	Slightly worn area is analysed
800	0.002	21.2	20.7	35.5	0.7	1.1	20.7	0.51	0.85	Area with oxidized transfer layer
	0.002	21.8	25.0	35.0	0.9	0.1	17.2	0.47	0.75	Area without transfer layer
	0.002	20.3	22.9	39.4	0.8	0.1	16.5	0.47	0.91	Unworn area (outside of track)
	0.006	21.4	23.1	31.3	0.8	1.4	22.0	0.48	0.70	Oxidized transfer layer
	0.018	22.6	22.4	30.8	0.7	1.2	22.3	0.50	0.68	Oxidized transfer layer
	0.054	20.4	22.7	18.0	1.1	2.5	35.3	0.47	0.42	Oxidized transfer layer with some damage of coating
	0.162	22.7	25.6	19.7	1.9	2.0	28.0	0.47	0.41	Oxidized transfer layer with damage of coating
	0.486	13.1	16.0	15.6	3.9	3.7	47.7	0.45	0.54	Oxidized transfer layer with damage of coating
	1.458	23.5	23.7	31.1	0.8	0.1	20.9	0.50	0.66	The test was run for 10% of duration and stopped due to undesirably high vibration and noise.

Table 6
Summary of results obtained by Raman spectroscopy.

Temp., 8C	253 MA substrate (SO) [45,46]	fcc-AlCrN coating (SO) [29,46,47]	β-Si_3N_4 [46–48,50]	α-Al_2O_3 [46,47,50]	Tetragonal ZrO_2 (YSZ) [47,49,50]
20	No oxides found.	Main structure was cubic CrN. No oxides found.	It was β-Si_3N_4. **Ball:** Transfer of coating to the ball was found after all tests. There was presence of Cr_2O_3 at all speeds. **Coating:** Transfer of ball material to the coating was hard to prove. Higher sliding speed results in higher Cr_2O_3 content in wear track of coating (most pronounced effect); (Fe_3O_4, γ-Fe_2O_3) and/or spinel ($FeCr_2O_4$, $Fe_{3-x}Cr_xO_4$, $Fe_{2-x}Cr_xO_3$, etc.) was found after sliding at 0.486 and 1.458 m s^{-1}.	It was α-Al_2O_3. **Ball:** Transfer of coating to the ball was found after all tests. There was presence of Cr_2O_3 at all speeds. **Coating:** Transfer of ball material to the coating was hard to prove.	It was tetragonal ZrO_2 with very low content of monoclinic phase. **Ball:** The content of coating material found was low (ball was worn quickly). **Coating:** Transfer of ball material to the coating was confirmed.
300	**Traces:** Cr_2O_3. **Possible:** Fe_3O_4, γ-Fe_2O_3, spinel ($FeCr_2O_4$, $Fe_{3-x}Cr_xO_4$, $Fe_{2-x}Cr_xO_3$, etc.).	**Found:** traces of Cr_2O_3	**SO:** It was β-Si_3N_4. **Ball:** Transfer of coating to the ball was found after all tests. There was presence of Cr_2O_3 at all speeds. **Coating:** Transfer of ball material to the coating was hard to prove. Higher sliding speed results in slightly higher Cr_2O_3 content in wear track of coating; spinel ($FeCr_2O_4$, $Fe_{3-x}Cr_xO_4$, $Fe_{2-x}Cr_xO_3$, etc.) was found after sliding at 0.486 and 1.458 m s^{-1}.	**SO:** It was α-Al_2O_3.	**SO:** It was tetragonal ZrO_2 with low content of monoclinic phase.
500	**Traces:** Cr_2O_3. **Possible:** Fe_3O_4, γ-Fe_2O_3, spinel ($FeCr_2O_4$, $Fe_{3-x}Cr_xO_4$, $Fe_{2-x}Cr_xO_3$, etc.).	**Found:** traces of Cr_2O_3	**SO:** It was β-Si_3N_4. **Ball:** Transfer of coating to the ball was found after all tests. There was presence of Cr_2O_3 at all speeds. **Coating:** Transfer of ball material to the coating was hard to prove. Higher sliding speed results in slightly higher Cr_2O_3 content in wear track of coating; spinel ($FeCr_2O_4$, $Fe_{3-x}Cr_xO_4$, $Fe_{2-x}Cr_xO_3$, etc.) was found after sliding at 0.486 and 1.458 m s^{-1}.	**SO:** It was α-Al_2O_3.	**SO:** It was tetragonal ZrO_2 with low content of monoclinic phase.
800	**Found:** Cr_2O_3, Fe_3O_4, γ-Fe_2O_3, spinel ($FeCr_2O_4$, $Fe_{3-x}Cr_xO_4$, $Fe_{2-x}Cr_xO_3$, etc.)	**Found:** Cr_2O_3 At 900 8C was found Cr_2O_3, α-Al_2O_3.	**SO:** It was β-Si_3N_4. **Ball:** Transfer of coating to the ball was found after all tests. There was presence of Cr_2O_3 at all speeds. α-Al_2O_3 was found after sliding at 0.486 and 1.458 m s^{-1}. **Coating:** Transfer of ball material to the coating was hard to prove. Cr_2O_3, spinel ($FeCr_2O_4$, $Fe_{3-x}Cr_xO_4$, $Fe_{2-x}Cr_xO_3$, etc.), α-Al_2O_3 (more at higher speeds) were always present.	**SO:** It was α-Al_2O_3. **Ball:** Transfer of coating to the ball was found after all tests. There was presence of Cr_2O_3 at all speeds. **Coating:** Transfer of ball material to the coating was hard to prove.	**SO:** It was tetragonal ZrO_2 with monoclinic phase (still lower content than that of tetragonal phase). **Ball:** The content of coating material found was extremely low (ball was worn quickly). **Coating:** Transfer of ball material to the coating was high.

*__SO__ – Results of static oxidation (2 h). The literature sources containing similar findings are referred.

temperature are compared. Protruding asperities of coating are in a frequent and more intensive contact with the ball that intensify oxidation and ball material transfer. The formation of glazed layers is possible [7,52]. Low concentration of N at 800 °C at speeds higher than 0.002 m s^{-1} and locally at other temperatures support possibility of glazed layer formation (Table 5). The high concentration of Fe (1.9 and 3.9 at. %) found after sliding at 800 °C with speed of 0.162 and 0.486 m s^{-1} indicates that the damage to the AlCrN coating is progressing substantially while the complete damage is still not present (Table 5). The iron is consumed to form various forms of spinel ($FeCr_2O_4$, $Fe_{3-x}Cr_xO_4$, $Fe_{2-x}Cr_xO_3$, etc.) at highest speeds (0.486 and 1.458 m s^{-1}) at all temperatures and at all speeds when temperature is 800 °C, Table 6.

3.3.2. Wear mechanism of Al_2O_3 ball tested against AlCrN coating

There is only minor (if compared to other balls) wear of Al_2O_3 ball when it is sliding on top of AlCrN coating during tests at room temperature (Fig. 3d). Wear of AlCrN coating is more pronounced when alumina counterbody is used as compared to sliding against Si_3N_4 ball (Fig. 4c). The formation of tribolayer in the wear scar of AlCrN coating is clearly evidenced in Fig. 6a. This is mostly due to formation of Cr_2O_3 since transfer of ball material to the coating was hard to prove by EDS or Raman spectroscopy due to presence of aluminium in the ball as well as in the coating (Table 6). Several single points with a removed coating originated from pinhole defects (Fig. 6b) or even larger areas of removed coating are observed. However, at 800 °C an amplified damage of the coating is revealed due to high stresses caused by the low wear and the small contact area of alumina ball even at the lowest speed. This results in a complete coating removal at the highest speed (Fig. 4d and e). Softening of the substrate plays an important role at 800 °C resulting in a progressive loose of support to the coating and development of undesirable tensile stresses. Longitudinal and perpendicular (to sliding direction) cracks are generated (Fig. 6c, e, f) and their size is increased when tested at higher speeds. Removal of tribolayer in form of chips (or flakes) is characteristic for sliding by alumina ball at 800 °C with only a minor chipping (delamination) on the edge of scar at the lowest speeds while leading to catastrophic chipping inside the wear scar at higher speeds (Fig. 6d and e).

3.3.3. Wear mechanism of ZrO_2 ball tested against AlCrN coating

The wear of zirconia balls is driven by its low hardness (more than 3 times lower than hardness of AlCrN coating) and a low thermal conductivity (Table 2) resulting in catastrophic abrasive wear (Fig. 3f) accompanied by melting or transformation tetragonal to monoclinic phase (Table 6) due to generated frictional heat (Table 4). At low speeds and temperatures there is mainly build-up layer on top of AlCrN coating (Figs. 4f, 7a and 7b) while at higher temperatures or speeds the damage to the coating is provoked (Fig. 4g, h and 7c-e) probably due to a larger size of the wear scars of balls providing longer time for transferring of the heat from ball to coating. Cracking of tribolayer and formation of a fine powder of wear debris was observed at the high temperature (Fig. 7f). The fresh fragments of the fractured coating increase the roughness of the disk and further accelerate the abrasive wear. A lower roughness of AlCrN coating is required to provide the reduction in coefficient of friction and wear rate.

As it was stated in previous research of authors [39] and supported by other researchers [18, for example], the wear of coatings and ball is a cyclic process with generation and removal of tribolayers. This is illustrated by Fig. 8a where the tribolayer on a top of the alumina ball is generated during sliding. The fracture and removal of the front edge of the layer is already initiated. The difference in colours of tribolayer in the rear part of the wear scar indicates that it consists from material of the ball and coating. Material transferred from the coating fills the voids

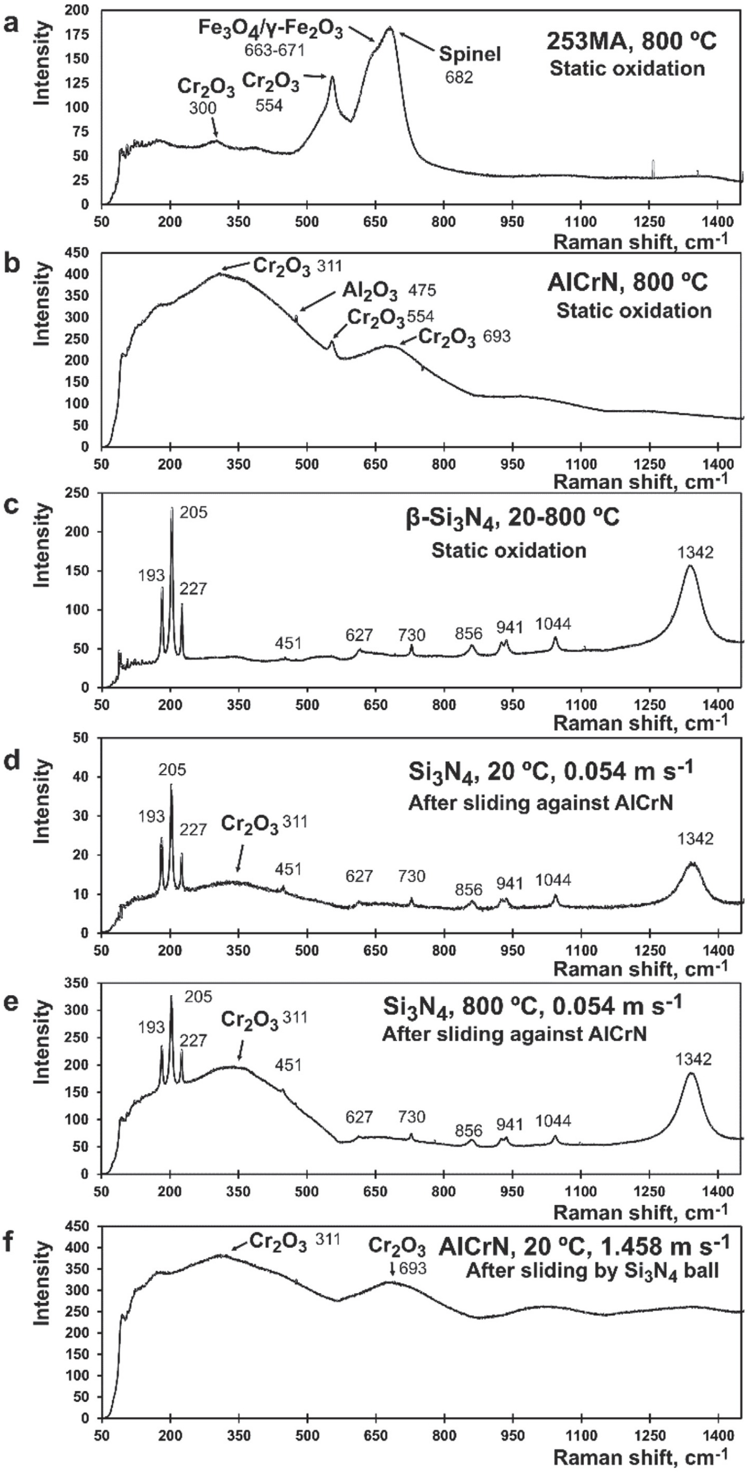

Fig. 9. Characteristic Raman spectra of coating and Si_3N_4 ball.

remained from brittle mechanical or fatigue fracture of alumina present close to the edge of wear scar even during testing at the lowest temperature and speed (Fig. 8b and c). Thermal-shock-induced fracture is intensified at higher speeds [42]. Transfer of AlCrN to much softer zirconia ball is present in some single locations at a low speed and temperature probably due to flash temperatures (Table 4, Fig. 8e). The transfer of AlCrN to the zirconia ball was confirmed by Raman spectroscopy after room temperature tests while only minor traces were found at 800 °C (Table 6). At high temperature and speed the wear of ball is catastrophic and the tribolayer has no chance to be established due to abrasive mode of wear (Fig. 8f). The scratches in the wear scar of zirconia ball are deep that indicates the severe abrasive wear due to its lowest hardness (compare Fig. 8d and e; Table 2).

3.4. Mapping of the AlCrN – Si_3N_4 tribopair behaviour

In order to simplify the interpretation of the results for Si_3N_4 balls, the maps were generated in Excel 2013 software from *Microsoft* (Fig. 10). According to a friction map shown in Fig. 10a, the lowest CoF is experienced by Si_3N_4 when tested at 300 °C in the speed range from 0.002 to 0.054 m s^{-1}. The wear map (Fig. 10b) shows that the lowest wear rates are obtained during sliding of Si_3N_4 against AlCrN coating at the highest temperature and speed. However, the risk of coating damage is increasing with rise of temperature and lower speeds should be preferred. The formation of cyclically regenerated discontinuous build-up tribolayers on AlCrN coating may reduce the stability of sliding (the ball is "jumping") that can lead to reduction of friction coefficient and lower wear rate [39] while disk positioning (runout) accuracy can result in

a. Map showing the effect of speed and temperature on coefficient of friction

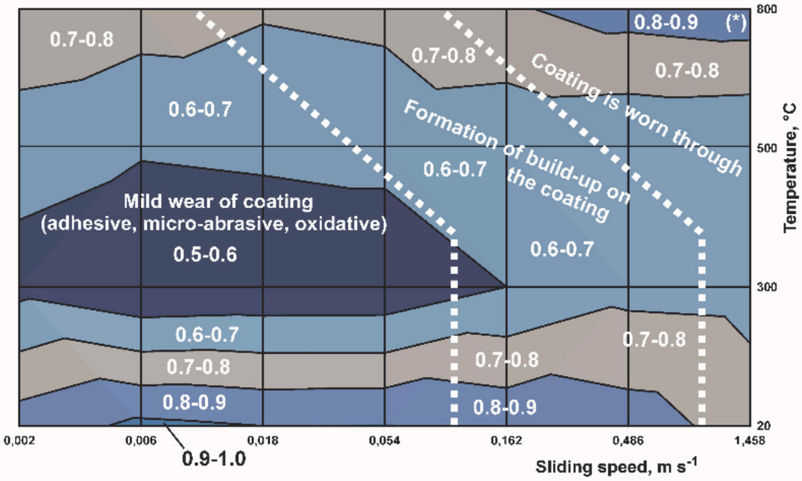

b. Map showing the effect of speed and temperature on wear rate of Si_3N_4 ball, x10^{-6} mm^3 N^{-1} m^{-1}

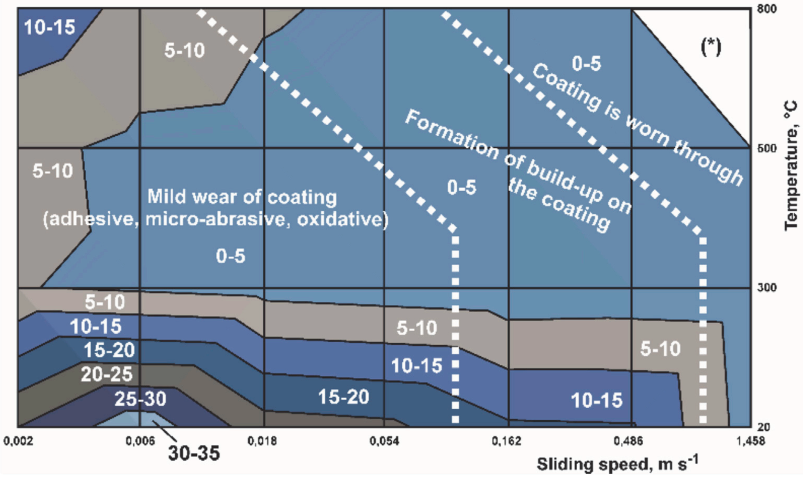

Fig. 10. Maps showing the effect of sliding speed and temperature on CoF and wear rate of Si_3N_4 ball sliding against AlCrN coating (reconstructed according to Fig. 3a and b). (*) The test at 800 °C with speed of 1.458 m s^{-1} was run for only 10% of test duration and was stopped due to undesirably high vibration and noise. "Coating is worn through" indicates high risk of partial or substantial coating loss.

generation of more intensive (especially at high speeds) mechanical impacts leading to a low- or high-cycle fatigue driven coating damage.

4. Discussion

Probably, the most important information for designers of new equipment are the limits (maximum temperature, speed, etc) for each studied tribocouple. The maps given in Fig. 10 can answer this question for the case of Si_3N_4 ball sliding against AlCrN coating. The maximum sliding speeds at the temperature of 20, 300, 500 and 800 °C are 0.486, 0.486, 0.162 and 0.054 m s^{-1} respectively. The temperatures between 300 and 500 °C are recommended as those providing the lowest friction coefficient and resulting in mild wear of AlCrN coating. It is known [33] that minor oxidation of AlCrN coating and formation Cr_2O is possible starting from the temperature of 700 °C. However, when the effect of oxygen is accompanied by friction during sliding (tribo-oxidation) the AlCrN coating with Al content 0.5 (acc. to at. % of metals) [28] the formation of CrO_2, Cr_2O_5 and CrO_3 is possible even at 300 °C. The thermodynamically stable Cr_2O_3 along with Al_2O_3 can be observed (mostly as a wear debris) already at 650 °C [28]. According to Raman spectroscopy result, the traces of Cr_2O_3 were found after static oxidation already at 300 °C while even room temperature sliding tests were favourable for oxidation as well. The formation of Cr_2O_3 provides reduction in friction coefficient (serving as a solid lubricant) while Al_2O_3 leads to higher CoF and increases the probability of abrasive wear [28,53]. The tested silicon nitride balls were made from the β-Si_3N_4 phase that is stable until temperature of 1000 °C. The crystallization of intergranular phases (that are softening at elevated temperatures) is avoided during sintering with the help of sintering aids [54]. The hardness of β- Si_3N_4 decreases only slightly by 10–20% when the temperature is increased from room to 800 °C [55]. This data leads to conclusion that lower friction coefficients of Si_3N_4 at 300 and 500 °C are caused by formation of lubricious chromium oxides (glazed layer) while the formation of Al_2O_3 is expected at 300, 500 °C and 800 °C when speed is higher than 0.162, 0.162 and 0.054 m s^{-1} respectively (see Fig. 3a, Tables 4 and 5). The Raman spectroscopy measurements confirmed that there is Al_2O_3 formation in the wear scar of AlCrN coating at 800 °C after sliding at speed 0.486 and 1.458 m s^{-1} (Table 6). The estimation of flash temperature presented in Table 4 indicates the possibility of protruding asperities melting during sliding at room temperature with the maximum studied speed of 1.458 m s^{-1}. This was supported by adhered and smeared fragments shown in Figs. 4b, 5a and 5b and according to EDS and Raman data. As it is shown in Table 5 highly oxidized material transferred from ball to the coating could be found after sliding with speed of 1.458 and even with as low as 0.006 m s^{-1}. It is also important to mention that decomposition of Si_3N_4 due to reaction with Cr_2O_3 formed on top of the AlCrN coating leads to the formation of series of chromium silicides (including Cr_3Si, Cr_5Si and $CrSi_2$) at temperatures higher than 1500–1700 °C [56] having poor wear resistance [57]. So, actually, the formation of unfavourable chromium silicides and Al_2O_3 is possible at high temperatures and speeds that leads to higher friction coefficient and wear rate. Recent investigations have shown that solid solution of silicon in AlCrN coating or amorphous Si-N accumulated at the AlCrN grain boundaries can enhance mechanical, tribological properties and oxidation resistance while this is not studied well yet [58]. The highest hardness and Young's modulus were observed for $(Cr_{94}Si_6)N$ (atomic %) coating [59]. This can give some hints to explain favourable behaviour of AlCrN - Si_3N_4 tribocouple at 300–500 °C while the confirmation of such hypothesis requires deeper research.

The α-Al_2O_3 is thermodynamically stable at all temperatures up to its melting point (2070 °C) that is almost twice higher than for Si_3N_4 [60]. The rise of bulk temperature is not critical for Al_2O_3 (max 302 °C) and the maximum service temperature is not reached even during testing at 800 °C (Table 2). However, the estimated rise in flash temperature is reaching 861 and 2544 °C (Table 4) that could be responsible for ball cracking of thermal origin observed in Fig. 8b and c. Alumina is the most reliable material among the studied ball materials in sliding against AlCrN coating at 800 °C due to the lowest coefficient of friction and the wear rate (Fig. 3c and d). This is also (along with high service temperature and melting point) influenced by the highest thermal conductivity and diffusivity that is reducing the risk of generation of high thermal gradients. However, high thermal conductivity and diffusivity are drawbacks for internal combustion cylinder liner materials that should provide insulation. Besides, alumina has lowest fracture toughness among materials investigated (Table 2). It is possible to expect that the delamination of tribolayer on top of AlCrN coating (Fig. 6d, e, f) could be avoided if conformal types of contacts providing uniform distribution of the load are applied.

Zirconia can change its structure between monoclinic, tetragonal and cubic structures at temperatures of 1200 °C and 2370 °C [61] while surface irregularities can experience these changes due to the rise of flash temperature or mechanical impacts caused by surface irregularities (Table 4). Change of the structure is accompanied with a significant change in volume that can lead to the fracturing of material and extreme wear. This is the main possible reason of catastrophic rise in wear rates of zirconia when tested at speeds higher than 0.162 and 0.006 m s^{-1} at temperatures of 20 and 800 °C respectively (Fig. 3f). The severe and catastrophic transfer of zirconia mostly in form of wear debris is illustrated in Fig. 7b, c and e.

The indentations (without sliding) were performed by alumina ball at temperatures from 20 to 900 °C and loads from 3 N to 10 N in order to illustrate that the damage of AlCrN coating is not caused by softening of the substrate alone. Only indents produced with 10 N load at 800 °C and with 5 and 10 N at 900 °C were possible to detect with the help of fringes (Fig. 11a1 and b1). The depth of indent produced by the load of 10 N at 800 and 900 °C is less than 0.2 and 0.5 μm respectively. No damage of the coating was found by SEM.

It is possible to expect that the performance of AlCrN coating and that of Al_2O_3 could be improved if the geometric precision of parts and their alignment are improved in real applications. The significant change in relative performance of materials caused by the change in testing methodology was demonstrated in Refs. [39,62]. The vertical movement of the ball was checked before the test (with an exchangeable ball, load 1 N and speed 1 rpm) with track radius of 26 mm and was usually in the range from 3 to 10 μm (measured by internal position sensor). Such runout accuracy can cause jumping of the ball and generation of impact stresses being higher than those assigned by envisaged test conditions. These values are comparable to the height of generated asperities (usually 0.2–5.0 μm) measured by the 3D profilometer (Fig. 4).

The testing with varied track radii is considered by authors as the most appropriate when it is required to check the performance of tribocouple in a wide range of sliding speeds (the difference between the lowest and highest speeds was 729 times) with the same device (drive). The tests with slowest sliding speed were performed with the smallest radius (10 mm) while fastest tests were performed with largest radius (22 mm). The tests with lowest sliding speed and largest track radius while the same sliding distance were performed at room temperature to check the influence of the track radius (number of completed revolutions). It was found that the change of test radius from 10 to 22 mm is causing the minor increase in wear rate (max. 10%) and decrease of final coefficient of friction (max. 20%) that is due to fact that coating has higher hardness and causes some abrasive wear during running-in and longer time is required for tests with larger wear track radius. However, it is expected that differences are smaller when higher test speeds are applied (compare Fig. 2a and c). The prolongation of Si_3N_4 ball test at room temperature and lowest speed (0.002 m s^{-1}) is proposed to compensate the influence of the running-in period (Fig. 2). Testing with varied track radii enables to avoid reconditioning (by polishing) of PVD coating between consecutive tests if they are performed with the same radius [23].

During testing of AlCrN coating deposited onto WC-Co substrate the surprising complete failure of film at temperatures of 600 °C was

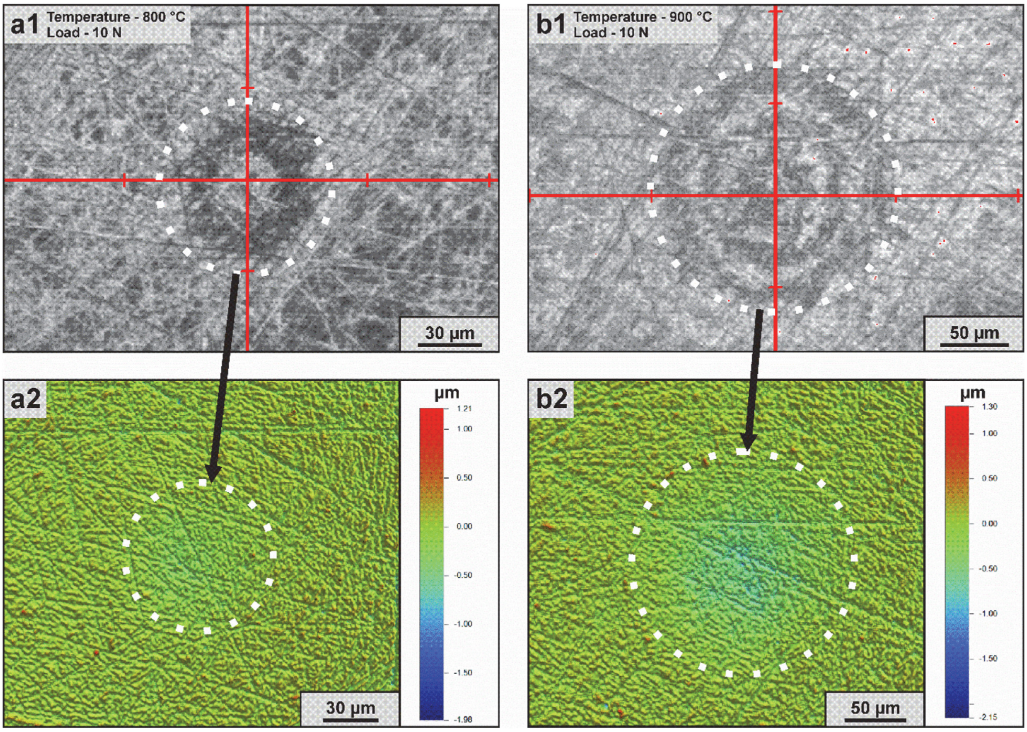

Fig. 11. Optical images with fringes and corresponding top views of scanned areas of AlCrN coating indented with the load of 10 N at temperatures of 800 °C and 900 °C. This is to illustrate that the damage of coating observed in Figs. 5–7 is not influenced by the load (3 N) and temperature (max 800 °C) only.

attributed by authors to adhesive problems of the coatings in the beginning of the sliding tests [22]. It was pointed out in Ref. [23] that WC-Co substrates (typical for cutting tools) experience high oxidation at temperatures over 600 °C that is causing severe wear of AlCrN coating tested against alumina ball even at speed as low as 0.2 m s^{-1}. It is possible to conclude that combination of AlCrN coating with 253 MA steel substrate enables to provide acceptable performance at 800 °C in comparison to WC-Co substrates. The coefficient of friction (0.75) obtained by other researchers [18] for Si_3N_4 ball sliding at room temperature against AlCrN coating applied onto hard WC-10 wt. % Co substrate with similar test duration at speed of 0.17 m s^{-1} was similar to that presented in Fig. 3a (0.87). The depth of wear track in AlCrN coating was about 0.5 µm that is extremely high for test with duration of only 30 min and thickness of coating being 1.0 µm (indication of accelerated test). Such fast wear is probably due to much higher maximum contact pressure applied during test (estimated as 2.3 GPa).

5. Conclusions

Based on the results obtained, the following conclusions are made:

- The wear of the AlCrN coating tested against Si_3N_4 ball in the speed range from 0.002 to 0.162 m s^{-1} is insignificant and highly affected by oxidation and transfer of material between the ball and the coating.
- An increase in the bulk and flash temperatures due to frictional heat is calculated and correlation with an initiation of coatings or balls failure is demonstrated.
- An increase in sliding speed results in decrease in the wear rates (expressed in mm N^{-1} m^{-1} units) of Si_3N_4, Al_2O_3 and ZrO_2 balls (until the initiation of AlCrN coating fracture).
- Zirconia ball exhibits the highest wear rate due to a low hardness and a low thermal conductivity. Silicon nitride and alumina has medium and the lowest wear respectively. The zirconia ball has catastrophic wear rate at 800 °C while the wear of alumina is still moderate.
- The lowest CoF of Si_3N_4 against AlCrN coating is observed when tested at 300 °C in the speed range from 0.002 to 0.054 m s^{-1}. Si_3N_4 ball has the lowest wear rate at the highest speed and temperature of 300 and 500 °C. However, the risk of coating damage is increasing with rise of temperature. The moderate speeds (below 0.486 m s^{-1}) should be preferred.
- Adhesive wear, oxidative wear, delamination, and cracking due to deformation of a stainless steel substrate caused by softening at high temperatures and vibration are main wear mechanisms of tested AlCrN coating. The balls experience also abrasive wear due to a higher hardness of AlCrN coating as compared to ZrO_2.
- The friction and wear maps generated for Si_3N_4 – AlCrN tribo-couple allow to select optimum combinations of temperature and sliding speed with tribological processes taken into account.

Acknowledgements

This work was supported by Estonian Ministry of Education and Research (IUT 19–29; base funding provided to R&D institutions, project B56). Authors would like to thank PhD A.Bogatov from Department of Mechanical and Industrial Engineering for help with nanoindentation measurements of AlCrN coating properties.

References

[1] Despeisse M, Baumers M, Brownc P, Charnley Ford SJ, Garmulewicz A, Knowles S, et al. Unlocking value for a circular economy through 3D printing: a research agenda. Technol Forecast Soc Change 2017;115:75–84.

[2] Guo N, Leu MC. Additive manufacturing: technology, applications and research needs. Front Mech Eng 2013;8(3):215–43.

[3] Vetter J, Michler T, Steuernagel H. Hard coatings on thermochemically pretreated soft steels: application potential for ball valves. Surf Coat Technol 1999;111:210–9.

[4] Bullock E, editor. Research and development of high temperature materials for industry. Elsevier; 1989.

[5] Blau PJ, editor. Friction, lubrication, and wear technology. ASM metals handbook. tenth ed., vol. 18. USA: ASM International; 1992.

[6] Sliney HA, DellaCorte C. The friction and wear of ceramic/ceramic and ceramic/metal combinations in sliding contacts. NASA TM-106348 report. US Department of Energy; 1993.

[7] Zum Gahr KH. Sliding wear of ceramic–ceramic, ceramic–steel and steel– steel pairs in lubricated and unlubricated contact. Wear 1989;133:1–22.

[8] Michalczewski R, Piekoszewski W, Szczerek M, Tuszynski W. The problems of resistance to scuffing of heavily loaded lubricated friction joints with WC/C coated parts. Ind Lub Trib 2014;66/3:434–42.

[9] Michalczewski R, Kalbarczyk M, Piekoszewski W, Szczerek M, Tuszynski W. The rolling contact fatigue of WC/C-coated spur gears. Proc Inst Mech Eng Part J J Eng Trib 2013;8/227:850–60.

[10] Hussainova I, Baronins J, Drozdova M, Antonov M. Wear performance of hierarchically structured alumina reinforced by hybrid graphene encapsulated alumina nanofibers. Wear 2016;368–369:287–95.

[11] Kawamura H. Development of ceramic engine parts for heat insulated engine. ASME Proc 1990:1–13. Paper No. 90-GT-384.

[12] Parker DA. Ceramics technology-application to engine components. Proc Inst Mech Eng 1985;199/A3:135–50.

[13] Bhatia SM, Pandey PC, Shan HS. Thermal cracking of carbide tools during intermittent cutting. Wear 1978;51:201–11.

[14] Umanskyi O, Storozhenko M, Hussainova I, Terentjev O, Kovalchenko A, Antonov M. Effect of TiB2 additives on wear behavior of NiCrBSi-based plasma-sprayed coatings. Mat Sc (Medžiagotyra) 2016;22/1:15–9.

[15] Beake BD, Ning L, Gey C, Veldhuis SC, Komarov A, Weaver A, et al. Wear performance of different PVD coatings during hard wet end milling of H13 tool steel. Surf Coat Tech 2015;279:118–25.

[16] Norrby N, Johansson MP, M'Saoubi R, Odén M. Pressure and temperature effects on the decomposition of arc evaporated Ti0.6Al0.4N coatings in continuous turning. Surf Coat Tech 2012;209:203–7.

[17] Mo JL, Zhu MH. Sliding tribological behaviors of PVD CrN and AlCrN coatings against Si3N4 ceramic and pure titanium. Wear 2009;267:874–81.

[18] Mo JL, Zhu MH. Tribological oxidation behaviour of PVD hard coatings. Tribol Int 2009;42:1758–64.

[19] Kawate M, Kimura Hashimoto A, Suzuki T. Oxidation resistance of Cr1−XAlXN and Ti1−XAlXN films. Surf Coat Tech 2003;165:163–7.

[20] Scheerer H, Hoche H, Broszeit E, Schramm B, Abele E, Berger C. Effects of the chromium to aluminum content on the tribology in dry machining using (Cr,Al)N coated tools. Surf Coat Tech 2005;200:203–7.

[21] Uchida M, Nihira N, Mitsuo A, Toyoda K, Kubota K, Aizawa T. Friction and wear properties of CrAlN and CrVN films deposited by cathodic arc ion plating method. Surf Coat Tech 2004;177–178:627–30.

[22] Polcar T, Cavaleiro A. High-temperature tribological properties of CrAlN, CrAlSiN and AlCrSiN coatings. Surf Coat Tech 2011;206:1244–51.

[23] Nohava J, Dessarzin P, Karvankova P, Morstein M. Characterization of tribological behavior and wear mechanisms of novel oxynitride PVD coatings designed for applications at high temperatures. Tribol Int 2015;81:231–9.

[24] Liew WYH, Jie JLL, Yan LY, Dayou J, Sipaut CS, Bin Madlan MF. Frictional and wear behaviour of AlCrN, TiN, TiAlN single-layer coatings, and TiAlN/AlCrN, AlN/TiN nano-multilayer coatings in dry sliding. Procedia Eng 2013;68:515–7.

[25] 1011EN-GB:3 High temperature austenitic stainless steel. Avesta: Centrum Tryck AB; 2004. Available from webpage, www.outokumpu.com/stainless (Accessed 07/01/2017).

[26] Roy M, Pauschitz A, Wernisch J, Franek F. Effect of mating surface on the high temperature wear of 253 MA alloy. Mater Corros 2004;55/4:259–73.

[27] Surzhenkov A, Adoberg E, Antonov M, Sergejev F, Mikli V, Viljus M, et al. Influence of laser hardening to the sliding wear resistance of the PVD (Al,Ti)N-G and nACo coatings. Key Eng Mater 2014;604:28–31.

[28] Contreras Sánchez AJ, Sánchez-López JC, Domínguez-Meister S, García-Luis A, Brizuela M. Tribological behaviour at high temperature of hard CrAlN coatings doped with y or Zr. Thin Solid Films 2014;550:413–20.

[29] Wang L, Nie X, Housden J, Spain E, Jiang JC, Meletis EI, et al. Material transfer phenomena and failure mechanisms of a nanostructured Cr–Al–N coating in laboratory wear tests and an industrial punch tool application. Surf Coatings Technol 2008;203/5:816–21.

[30] Rainforth WM. The wear behaviour of oxide ceramics-a review. J Mater Sci 2004;39:6705–21.

[31] Davis JR. Metals handbook. second ed. ASM International; 1998.

[32] Barber GC, Ludema KC. The break-in stage of cylinder-ring wear: a correlation between fired engines and a laboratory simulator. Wear 1987;118:57–75.

[33] Chim YC, Ding XZ, Zeng XT, Zhang S. Oxidation resistance of TiN, CrN, TiAlN and CrAlN coatings deposited by lateral rotating cathode arc. Thin Solid Films 2009;517/17:4845–9.

[34] Samani MK, Chen GCK, Ding XZ, Zeng XT. Thermal conductivity of CrAlN and TiAlN coatings deposited by lateral rotating cathode arc. Key Eng Mater 2010;447–448:705–9.

[35] Ashby MF. Materials selection in mechanical design. fourth ed. Elsevier; 2011.

[36] Somiya S. Handbook of advanced ceramics - materials, applications, processing, and properties. second ed. Elsevier; 2013.

[37] Schlichting KW, Padture NP, Klemens PG. Thermal conductivity of dense and porous yttria-stabilized zirconia. J Mater Sci 2001;36:3003–10.

[38] Ashby MF, Abulawi J, Kong HS. Temperature maps for frictional heating in dry sliding. Tribol Trans 1991;34:577–87.

[39] Antonov M, Hussainova I, Adoberg E. Effect of loading system inertia on tribological behaviour of ceramic–ceramic, ceramic–metal and metal–metal dry sliding contacts. Tribol Int 2013;65:207–14.

[40] Antonov M, Goljandin D, Andreev A, Voltsihhin N, Hussainova I. Sliding wear behaviour of basalt containing composites with additions of either metallic and/or ceramic phases. In: Proc. of the int. Conf. BALTTRIB'2013. Aleksandras Stulginskis University; 2013. ISSN 1822–8801.

[41] Blau PJ. On the nature of running-in. Tribol Int 2005;38:1007–12.

[42] Hsu SM, Shen MC. Wear maps. In: Bhushan B, editor. Modern tribology handbook. USA: CRC press; 2000.

[43] Podgursky V, Hantschel T, Bogatov A, Kimmari E, Antonov M, Viljus M, et al. Rippling on wear scar surfaces of nanocrystalline diamond films after reciprocating sliding against ceramic balls. Tribol Lett 2014;55/3:493–501.

[44] Bobzin K, Lugscheider E, Nickel R, Bagcivan N, Krämer A. Wear behavior of Cr1−xAlxN PVD-coatings in dry running conditions. Wear 2007;263:1274–80.

[45] Natesan K. Study of metal dusting phenomenon and development of materials resistant to metal dusting. Annual report ANL-02/05. USA: U.S. Department of Energy; 2002.

[46] McCarty KF, Boehme DR. A Raman study of the systems Fe3−xCrxO4 and Fe2−xCrxO3. J Solid State Chem 1989;79/1:19–27.

[47] Ipaz L, Aperador W, Caicedo J, Esteve J, Zambrano G. A practical application of X-ray spectroscopy in Ti-Al-N and Cr-Al-N thin films. In: Sharma SK, editor. X-Ray spectroscopy. Croatia: InTech; 2012. p. 21–38.

[48] Riedel R, Zerr A, Miehe G, Serghiou G, Schwarz M, Kroke E, et al. Synthesis of cubic silicon nitride. Nature 1999;400/6742:340–2.

[49] Li C, Li M. UV Raman spectroscopic study on the phase transformation of ZrO2, Y2O3-ZrO2 and SO42-/ZrO2. J Raman Spectrosc 2002;33/5:301–8.

[50] Database of raman spectra. Available online. www.rruff.info. Si3N4-β (ID R120129), Cr2O3 Eskolaite (ID R060892), Corundum (ID R040096).

[51] Baronins J, Podgursky V, Antonov M. Bereznev S Hussainova I. Electrochemical behaviour of TiCN and TiAlN gradient coatings prepared by lateral rotating cathode arc PVD technology. Key Eng Mater 2017;721:414–8.

[52] Pauschitz A, Roy M, Franek F. Mechanisms of sliding wear of metals and alloys at elevated temperatures. Tribol Int 2008;41:584–602.

[53] Poliarus O, Umanskyi O, Ukrainets M, Kostenko O, Antonov M, Hussainova I. Influence of Cr, Ti and Zr oxides formation on high temperature sliding of NiAl-based plasma spray coatings. Key Eng Mater 2016;674:308–12.

[54] Hoffmann MJ. High-temperature properties of Si3N4 ceramics. MRS Bull 1995;20/2:28–32.

[55] Martienssen W, Warlimont H. Springer handbook of condensed matter and materials data. Springer Berlin Heidelberg; 2006.

[56] Alem A, Pugh MD. The influence of chromium oxide on the sintering behavior of silicon nitride. Int J Appl Ceram Technol 2013;10(S1):E258–66.

[57] Salas O, Kearns K, Carrera S, Moore JJ. Tribological behavior of candidate coatings for Al die casting dies. Surf Coat Technol 2003;172:117–27.

[58] Liu CB, Pei W, Huang F, Chen L. Improved mechanical and thermal properties of CrAlN coatings by Si solid solution. Vacuum 2016;125:180–4.

[59] Castaldi L, Kurapov D, Reiter A, Shklover V, Schwaller P, Patscheider J. High temperature phase changes and oxidation behavior of Cr–Si–N coatings. Surf Coat Technol 2007;202:781–5.

[60] McHale JM. Surface energies and thermodynamic phase stability in nanocrystalline aluminas. Science 1997;277/5327:788–91.

[61] Platt P, Frankel P, Gass M, Howells R, Preuss M. Finite element analysis of the tetragonal to monoclinic phase transformation during oxidation of zirconium alloys. J Nucl Mater 2014;454/1:290–7.

[62] Yung DL, Antonov M, Veinthal R, Hussainova I. Wear behaviour of doped WC–NI based hardmetals tested by four methods. Wear 2016;352–353:171–9.

PAPER III

Baronins, J., Antonov, M., Bereznev, S., Raadik, T., Hussainova, I., Raman spectroscopy for reliability assessment of multilayered AlCrN coating in tribo-corrosive conditions. *Coatings*, 2018, 8 (7), 229–241.

coatings

MDPI

Article

Raman Spectroscopy for Reliability Assessment of Multilayered AlCrN Coating in Tribo-Corrosive Conditions

Janis Baronins [1], Maksim Antonov [1,*], Sergei Bereznev [2], Taavi Raadik [2,3] and Irina Hussainova [1]

[1] Department of Mechanical and Industrial Engineering, Tallinn University of Technology, 12616 Tallinn, Estonia; Janis.Baronins@ttu.ee (J.B.); Irina.Hussainova@ttu.ee (I.H.)
[2] Department of Materials and Environmental Technology, Tallinn University of Technology, 12616 Tallinn, Estonia; Sergei.Bereznev@ttu.ee (S.B.); Taavi.Raadik@ttu.ee (T.R.)
[3] European Space Agency ESA-ESTEC, Materials and Processes Section, 2201 Noordwijk, The Netherlands
* Correspondence: Maksim.Antonov@ttu.ee; Tel.: +372-620-335-5

Received: 18 May 2018; Accepted: 20 June 2018; Published: 26 June 2018

Abstract: In this study, a multilayered AlCrN coating has been employed as a protective layer for steel used in tribo-corrosive conditions. The coating was deposited by a lateral rotating cathode arc PVD technology on a AISI 316L stainless steel substrate. A ratio of Al/(Al + Cr) was varied from 0.5 up to 0.6 in the AlCrN layer located above Cr adhesion and gradient CrN interlayers. A Raman spectroscopy and potentiodynamic polarization scan were used to determine the resistance in tribo-corrosive (3.5 wt % NaCl) conditions. Correlation between sliding contact surface chemistry and measured tribological properties of material was supported with static corrosion experiments. The corrosion mechanisms responsible for surface degradation are reported.

Keywords: multilayered AlCrN coating; Raman spectroscopy; tribo-corrosion; sliding wear

---

1. Introduction

One of the problems in the industrial application of moving bodies concerns the mechanical interaction between sliding surfaces and surface chemical reactions or corrosion occurring in reactive environments such as an aqueous media. A simplified description of tribo-corrosion phenomenon is related to a material transformation process due to simultaneous corrosion and wear taking place at contacting surfaces in relative motion [1].

Corrosion resistance is one of the most important factors to be taken into consideration for manufacturing metal products, as the formation of rust can have a devastating impact on the performance. Protection of the metal surfaces with physical vapour deposited coatings is a widely used technique. It could be assumed that such treatment will be even more relevant in future due to boosting of 3D metal printing technologies (additive manufacturing) [2]. Reliable lifetime prediction for a component used in an aqueous corrosive environment requires the identification of corrosion failure modes. Such failure modes can be pitting (if halide ions are present), stress-corrosion caused cracking by hydrogen embrittlement and corrosion fatigue [3].

The effect of mechanical stimulation on chemical degradation of materials and, vice-versa, the influence of corrosion on the mechanical response of contacting materials are of great concern for modern technologies including power generation, marine, and offshore industries. Materials properties, surface transformations, and electrochemical reactions are important aspects to be considered during materials selection for any specific application as cumulative effects of mechanical and chemical factors can result in unexpected behaviour and catastrophic loss of integrity. However, the chemo-mechanical mechanisms of tribo-corrosion are not yet well-understood and are extremely complex as they involve a great number of parameters [1,4–6]. A realistic evaluation of materials reliability is further hindered by the experimental difficulties in process characterization. Moreover, the overall rate of material degradation is rarely the sum of just corrosion and wear but is influenced by multiple reactions and transformations that take place during tribo-corrosive interactions. Therefore, an attempt to use Raman spectroscopy as a non-destructive and relatively fast method for understanding processes of tribo-corrosion is of potential benefit [7].

Nowadays the use of protective coatings containing carbon, oxygen, or nitrogen (e.g., carbides, nitrides, carbonitrides, or oxynitrides) is considered to be a practical method for improvement of the performance of metals and alloys [8–10]. Transition metal nitrides ensure the high hardness, acceptable wear, and corrosion resistance when applied as physical vapour deposited (PVD) coatings to enable application under aggressive environments [11,12]. Dominating phase transition changes from cubic to hexagonal have been found in $Al_xCr_{1-x}N$ by increasing x up to about 0.71 [13]; however, this value has not been strictly defined.

In many cases, a ceramic coating cannot be applied directly to an SS substrate due to insufficient bonding efficiency. As the result of this, intensive delamination of a coating can take place. It is especially harmful, if emission of Cr containing particles takes place that can oxidize into a toxic and cancerogenic Cr(VI) [14]. Accordingly, an adhesive interlayer with as possible similar lattice parameters can be applied. In such situation, a process of inter-diffusion between coating and substrate may occur. Cohesive energy densities or solubility parameters should match according to thermodynamic considerations to attain good bonding between a substrate and an adhesive layer [15]. A combination of Fe and Cr satisfy these conditions as both have bcc structures. It is well known that specific interactions between the components enable blending the miscible materials [16]. The ideal work of adhesion properties of the Cr(100)/Fe(100) and Cr(110)/Fe(110) abrupt interfaces has been predicted to be about 5.4 $J\cdot m^{-2}$. Endothermic intermixing occurs at the interface of Cr film and Fe substrate, exhibiting a very strong adhesion caused by strong covalent bonding in addition to metallic cohesion and nearly lack of strain [14]. Intermixing causes a favourable concentration gradient transition zones distinguished by thermodynamic compatibility of a substrate-coating system [17].

Herein, the tribo-corrosive processes occurring at multilayered AlCrN PVD coatings deposited over stainless steel (SS) substrate demonstrating an applicability of Raman spectroscopy for determination of corrosion products and possible coating failures under static and tribologically initiated conditions is reported.

2. Materials and Methods

2.1. Materials

Austenitic conventional (produced by casting and rolling) SS AISI 316L (UNS S31603, dimension: 25 mm × 15 mm × 5 mm) supplied by *Outokumpu* (Helsinki, Finland) was used as the substrate material for the compositions described. Selected Fe based SS typically contains Cr (17.2 wt %) C (0.02 wt %), Ni (10.1 wt %) and Mo (2.1 wt %) according to properties provided by the producer. A small concentration of several other elements like Si, P, S, Mn, and N can be detected during elemental analysis.

An arithmetical mean roughness of the substrates $R_a \leq 0.02$ μm was reached using a Phoenix 4000 (*Buehler*, Lake Bluff, IL, USA) polishing system by applying SiC papers (Buehler) down to grade P4000 (*MicroCut S*, *Buehler*). Substrates were cleaned with an isopropanol for 50 min in an ultrasonic bath and then sputter-cleaned in a chamber with argon plasma with the bias voltage of 850 V at 425 °C for 1 h. Chromium adhesive and gradient CrN interlayers were used in order to provide sufficient adhesion of the AlCrN coating to the substrate. The structure of alternating layers with an Al/(Al + Cr) ratio of 0.6 and 0.5 was produced by varying the Cr cathode arc current, [5]. The adhesion of the coating to the substrate was characterised as class 1 according to VDI 3198. The thickness of the AlCrN coating was established as 3 μm and the thickness of the Cr/CrN interlayer was about 0.3 μm (Kalotest method by

BAQ GmbH KaloMAX ball cratering device according to EN1071-2007). The deposition temperature for the substrate was 450 °C. The schematic representation of the coating described is given in Figure 1a. A dominating cubic CrN phase was confirmed by XRD in the structure of the AlCrN PVD coating after deposition, as demonstrated in Figure 1b (minerals with similar XRD signals are indicated). The main properties of the coating are listed in Table 1.

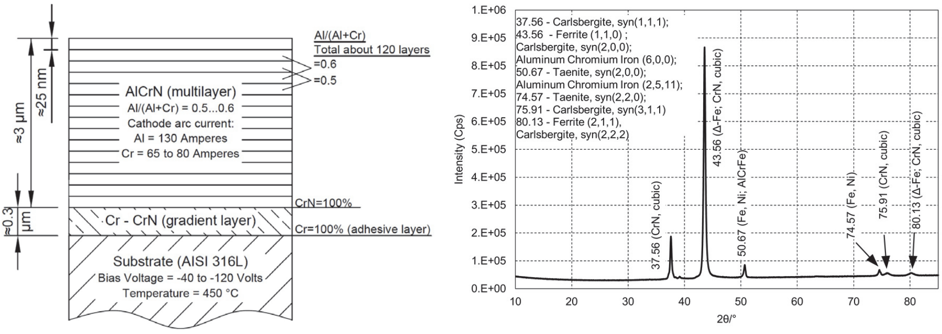

(**a**) (**b**)

Figure 1. A schematic illustration of the multilayered AlCrN PVD coating on the stainless steel substrate (**a**); and XRD (made by *Rigaku Ultima IV*, Tokyo, Japan) diffractogram of AlCrN PVD coating deposited onto stainless steel AISI 316L substrate, indicating a dominating cubic CrN phase in the coating (**b**).

Counter-body balls of yttria-stabilized tetragonal zirconia (YSZ, 95% ZrO_2, 5% Y_2O_3, *Tosoh/Nikkato*, Tokyo, Japan) were used in this research. The main properties of the balls are listed in Table 1.

Table 1. Properties of coating and ball materials.

Properties	AlCrN	YSZ
Hardness at 20 °C, GPa	30.6 ± 2.8 [5] *	10.5 **
Fracture toughness K_{IC}, MPa·$m^{0.5}$	6.4 [18]	6.0 **
Young's modulus of elasticity, GPa	585 ± 54 [5] *	210 **
Thermal conductivity 20 °C, W $m^{-1}\cdot K^{-1}$	1.5 [19]	3 **
Max service temperature, °C	900 [20]	1200 **
Density, kg·m^{-3}	–	6000 **
Thermal diffusivity, $\times 10^{-6}\cdot m^2\cdot s^{-1}$	–	0.9 [21]
Diameter, mm	–	10

Notes: * Property from coating from the same production line; ** Properties are provided by producer.

2.2. Characterization of Materials

Surface morphology was studied using a scanning electron microscope (SEM) *Hitachi TM1000* (Tokyo, Japan) equipped with an energy-dispersive X-ray source (EDS).

Raman spectral analysis was performed at room temperature using a high resolution micro-Raman spectrometer (*Horiba Jobin Yvon HR800*, Kyoto, Japan) equipped with a multichannel charge-coupled device (CCD) detection system. The device was set in the backscattering configuration. An Nd-YAG induced laser (λ = 532 nm) with a spot size of 10 µm in diameter was used for excitation. The results were obtained with laser beam powers of 2.8 mW (factor of filter was 0.0912) and 15.8 mW (factor of filter was 0.5147). The laser beam power was kept unchanged for all test materials (including transferred material). Crystal phases of the AlCrN PVD coating were detected by X-ray diffractometer (XRD) *Rigaku Ultima IV* (Tokyo, Japan). Obtained results were compared with measurement results from X-ray diffractometer *Bruker D5005 AXS* (Billerica, MA, US). A monochromatic CuKα radiation in 2θ scan mode was applied. Commercially available database ICDD-PDF-4+*2016* was used for the identifications of crystal phases.

2.3. Evaluation of Coating Reliability

Selected laboratory-scale experimental methods and approaches for improvement of reliability of the AlCrN PVD coating on the steel substrate for use in aggressive environments are listed in Table 2. The selection was done according to applicability for determination of coating reliability under static and tribologically influenced conditions. Visual observation, imaging techniques (optical, SEM, 2D or 3D profiling), ball cratering, adhesion or scratch testing are mainly suitable for preliminary estimation of properties and prediction of performance while electrochemical or tribo-corrosive tests (accompanied with electrochemical measurements) provide the possibility for tracking the performance of materials In-Situ. To great extent, only Raman spectroscopy can assist in an evaluation of the composition of a thin layer formed during tribological testing of material.

Table 2. Applicability of different methods for laboratory evaluation of various aspects of reliability of coatings intended for corrosive tribo-applications.

Task	Method												
	Visual and Tactile Observation	**Optical Microscopy**	**SEM**	**2D Contact Profilometry**	**3D Topography**	**KaloMax Ball Cratering**	**Adhesion Testing**	**Scratch Testing**	**Electrochemical Corrosion Tests**	**Tribo-Corrosive Test***	**EDS**	**Raman Spectroscopy**	**XRD**
Preliminary evaluation	+	+	+	++	+++	+++	+++	+++	+	NCH	++	++	+++
Wear or corrosion rate	-	+	+	+++	+++	NCH	NCH	NCH	++	+++	-	-	-
Destruction mechanisms	+	+	++	++	+++	NCH	NCH	+	+	++	+	+++	++
Elemental or phase composition of thin tribo-layer	-	-	- SE	NCH	NCH	NCH	NCH	-	0	0	-	+++	-
Elemental or phase composition of thick (≈>1 um) tribo-layer	-	0	+ BSE	NCH	NCH	NCH	NCH	-	0	0	++	+++	++
In-Situ measurement of corrosion intensity and/or evolution of coating damage	0	0	NCH	NCH	NCH	NCH	NCH	NCH	+++	+++	-	-	+

Notes: "+" is showing how useful could be the equipment (+ min, ++ average, +++ max); "-" means that equipment is rather not useful; "0"–only qualitative estimation or indirect conclusion; NCH–not considered here; SE and BSE–Secondary electron and Backscattered electrons of SEM; * Assisted with potentiostat/galvanostat.

2.3.1. Potentiodynamic Polarization Test

The typical three-electrode cell was used with the Pt counter-electrode (CE) with a working surface area of 2 cm^2 and the saturated calomel reference electrode (SCE). Potentiodynamic polarization measurements were performed in a 3.5 wt % NaCl aqueous solution to estimate the influence of the microdefects (micropores and macrodroplets) detected by SEM, Figure 2a. The corrosion current density (i_{corr}) was measured at room temperature to evaluation corrosion reaction kinetics. A corrosion potential ($E_{\mathrm{corr\ calc}}$) was calculated from the intercept on Tafel plot. Pristine SS substrates, as well as coated substrates, were tested.

Specimens were isolated with a nonconductive tape and the remaining exposed surface area of about 1 cm^2 was used as working electrodes (WE). *Autolab PGSTAT30* galvanostat–potentiostat with general purpose electrochemical system (*GPES*) software (*Metrohm Autolab B.V., Utrecht*, The Netherlands) was employed for data recording. Open circuit potential (OCP) stabilization was done by immersing the samples into 3.5 wt % NaCl solution for either 10 min or 24 h before the test to estimate the change in polarization resistance. The limits of positive scanning linear sweep voltammetry were set from −0.7 up to 0 V for the coatings and from −0.8 up to 0 V for the substrate. Scanning rate was selected 5 mV·s^{-1}. Software *NOVA* (version 2.1.2, *Metrohm Autolab B.V.*) was used to analyse the Tafel plot. Penetration rate CR (the thickness loss per unit of time mm·year^{-1}]), protective efficiency $P_{\text{ i}}$ [%], porosity F [%] of the coating, the polarization resistances of the substrate and coating-substrate systems R_{pm} and R_{p} [$\Omega\cdot\text{cm}^{-2}$] were calculated according to ASTM G59-97e1-Standard Test Method for Conducting Potentiodynamic Polarization Resistance Measurements [22].

2.3.2. Tribo-Corrosion at Open Circuit Potential

Tribo-corrosion experiments were carried out using universal materials tester (UMT-2) from CETR (*Bruker*, Billerica, MA, US) in a reciprocating mode (amplitude 1×10^{-3} m, frequency 1 Hz). The counter ball was located above the specimen and, therefore, wear debris tend to remain in a wear scar. All tests were done in ambient atmosphere environment (temperature 20 ± 2 °C, relative humidity 50% ± 5%). The specimens were fixed in the electrochemical cell installed on the reciprocating table as shown in Figure 2b. The electrochemical cell was filled with 50 mL of 3.5 wt % NaCl aqueous electrolyte solution. A level of a liquid of 1 cm above the tribological contact was provided. The specimen was connected to the potentiostat as WE. Standard Ag/AgCl as RE and Pt as CE were utilized in the three-electrode mode. EmStat^{3+} potentiostat and *PSTrace* software (*PalmSens BV*, Houten, The Netherlands) was used for data recording and processing.

An exposed surface area of 1 cm^2 was left by isolating the remaining surface of specimens with a nonconductive tape. Exposed surfaces were cleaned step-by-step with acetone, ethanol and then dried before applying electrolyte. The material was immersed in the liquid for 1 h before test without data recording for preliminary stabilization. Recorded data for coated and uncoated materials were divided into three periods: (1) Stabilization (1000 s); (2) tribo-corrosion (7200 or 43,200 s that corresponds to 2 or 12 h); and (3) passivation (1000 s). The load was 1 kg (9.8 N) during 7200 or 43,200 s tests and 3 kg (29.4 N) during 7200 s tests. The initial maximum Hertzian contact pressure was either 1.31 or to 1.88 GPa for 1 or 3 kg tests, respectively.

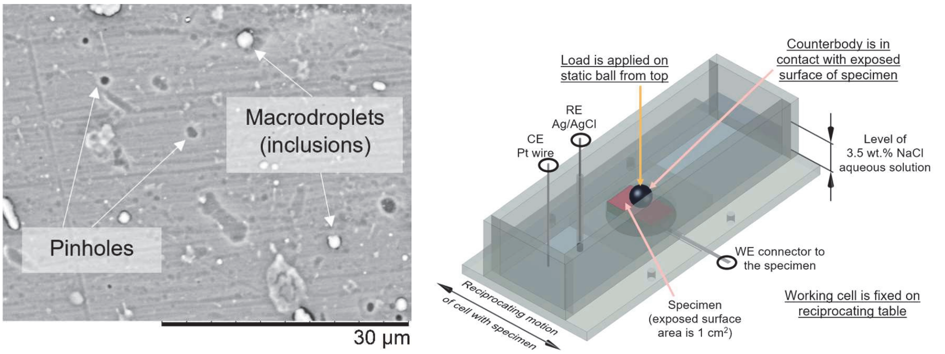

(**a**) (**b**)

Figure 2. Surface defects on the as-deposited AlCrN coating on the stainless steel AISI 316L substrate were detected in a SEM micrograph (**a**); and a schematic illustration of reciprocating tribo-corrosion test setup (**b**).

3. Results and Discussion

3.1. Potentiodynamic Polarization Test of Statically Corroded Uncoated and Coated SS AISI 316L

The Tafel plots and calculated potentiodynamic polarization results of the SS substrate and the coated specimens are presented in Figure 3 and Table 3, respectively. The $E_{\text{corr calc}}$ and i_{corr} of the bare AISI 316L after 10 min of immersion were found to be −0.423 V vs. SCE and 1.9 μA·cm^{-2}, respectively. $E_{\text{corr calc}}$ shifts toward more positive value (to about −0.340 V vs. SCE) after applying the AlCrN PVD coating on the SS substrate. About 1.2 times lower i_{corr} was measured as compared to the AISI 316L, reaching improvement in the protective efficiency (P_{i}) by 15.9%.

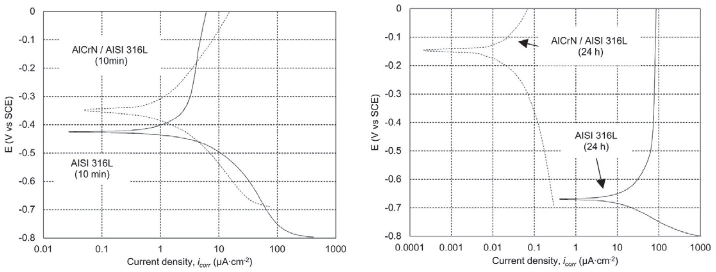

(**a**) (**b**)

Figure 3. Potentiodynamic polarization curves (Tafel plots) of uncoated and AlCrN PVD coated AISI 316L specimens indicating corrosion potential: (**a**) after 10 min immersion; (**b**) after 24 h immersion.

Table 3. Potentiodynamic polarization of uncoated and coated specimens.

Material	**Potentiodynamic Polarization Measurements (From NOVA)**					**Calculation Results**		
	Corrosion Current Density	**Polarization Resistance**	**Calculated Corrosion Potential**	**Tafel Slope**	**Tafel Slope**	**Corrosion Rate**	**Protective Efficiency**	**Porosity**
	i_{corr}	R_{pm}, R_{p}	$E_{\text{corr calc}}$	$\lvert\beta_{\text{a}}\rvert$	$\lvert\beta_{\text{c}}\rvert$	CR	P_{i}	F
	[μA·cm^{-2}]	[Ω·cm^{-2}]	[V]	[V·Decade^{-1}]	[V·Decade^{-1}]	[mm·Year^{-1}]	[%]	[%]
AISI 316L, 10 min	1.9	1.43 × 10^{4}	−0.423	0.718	0.069	2.0 × 10^{-2}	–	–
AlCrN/AISI 316L, 10 min	1.6	3.76 × 10^{4}	−0.340	0.399	0.212	1.7 × 10^{-2}	15.9	29
AISI 316L, 24 h	22.1	1.71 × 10^{3}	−0.669	0.312	0.121	2.3 × 10^{-1}	–	–
AlCrN/AISI 316L, 24 h	0.05	2.33 × 10^{6}	−0.153	0.488	0.517	4.9 × 10^{-4}	99.8	0.002

A significant passivation of the AlCrN PVD coated sample was found after immersion for 24 h. $E_{\text{corr calc}}$ significantly shifts toward a positive value (−0.153 V vs. SCE) and i_{corr} was found to be ≈30 times lower (0.05 μA·cm^{-2}) as compared to the coating after 10 min immersion. The i_{corr} was also found being ≈40 and ≈450 times lower as compared with the tested substrate after 10 min and 24 h immersion, respectively.

Decrease in CR down to 4.9 × 10^{-4} mm·year^{-1} and F down to 0.002% for the AlCrN PVD coated sample was detected after 24 h immersion. It confirms a hydrolyzation reaction with the AlN on the surface and inside the pores. One of possible reaction is known as the Bowen's model [23] reporting degradation of the AlN in an aqueous medium. In the present work, the reaction passivates as the AlN is embedded into a monolithic dense coating and the reaction occurs only on the surface. Corrosion products such as an amorphous aluminium monohydroxide ($\text{AlOOH}_{\text{(amorph)}}$) and a crystalline aluminium hydroxide ($\text{Al(OH)}_{3\text{(crystal)}}$) form an additional passivation layer. Increased P_{i} up to 99.8% confirms the inertness of transition metal (e.g., Cr) nitrides [24].

3.2. Tribo-Corrosive Wear Test of Uncoated and Coated SS AISI 316L

Evolution in OCP before, during and after the short (2 h) wear tests of the bare and coated SS are presented in Figure 4a. Loss of protective oxide film developed on the surface of the bare SS was continuously observed during the whole stabilization period (1000 s) before starting the wear test. OCP shifts towards negative values from about −0.400 down to about −0.680 V vs. Ag/AgCl during stabilization.

Sharp shifting towards more negative values of OCP was measured at the beginning of wear test. Stabilized OCP value of about −0.780 V vs. Ag/AgCl remains practically unchanged until the end of the test. A sharp increase in coefficient of friction (CoF) from about 0.10 up to about 0.74 in the first 1200 s of the wear test (running-in period) indicates a rapid formation of a wear track representing a removed protective oxide layer and an enlarging tribocontact area. Instability in CoF was observed as a fluctuation from 0.70 to 0.74, exhibiting arrangement of the tribosystem (second running-in period). A slightly higher, but stable CoF of about 0.79 was measured after 2600 s of the test running, which indicates reaching a steady-state regime.

Some fluctuations in OCP from −0.230 to −0.160 V vs. Ag/AgCl were observed with the AlCrN PVD coated steel before wear test. These fluctuations are related to the solution penetration into the pores, other defects presented on the surface of the coatings, and reaction with the available AlN, causing a formation of the passive layer that consists of Al-based reaction products. Simultaneous evolution during the first 1600 s and stabilization in OCP and CoF values of about −0.210 V vs. Ag/AgCl and 0.58 were observed corresponding to the running-in and the steady-state regime, respectively. At these particular conditions, neither failure nor observable degradation of the coating was detected.

The test duration was increased up to 12 h with the application of 1 or 3 kg load as shown in Figure 4b. The fluctuations in OCP from −0.320 up to −0.250 V vs. Ag/AgCl were generally observed with the AlCrN PVD coated steel before wear test initiation, Figure 4b. Evolution of CoF during a running-in period (about 4000 s from the beginning of wear test) is similar to the evolution of CoF at 1 and 3 kg loads. An increase in CoF was measured from 0.42 up to the steady-state value of 0.69. A second CoF stabilization period was observed after about 21,000 s of test running, changing CoF to the final steady-state value of 0.65 (1 kg) and 0.62 (3 kg).

A passivation effect of the coated specimen was detected during the test under 1 kg load. The OCP slightly changed from −0.240 up to a more positive value of −0.150 V vs. Ag/AgCl. A rapid change to more negative OCP value of −0.300 V vs. Ag/AgCl was detected after 9000 s of sliding. It can be explained by an increased rate of a continuous mechanical destruction of the passivating layer. A slight passivation effect occurs after about 25,000 s as OCP was measured to be changing from −0.300 up to the final steady-state value of −0.280 V vs. Ag/AgCl.

Sharp shifting in OCP toward more negative values from −0.240 down to −0.440 V vs. Ag/AgCl was observed after the first 3300 s of the test under 3 kg load as shown in Figure 4b. This value remained stable for about 18,000 s of sliding indicating an inability of corrosion products to create a stable passivation layer under this load. However, the critical failure of the coating was recognized after about 18,000 s of the test run. The OCP was measured to be almost continuously shifting towards negative values from −0.440 down to about −0.700 V vs. Ag/AgCl at the end of the test.

It was also found that passivation effect of the immersed AlCrN coating occurs after about 45,400 s of static oxidation as demonstrated in Figure 5. The stabilized OCP is more positive than during tribo-corrosion tests (Figure 4b).

No typical iron based oxides on the pristine surface of the SS AISI 316L were found in the Raman spectra, Figure 6a. However, the Raman peak of Cr_2O_3 with a low intensity at 310 cm^{-1} indicates the development of the oxide layer at the ambient conditions. An increase in intensities of peaks collected from the area of a wear scar of the pristine SS points out to the formation of a thick layer of iron-based oxides and hydroxides [7]. A broad peak was observed in a range between 680 and 700 cm^{-1} indicates the presence of the corrosion product Fe_3O_4, Figure 6a. It should be noted that almost identical spectrum was obtained even after 24 h of static sample expose into the NaCl solution. Well-pronounced broad peaks appear in the spectra of the AlCrN PVD coated SS at 300, 690–706, 1000 and 1331–1388 cm^{-1}, Figure 6b. These peaks belong to the vibration of Cr and N ions and their intensities decrease after immersion in the 3.5 wt % NaCl solution for 12 h. The peak at 1000 cm^{-1} disappears, but a broad peak at 1331–1388 cm^{-1} turns into new peaks of low intensities as demonstrated in Figure 6b. It could be explained by the low and medium intensity combination of Raman active modes and overtones of α-Cr_2O_3 on the surface of coated material [25].

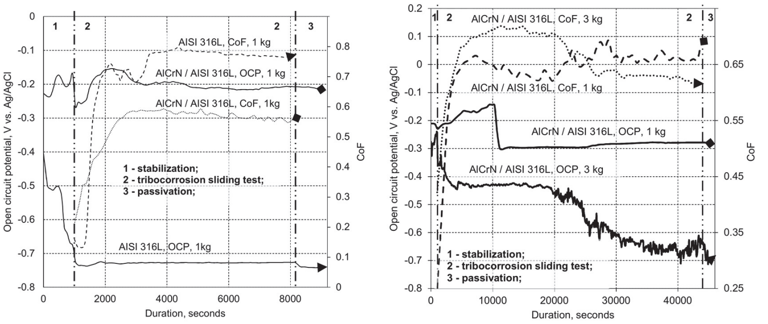

(**a**) (**b**)

Figure 4. Chronopotentiometry results to show comparison in evolution of CoF and open circuit potential (vs. Ag/AgCl) of uncoated and the AlCrN PVD coated AISI 316L samples during short (2 h) (**a**); and extended (12 h) tribo-corrosion test of coated AISI 316L sample (**b**).

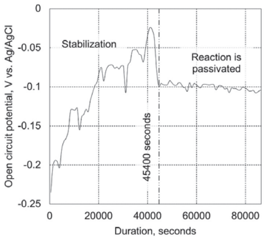

Figure 5. Chronopotentiometry result to show evolution of open circuit potential (vs. Ag/AgCl) of AlCrN PVD coated AISI 316L sample in the 3.5 wt % NaCl solution (static test duration–86,400 s/24 h).

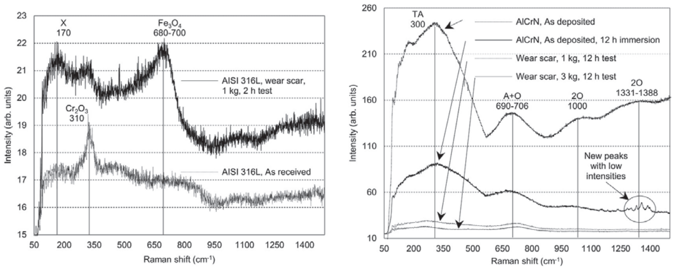

(**a**) (**b**)

Figure 6. Raman spectra illustrates vibration modes and oxides on pristine surface of AISI 316L and in a wear scar after 2 h (1 kg) tribo-corrosion wear test (**a**); and observed changes of intensities and shifting of peaks on coated specimens before and after 12 h immersion; and after extended (12 h) tribo-corrosion wear tests in 3.5 wt. NaCl % under 1 and 3 kg loads (**b**).

The typical grooves in the wear scar of the AISI 316L SS after the short tribo-corrosion test are demonstrated in Figure 7a. Several areas of the CrN rich interlayers and micro-droplet inclusions were exposed during an extended (12 h) tribo-corrosion test under 1 kg load, Figure 7b. Several areas of the uncovered CrN interlayer and extensive cracking in the middle region were found after the extended wear test under 3 kg load, Figure 7c. EDS analysis indicated a critical decrease in an atomic content of Al and appearance of elements typical for AISI 316L in the delaminated areas. The simplified schematic illustration of the static and dynamic corrosion processes is made based on the results obtained, Figure 8. The overview assignment of the Raman peaks of the uncoated and AlCrN coated SS AISI 316L before and after the corrosion and tribo-corrosion tests are presented in Table 4.

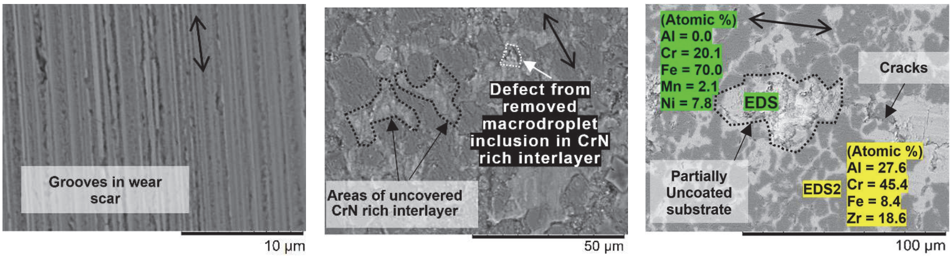

(**a**) (**b**) (**c**)

Figure 7. SEM micrographs show grooves inside wear scars after short (2 h) tribo-corrosion test with AISI 316L (**a**), and defects after extended (12 h) tribo-corrosion tests with AlCrN coated AISI 316L specimens under 1 kg (**b**), and 3 kg loads (**c**). Double arrowed line shows reciprocating sliding direction; elemental analysis was done with EDS inside and close to the marked area.

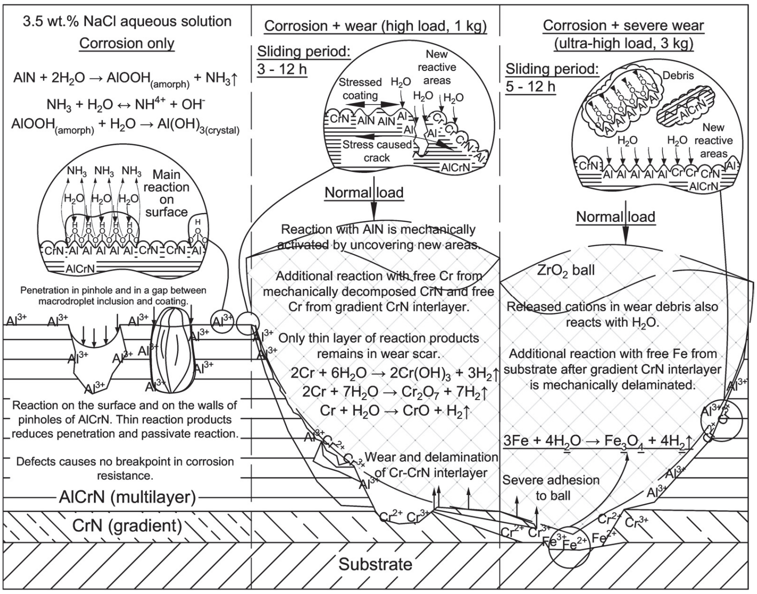

Figure 8. Simplified schematic illustration indicates main processes on the surface and in the wear scar during static corrosion and 12 h tribo-corrosion tests. A period when damage of interlayer or substrate took place in case of 1 or 3 kg tests, respectively is indicated. A ball is shown only for illustration without scaling. Mainly released cations are indicated.

Table 4. Assignment of Raman peaks before and after corrosion and tribo-corrosion tests.

Material	Test	Peak Position [cm^{-1}]	Peak Assignment	Peak Intensity	Peak Configuration	Comments
AISI 316L	As received	310	Cr_2O_3	Low	Sharp	Slight oxidation after polishing
	24 h static immersion	680–700	$Fe_3O_4/\gamma\text{-}Fe_2O_3$	Low	Broad	Development of Fe based oxides and hydroxides
	Tribo-corrosion 2 h, 1 kg	680–700	$Fe_3O_4/\gamma\text{-}Fe_2O_3$	Low	Broad	Development of Fe based oxides and hydroxides
AlCrN PVD on AISI 316L	As deposited	300	TA mode-vibration of Cr ions	High	Broad	Cubic CrN structure
		690–706	A+O optic mode-vibration of N ions	High	Broad	Cubic CrN structure
		1000	2 O-second order transition	Low	Broad	Cubic CrN structure
		1331–1388	2 O-second order transition	Low	Broad	Cubic CrN structure
	12 h static immersion	300	TA mode-vibration of Cr ions	High	Broad	*
		690–706	A+O optic mode-vibration of N ions	High	Broad	*
		1000	2 O-second order transition	Low	Broad	*
		1331–1388	-	Low	Sharp	Possible formation of Al based corrosion products
	Tribo-corrosion 12 h, 1 kg	300	TA mode-vibration of Cr ions	Low	Broad	*
		690–706	A+O optic mode-vibration of N ions	Low	Broad	*
	Tribo-corrosion 12 h, 3 kg	300	TA mode-vibration of Cr ions	Low	Broad	Formation of corrosion products
		690–706	A+O optic mode-vibration of N ions	Low	Broad	Formation of corrosion products.

Note: * Intensity decreases due to the formation of amorphous AlOOH [22].

4. Discussion

The reaction and the subsequent passivation effect in the 3.5 wt % NaCl solution can be attributed to the formation of a very thin and mainly amorphous layer on the surface of the AlCrN coating [26]. This layer consists mainly of $AlOOH_{(amorph)}$, which foremost is a result of the reaction between H_2O and AlN on the surface of the coating (including pinholes, gaps between microdroplet inclusions, etc.). The reactions are more intensive on the more defected areas of the surface. The applied incident powers of Nd-YAG induced laser (λ = 532 nm) of the Raman spectrometer checked from 0.05 up to 22 mW was not appropriate enough to detect this thin amorphous oxide layer due to massive side effects such as noise and/or weak signals. The CoF measurements in the conditions of the tribo-corrosive reciprocating sliding test demonstrate even lower final value at the ultra-high load (3 kg) as compared to the same test at a load of 1 kg. It indicates an intensive forming of a quite soft abrasive body of severely hydrolysed surfaces of the AlCrN-based wear debris (self-lubrication) at the extreme conditions as schematically shown in Figure 8. Self-lubrication effect provided by the hydrolyzation reaction with AlN can provide an improved reliability as a protective factor in a short period of overloading situations. It leads to significantly increased lifetime of coating in underwater conditions in addition to a high resistance to corrosion due to a presence of the interstitial compound of CrN.

It was found that the AlCrN coating is performing sufficiently better than TiCN or TiAlN coatings deposited onto the same SS substrate and tested by authors under the same tribo-corrosive conditions that indicate its higher reliability as the coating for protection of a soft steel substrate that can be produced by 3D printing (additive manufacturing technology) [2]. These TiCN and TiAlN coatings failed during 2-h sliding test with 1 kg load while the AlCrN coating was providing sufficient resistance up to the end of 12-h test with 1 kg load and failed only after 20,000 s of sliding with 3 kg load.

5. Conclusions

The multilayered AlCrN hard coating with the Cr adhesion and the gradient CrN interlayer was deposited on the SS substrate AISI 316L in a dominating cubic CrN structure by LARC PVD. The protective efficiency of the gradient AlCrN PVD coating increases up to 99.8% indicating a passivation layer developed through Al-based reaction products due to the reduced penetration rate of the corrosive media. The presence of surface defects (pinholes, inclusions, etc.) does not significantly affect the failure of coating in static corrosive conditions.

Tribo-corrosion tests performed in 3.5 wt % NaCl solution allows evaluation of the coating reactivity due to the AlN passivation effect combined with the presence of Al-based corrosion products. Change in OCP from −0.18 down to −0.3 V vs. Ag/AgCl after about 2 h-long sliding test under 1 kg load is related to the unprotected layer of Cr rich gradient CrN interlayer due to the partially lost layer of the AlCrN. An appearance and evolution of severe damages in the coating causes OCP shifting down to −0.42 V vs. Ag/AgCl at the beginning of sliding test under 3 kg load, indicating a mechanically initiated reaction with free Al from the AlN and free Cr from the AlCrN and CrN interlayer. The CoF of the coated samples remains about 25% lower (about 0.6) even after partial degradation as compared to the pristine SS under threefold lower load, indicating a reliability of the coating in tribo-contact even after a loss of chemical protection.

Author Contributions: Conceptualization, M.A. and I.H.; Methodology, J.B.; Software, T.R.; Validation, M.A., S.B. and I.H.; Formal Analysis, J.B.; Investigation, J.B.; Resources, M.A., S.B. and T.R.; Data Curation, J.B.; Writing-Original Draft Preparation, J.B.; Writing-Review & Editing, M.A. and I.H.; Visualization, J.B.; Supervision, M.A., I.H.; Project Administration, M.A.; Funding Acquisition, M.A. and I.H.

Funding: This research was supported by the Estonian Research Council under the personal grant (PUT1063) (I. Hussainova), Estonian Ministry of Higher Education and Research under Projects (IUT19-29 and IUT19-28), the European Union through the European Regional Development Fund, (Project TK141) and TTÜ base finance projects (B54, B56 and SS427) (M. Antonov).

Acknowledgments: The authors would like to thank Heinar Vagiström for the help with preparation of AlCrN PVD coatings. The authors would also like to thank Rainer Traksmaa and Arvo Mere for the help with XRD measurements.

Conflicts of Interest: The authors declare no conflict of interest. The founding sponsors had no role in the design of the study; in the collection, analyses, or interpretation of data; in the writing of the manuscript, and in the decision to publish the results.

References

1. Wood, R.J.K. Tribo-corrosion of coatings: A review. *J. Phys. D: Appl. Phys.* **2007**, *40*, 5502–5521. [CrossRef]
2. Holovenko, Y.; Antonov, M.; Kollo, L.; Hussainova, I. Friction studies of metal surfaces with various 3D printed patterns tested in dry sliding conditions. *Proc. Inst. Mech. Eng. Part J J. Eng. Tribol.* **2018**, *232*, 43–53. [CrossRef]
3. Ricker, R.E.; Papavinasam, S.; Berke, N.; Brossia, S.; Dean, S.W. On using laboratory measurements to predict corrosion service lives for engineering applications. *J. ASTM Int.* **2008**, *5*, 1–10. [CrossRef]
4. Fischer, A.; Mischler, S. Tribocorrosion: Fundamentals, materials and applications. *J. Phys. D Appl. Phys.* **2006**, *39*, 3120–3219. [CrossRef]
5. Antonov, M.; Afshari, H.; Baronins, J.; Adoberg, E.; Raadik, T.; Hussainova, I. The effect of temperature and sliding speed on friction and wear of Si_3N_4, Al_2O_3, and ZrO_2 balls tested against AlCrN PVD coating. *Tribol. Int.* **2018**, *118*, 500–514. [CrossRef]
6. Stack, M.M.; Antonov, M.M.; Hussainova, I. Some views on the erosion–corrosion response of bulk chromium carbide based cermets. *J. Phys. D Appl. Phys.* **2006**, *39*, 3165–3174. [CrossRef]
7. Larroumet, D.; Greenfield, D.; Akid, R.; Yarwood, J. Raman spectroscopic studies of the corrosion of model iron electrodes in sodium chloride solution. *J. Raman Spectrosc.* **2007**, *38*, 1577–1585. [CrossRef]

8. Fenker, M.; Balzer, M.; Kappl, H. Corrosion protection with hard coatings on steel: Past approaches and current research efforts. *Surf. Coat. Technol.* **2014**, *257*, 182–205. [CrossRef]
9. Dinu, M.; Mouele, E.; Parau, A.; Vladescu, A.; Petrik, L.; Braic, M. Enhancement of the corrosion resistance of 304 stainless steel by Cr–N and Cr(N,O) coatings. *Coatings* **2018**, *8*, 132. [CrossRef]
10. Gutsev, D.; Antonov, M.; Hussainova, I.; Grigoriev, A.Y. Effect of SiO_2 and PTFE additives on dry sliding of NiP electroless coating. *Tribol. Int.* **2013**, *65*, 295–302. [CrossRef]
11. Zhang, L.; Chen, Y.; Feng, Y.; Chen, S.; Wan, Q.; Zhu, J. Electrochemical characterization of AlTiN, AlCrN and AlCrSiWN coatings. *Int. J. Refract. Met. Hard Mater.* **2015**, *53*, 68–73. [CrossRef]
12. Baronins, J.; Podgursky, V.; Antonov, M.; Bereznev, S.; Hussainova, I. Electrochemical behaviour of TiCN and TiAlN gradient coatings prepared by lateral rotating cathode arc PVD technology. *Key Eng. Mater.* **2016**, *721*, 414–418. [CrossRef]
13. Kaindl, R.; Franz, R.; Soldan, J.; Reiter, A.; Polcik, P.; Mitterer, C.; Sartory, B.; Tessadri, R.; O'Sullivan, M. Structural investigations of aluminum-chromium-nitride hard coatings by Raman micro-spectroscopy. *Thin Solid Films* **2006**, *515*, 2197–2202. [CrossRef]
14. Johnson, D.F.; Jiang, D.E.; Carter, E.A. Structure, magnetism, and adhesion at Cr/Fe interfaces from density functional theory. *Surf. Sci.* **2007**, *601*, 699–705. [CrossRef]
15. Lukaszkowicz, K.; Sondor, J.; Balin, K.; Kubacki, J. Characteristics of CrAlSiN + DLC coating deposited by lateral rotating cathode arc PVD and PACVD process. *Appl. Surf. Sci.* **2014**, *312*, 126–133. [CrossRef]
16. Rana, D.; Mandal, B.M.; Bhattacharyya, S.N. Analogue calorimetric studies of blends of poly(vinyl ester)s and polyacrylates. *Macromolecules* **1996**, *29*, 1579–1583. [CrossRef]
17. Benedek, I.; Feldstein, M.M. Fundamentals of pressure sensitivity. In *Handbook of Pressure-Sensitive Adhesives and Products*; CRC Press: Boca Raton, FL, USA, 2008.
18. Kawate, M.; Kimura Hashimoto, A.; Suzuki, T. Oxidation resistance of $Cr_{1-x}Al_xN$ and $Ti_{1-x}Al_xN$ films. *Surf. Coat. Technol.* **2003**, *165*, 163–167. [CrossRef]
19. Samani, M.K.; Chen, G.C.K.; Ding, X.Z.; Zeng, X.T. Thermal conductivity of CrAlN and TiAlN coatings deposited by lateral rotating cathode arc. *Key Eng. Mater.* **2010**, *447–448*, 705–709. [CrossRef]
20. Nohava, J.; Dessarzin, P.; Karvankova, P.; Morstein, M. Characterization of tribological behavior and wear mechanisms of novel oxynitride PVD coatings designed for applications at high temperatures. *Tribol. Int.* **2015**, *81*, 231–239. [CrossRef]
21. Somiya, S.; Aldinger, F.; Spriggs, R.M.; Uchino, K.; Koumoto, K.; Kaneno, M. Handbook of Advanced Ceramics: Materials, Applications, Processing, and Properties. In *Handbook of Advanced Ceramics*; Elsevier: New York, NY, USA, 2003.
22. *ASTM G59-97e1 Standard Test Method for Conducting Potentiodynamic Polarization Resistance Measurements*; ASTM International: West Conshohocken, PA, USA, 1997.
23. Bowen, P.; Highfield, J.G.; Mocellin, A.; Ring, T.A. Degradation of aluminum nitride powder in an aqueous environmet. *J. Am. Ceram. Soc.* **1990**, *73*, 724–728. [CrossRef]
24. Yang, M.; Allen, A.J.; Nguyen, M.T.; Ralston, W.T.; MacLeod, M.J.; DiSalvo, F.J. Corrosion behavior of mesoporous transition metal nitrides. *J. Solid State Chem.* **2013**, *205*, 49–56. [CrossRef]
25. Gomes, A.S.O.; Yaghini, N.; Martinelli, A.; Ahlberg, E. A micro-Raman spectroscopic study of $Cr(OH)_3$ and Cr_2O_3 nanoparticles obtained by the hydrothermal method. *J. Raman Spectrosc.* **2017**, *48*, 1256–1263. [CrossRef]
26. Barshilia, H.C.; Selvakumar, N.; Deepthi, B.; Rajam, K.S. A comparative study of reactive direct current magnetron sputtered CrAlN and CrN coatings. *Surf. Coat. Technol.* **2006**, *201*, 2193–2201. [CrossRef]

Curriculum vitae

Personal data

Name: Janis Baroninš
Date of birth: 15.08.1987
Place of birth: Riga
Citizenship: Latvia

Contact data

E-mail: Janis.baronins@ttu.ee; jbaronins@gmail.com

Education

2014 – 2018	Tallinn University of Technology, PhD
2011 – 2014	Riga Technical University, MSC
2007 – 2011	Riga Technical University, BSC
2003 – 2007	Riga State technical school

Language competence

Latvian	Native
English	Fluent
Russian	Basic
German	Basic

Professional employment

2006 – 2006	Rudus Latvia, Ltd, Laboratory assistant
2006 – 2007	HC Betons, Ltd, Laboratory assistant
2011 – 2013	Riga Technical University, Laboratory assistant
2012 – 2013	Arcers Ltd, NATO project, Quality manager

Projects in progress

B56 "Innovative polycrystalline diamond (PDC) drag bit for soft ground tunnel boring machines (1.05.2016−30.04.2019)", Maksim Antonov, Tallinn University of Technology, School of Engineering, Department of Mechanical and Industrial Engineering.

ETF8850 "Self-organisation of minerals based adaptive tribomaterials (1.01.2011−31.12.2014)", Maksim Antonov, Tallinn University of Technology, Faculty of Mechanical Engineering.

SS427 "INNOVAATILISTE TEHNOLOOGIATE ARENDAMINE METALL-KERAAMILISTE MATERJALIDE VALMISTAMISEKS"

Industrial property

Invention: Transformable multi-sample apparatus for dry erosion testing of materials up to 1000 °C in the presence of corrosive gases; Owners: Tallinn University of Technology; Authors: Maksim Antonov, Janis Baroninš, Irina Hussainova; Priority number: P201800011; Priority date: 6.06.2018.

Invention: Sorbent with ferromagnetic properties; Owners and authors: Andrei Shishkin, Viktors Mironovs, Janis Baroninš, Juris Treijs; Priority number: LV14822 B; Priority date: 20.06.2014.

Invention: Ferromagnetic sorbent; Owners and authors: Andrei Shishkin, Mironovs Viktors, Janis Baroninš, Treijs Juris; Priority number: LV 14820 B; Priority date: 20.06.2013.

Invention: Method and device for manufacturing multilayer articles of sheet materials and device for the same; Owners and authors: Viktors Mironovs, Andrejs Šiškins, Janis Baroninš; Priority number: LV14424 B (Latvia) and LV20110000122 20110922 (Espacenet); Priority date: 20.01.2012.

Invention: Magnetic stirrer; Owners and authors: Viktors Mironovs, Andrejs Šiškins, Vjačeslavs Lapkovskis, Janis Baroninš; Priority number: LV14382; Priority date: 14.06.2011.

Invention: Method and device for mixing of powder materials; Owners and authors: Viktors Mironovs, Vjačeslavs Lapkovskis, Andrejs Šiškins, Janis Baroninš; Priority number: LV14383; Priority date: 10.06.2011.

Elulookirjeldus

Isikuandmed

Nimi: Janis Baroninš
Sünniaeg: 15.08.1987
Sünnikoht: Riia
Kodakondsus: Läti

Kontaktandmed

E-post: Janis.baronins@ttu.ee; jbaronins@gmail.com

Hariduskäik

2014 – 2018	Tallinna Tehnikaülikool, PhD
2011 – 2014	Riia Tehnikaülikool, MSc
2007 – 2011	Riia Tehnikaülikool, BSc
2003 – 2007	Riia Riiklik Tehnikakool

Keelteoskus

Läti	emakeel
Inglise	kõrgtase
Vene	algtase
Saksa	algtase

Teenistuskäik

2006 – 2006	Rudus Latvia, Ltd, laborant
2006 – 2007	HC Betons, Ltd, laborant
2011 – 2013	Riia Tehnikaülikool, laborant
2012 – 2013	Arcers Ltd, NATO projekt, kvaliteedijuht

Projektid

B56 "Innovatiivsed polükristallilisest teemandist kuluvosad pehme pinnase tunneli puurimisseadmete tarbeks" (1.05.2016−30.04.2019), Maksim Antonov, Tallinna Tehnikaülikool, Inseneriteaduskond, Mehaanika ja tööstustehnika instituut.

ETF8850 "Isesobituvad adaptiivsed tribomaterjalid mineraalide baasil" (1.01.2011−31.12.2014), Maksim Antonov, Tallinna Tehnikaülikool, Inseneriteaduskond, Mehaanika ja tööstustehnika instituut.

SS427 "Innovaatiliste tehnoloogiate arendamine metall-keraamiliste materjalide valmistamiseks"

Tööstusomand

Patentne leiutis: Transformeeritav multi-proovi seade materjalide kuiverosioonil katsetamiseks söövitavate gaaside keskkonnas kuni 1000 °C; Omanik: Tallinna Tehnikaülikool; Autorid: Maksim Antonov, Janis Baroninš, Irina Hussainova; Prioriteedi number: P201800011; Prioriteedi kuupäev: 6.06.2018.

Patentne leiutis: Ferromagnetiliste omadustega sorbent; Omanikud ja autorid: Andrei Shishkin, Viktors Mironovs, Janis Baroninš, Juris Treijs; Prioriteedi number: LV14822 B; Prioriteedi kuupäev: 20.06.2014. 101

Patentne leiutis: Ferromagnetiline sorbent; Omanikud ja autorid: Andrei Shishkin, Mironovs Viktors, Janis Baroninš, Treijs Juris; Prioriteedi number: LV14820 B; Prioriteedi kuupäev: 20.06.2013.

Patentne leiutis: Meetod ja seade mitmekihiliste lehtmaterjalide valmistamiseks; Omanikud ja autorid: Viktors Mironovs, Andrejs Šiškins, Janis Baroninš; Prioriteedi number: LV14424 B (Latvia) and LV20110000122 20110922 (Espacenet); Prioriteedi kuupäev: 20.01.2012.

Patentne leiutis: Magnetsegaja; Omanikud ja autorid: Viktors Mironovs, Andrejs Šiškins, Vjačeslavs Lapkovskis, Janis Baroninš; Prioriteedi number: LV14382; Prioriteedi kuupäev: 14.06.2011.

Patentne leiutis: Meetod ja seade pulbermaterjalide segamiseks; Omanikud ja autorid: Viktors Mironovs, Vjačeslavs Lapkovskis, Andrejs Šiškins, Janis Baroninš; Prioriteedi number: LV14383; Prioriteedi kuupäev: 10.06.2011.